opera
Osaka Prefecture University Education and Research Archives
大阪府立大学 学術情報リポジトリ

Title	Novel Chemical Vapor Deposition Process of ZnO Thin Films using Non equilibrium Plasma Generated near Atmospheric Pressure
Author(s)	野瀬, 幸則
Editor(s)	
Citation	
Issue Date	2016-02
URL	http://hdl.handle.net/10466/15116
Rights	

http://repository.osakafu-u.ac.jp/dspace/

Novel Chemical Vapor Deposition Process of ZnO Thin Films using Nonequilibrium Plasma Generated near Atmospheric Pressure

Yukinori Nose

February 2016

Doctoral Thesis at Osaka Prefecture University

Table of Contents

Chapter 1: General introduction

1-1 Research backgrounds 1

1-2 Objectives and composition of this thesis 9

References 14

Chapter 2: Development of chemical vapor deposition system using nonequilibrium N_2/O_2 plasma generated near atmospheric pressure

2-1 Introduction 21

2-2 Experimental 23

2-2-1 Source materials for CVD 23

2-2-2 CVD system using N_2/O_2 direct plasma generated near atmospheric pressure 27

2-2-3 Film characterization 30

2-3 Results and discussions 31

2-3-1 Analysis of plasma by optical emission spectroscopy..................... 31

2-3-2 Characterization of ZnO films 33

2-3-3 Position dependence of growth rate 35

2-3-4 Analysis of the limiting factor of CVD 37

2-4 Conclusions 39

References 40

Chapter 3: Orientation control of low temperature grown ZnO films and the electrical property

3-1 Introduction.. 45

3-2 Experimental 47

3-3 Results and discussions.. 49

3-3-1 Growth temperature dependence on the crystallinity...................... 49

3-3-2 Orientation control and the kinetics.. 51

3-3-3 Electrical properties of ZnO films 55

3-4 Conclusions 59

References 60

Chapter 4: Evaluation of the electronic state for highly resistive ZnO epitaxial films

4-1 Introduction.. 65

4-2 Experimental 67

4-3 Results and discussions.. 69

4-3-1 Crystallinity and morphology of epitaxial ZnO films 69

4-3-2 Optical properties of epitaxial ZnO films 73

4-3-3 Electrical property of ZnO epitaxial films 77

4-3-4 Extrinsic impurities and nitrogen acceptors 83

4-3-5 Electronic state of highly resistive ZnO films 89

4-4 Conclusions..91

References..92

Chapter 5: Novel chemical vapor deposition route of ZnO films: nonequilibrium N_2 plasma with small amount of O_2 below 1%

5-1 Introduction 99

5-2 Experimental..101

5-3 Results and discussions 105

5-3-1 Effect of small amount of O_2 addition on the plasma and basic properties of ZnO films 105

5-3-2 Evaluation of non-radiative species using Q-mass and gas sensor113

5-3-3 Evaluation of the oxidation state by XPS 117

5-3-4 Reaction scheme...119

5-3-5 Evaluation of the deep levels by thermally stimulated current measurement 121

5-3-6 Assignment of the trap states 128

5-3-7 Application of this novel CVD process 133

5-4 Conclusions 134
References 135

Chapter 6: Chemical vapor deposition using nonequilibrium N_2/O_2 remote plasma generated near atmospheric pressure

6-1 Introduction.. 145
6-2 Difference in growth process: Direct and Remote regions.. 147
6-3 Experimental setup for remote plasma CVD.................. 151
6-4 Results and discussions 153
6-4-1 Extraction of excited species to remote region 153
6-4-2 Characterization of ZnO films 157
6-5 Conclusions 163
References 164

Chapter 7: General conclusions 167

Acknowledgement 173

Original articles regarding this thesis 175

Other article regarding this thesis 176

Chapter 1: General introduction

1-1 Research backgrounds

Oxygen is an element with the largest Clarke number and commonly exists in minerals on earth in the form of “oxide”. Oxide is stable in ambient and shows a variety of physical and chemical properties such as dielectric,[1)1-3)] conductor,[4-6)] superconductor,[7-10)] ferroelectrics,[11-14)] ferromagnetics,[15,16)] catalysts [17)] and so on. The variety has enabled a wide range of the material design for functional devices.[18)] Since the discovery of high-T_c superconductors,[19)] crystal growth of oxides and the peripheral technology have rapidly made progress.[20,21)] Now, the field of oxide electronics is getting advances into the backbone of semiconductor electronics in association with the crystal growth techniques peculiar to oxides.[5,20,22,23)]

In such trends in oxide electronics, zinc oxide (ZnO) as a semiconductor has attracted much attention for a long time. ZnO is a transparent semiconductor with a direct bandgap of 3.37 eV at ambient temperature and pressure. ZnO has hexagonal wurtzite structure where each elements (Zn and O) form tetrahedral coordination as illustrated in **Fig. 1-1**. The crystal structure has no inversion symmetry along $\langle 0001 \rangle$ direction due to the distortion of tetrahedron from the regular one, which result in the origin of spontaneous polarization and piezoelectricity along c-axis direction.[24,25)] ZnO have very high electro-mechanical coupling coefficient (k^2) in semiconductors, which have allowed the application to thin film piezoelectric devices on non-piezoelectric substrates such as surface acoustic wave (SAW) resonator and filter for telecommunications.[26-31)] Recent progress on thin film growth technology has enabled

the growth of high quality single-crystalline ZnO epitaxial films with atomically flat surface [32] utilizing commercially available high quality single crystal substrates [33] and their surface treatments.[34,35] Since the demonstration of excitonic stimulated light emission at high temperature,[36] ZnO has been expected as a host material of short-wavelength light emitter utilizing its extremely high exciton binding energy of 60 meV.[37] The successful formation of p-type ZnO proved by the electroluminescence from p-i-n homojunction of ZnO [38] accelerated the researches toward the realization of reliable and reproducible p-type ZnO films.[39] As a result, the light emitting efficiency of ZnO-based light emitting diodes (LEDs) had rapidly improved to two-digits under the commercially available InGaN-based LEDs without any elaborate light extraction structures.[40] Such a remarkable advances in the quality of ZnO-based materials has established their position as one of the purest semiconductors.[41,42]

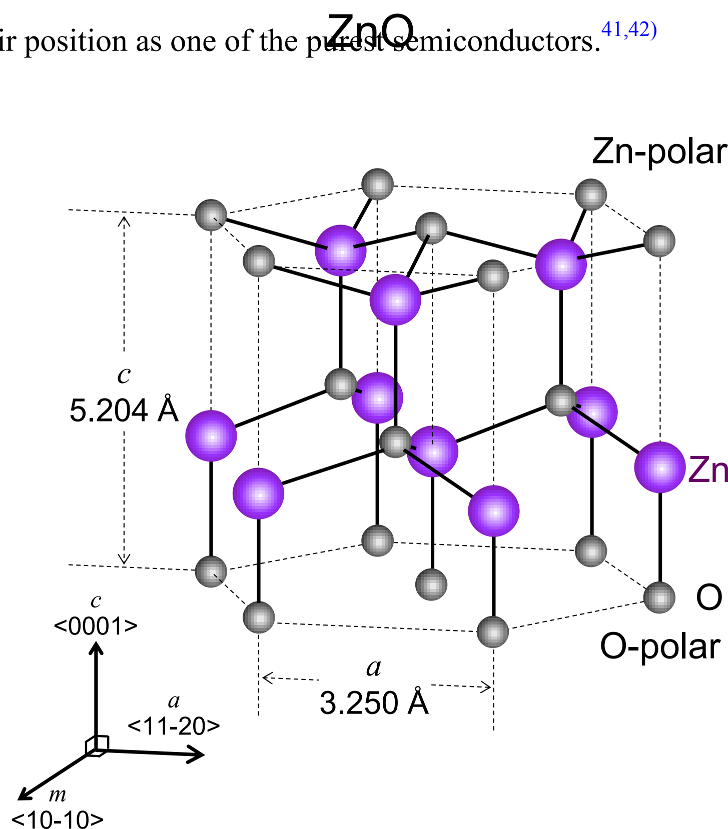

Fig. 1-1. Crystal structure and lattice parameter of wurtzite-structured zinc oxide.[24,25]

Although ZnO have many inherent advantages in terms of its material properties compared with III-V semiconductor such as gallium nitride (GaN),[33,36,37,43] the problem, oxygen deficiency (zinc excess), has still remained as an obstacle to the practical application of ZnO-based devices,[44] despite enormous efforts have been devoted to overcome the serious problem as a semiconductor, and various crystal growth techniques have proposed and assessed.[45] ZnO generally shows a single polarity of n-type and the opposite (p-type) is very difficult to form, which is one of the most serious but universal issue in many wide bandgap semiconductors.[46-55] According to the first principle calculation given Janotti and Van de Walle,[56] donor-type defects such as zinc interstitial (Zn_i) and oxygen vacancy (V_O) are predicted to be formed easily in nominally un-doped ZnO in Zn-rich equilibrium state. (**Fig. 1-2** left) However, note that the formation energies of each point defects in O-rich state are higher positive value than those in Zn-rich state when the Fermi level locates from midgap (i-type) to valence band maximum (p-type).[56,57] (**Fig. 1-2** right) Their calculation implicitly recommends that crystal growth techniques enable O-rich state are the promising route for suppressing donor-type intrinsic defects. From an experimental viewpoint, crystal growth techniques with reactive oxygen sources are important for the realization of pure ZnO films with high quality either the final goal is intrinsic or p-type ZnO.[32,57,58] In case of conventional vacuum-based thin film growth techniques such as molecular beam epitaxy (MBE), pulsed laser deposition (PLD), sputtering and low pressure chemical vapor deposition (LPCVD), the generation of oxygen deficiency (Zn excess) is difficult to suppress owing to the high equilibrium vapor pressure of oxygen. In the history of semiconductors such as Si, GaAs and GaN, the incorporation oxygen has been

forbidden during the crystal growth. In contrast to that, oxide semiconductors contain oxygen as a major element, which is suitable for the growth near atmospheric pressure (AP). And sometimes the crystal growth is performed even in the moisture at AP.[59-61] In this thesis, the author proposes "nonequilibrium (cold) plasma process near atmospheric pressure (AP)" which is potentially able to generate oxidative excited species with extremely high density.[62]

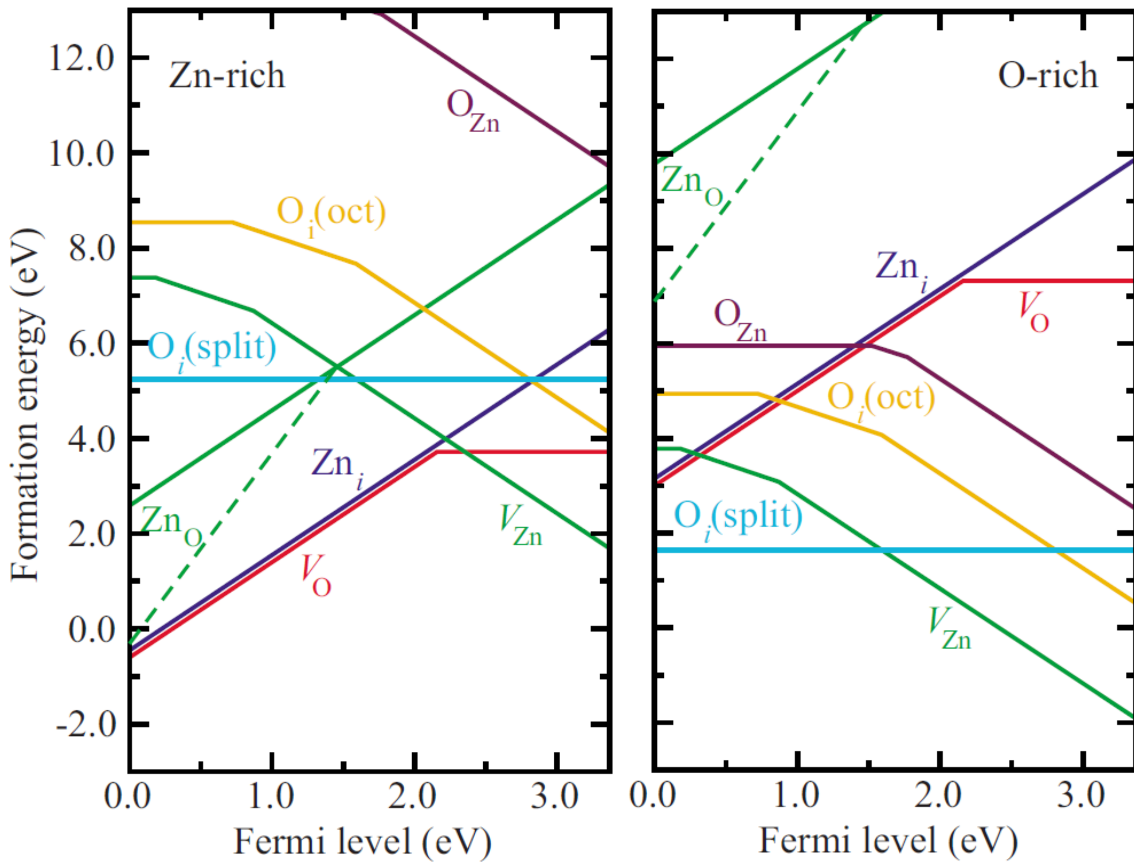

Fig. 1-2. Formation energy of native point defects in ZnO against the position of Fermi level calculated by A. Janotti, and C. G. Van de Walle.[56] The inflection points indicate the change of charged state. The words Zn-rich and O-rich indicate the diviation from the ideal stoichiometric composition.

Conventionally, nonequilibrium plasma has been generated at low pressure (LP), because a stable glow discharge suitable for materials processing is easy to generate at a specific LP according to Paschen's law.[63] Such nonequilibrium glow discharge has played important roles in the manufacturing processes of semiconductor devices. (e.g. sputtering, dry etching, ashing, surface modification, and so on.) On the other hand, glow-to-arc transition rapidly occurs near AP, which has been employed in thermal spraying, nuclear fusion reactions, etc. utilizing the extremely high gas temperature. In the late 1980s, Okazaki and her co-workers had succeeded in the formation of stable glow discharge at AP under several specific conditions.[64] Their requirements are as follows: (i) Dilution of process gases by a large amount of helium (He), (ii) Covering of at least one side electrode by dielectric materials and (iii) Application of alternating voltage above 1 kHz. Since their pioneering research, nonequilibrium plasma expanded its processing objects out of vacuum chamber not only for material processing [63,65] but also for biomedical processing etc.[66,67] However, the dilution by He is an expensive process due to the high cost and unstable supply of noble gases.[68] The stabilization technique of AP plasma without He was a big demand toward the practical application of this plasma.

The generation of nonequilibrium AP plasma using general-purpose gases such as N_2, O_2 and Ar had also been proposed in 1993 by Okazaki *et al*.[69] However, stability of the plasma was greatly affected by impurities, and a stable glow discharge was difficult to maintain mainly due to the shorter lifetime of metastable radicals compared with He (as long as 6×10^5 s). Under such technological difficulty, Yuasa *et al*. had succeeded in the formation of stable N_2 plasma at AP by the improvement of dielectric materials and voltage waveforms.[70,71]

In our research group, Hayakawa *et al*. had succeeded in the formation of nonequilibrium glow discharge of N_2 near AP accompanied by the low gas temperature of 400 K and high electron temperature of 3000 – 12000 K. They applied this nonequilibrium N_2 plasma near AP to the direct nitridation of silicon (denoted as SiN) and oxinitridation of silicon (denoted as SiON) for the application to gate insulators in field effect transistors (FETs). The results are briefly summarized in **Fig. 1-3**.[72)] Compared with the SiN dielectric layer formed by conventional radio frequency (RF) plasma operated at LP, pure N_2 plasma generated near AP is able to form dense SiN layer with smaller leakage current. They had also succeeded in the formation of SiN layer even at ambient temperature, indicating the high reactivity of nitrogen excited species in pure N_2 plasma generated near AP. Additionally, N_2 plasma with as low as 250 ppm additional O_2 strongly enhances the oxidation of Si, and SiON layer shows much lower leakage current compared with SiN layer. Based on the analysis of leakage current by Wentzel-Kramers-Brillouin (WKB) approximation, the effective mass in SiON layer is calculated to be 0.62 m_0, which is higher than the reported value of SiON layer with almost the same chemical composition, indicating the high oxidizability of the N_2-based N_2/O_2 plasma generated near AP. Despite being oxidative, however, this plasma had never been employed in the chemical vapor deposition (CVD) of oxide films. Regarding the CVD of ZnO films using AP plasma, although a few reports exist,[73-76)] all of them are employed under He dilution of source gases. To the knowledge of the author, no experimental verification and report exist which focused on the advantages of AP plasma as oxidation source in CVD process of oxide

semiconductors. Of course, the potential application of AP plasma process for the CVD of oxide films has not clearly understood until now.

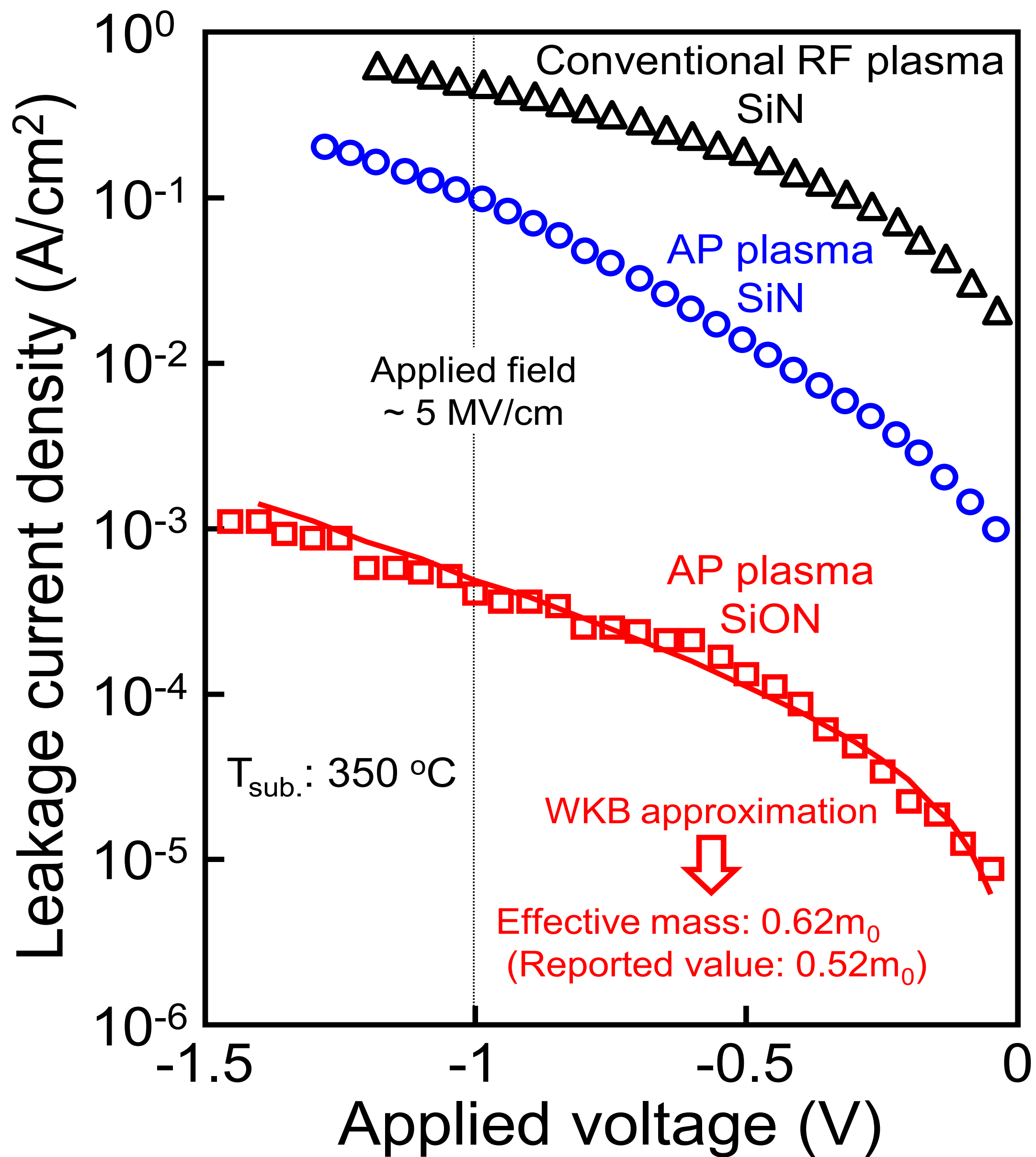

Fig. 1-3. Leakage current characteristics of metal-insulator-semiconductor (MIS) capacitor at accumulation side. Ultrathin dielectric layes (~ 2 nm) are formed at 350 °C by irradiating conventional RF plasma and AP plasma to p-type Si substrates.[72)]

1-2 Objectives and composition of this thesis

Based on the research backgrounds described in 1-1, the author intends to apply this N_2-based nonequilibrium plasma generated near AP to the CVD process of ZnO films as a novel process. The author develops two different CVD systems optimized for the deposition of ZnO films and studies on the effect of excited species on the formation process of ZnO films. On the basis of plasma analysis and film characterization techniques, reaction processes in the plasma and resulting electronic state of ZnO films are elucidated in detail. The objectives of this thesis are set as follows.

<Objectives>

Experimental verification of the advantages of N_2-based nonequilibrium plasma generated near atmospheric pressure to the reduction of residual electron and nitrogen doping to ZnO films for the application to next generation CVD process of ZnO based semiconductor.

This thesis is composed of seven chapters as briefly summarized in **Fig. 1-4**.

In chapter 1, the author has described the research backgrounds and the objectives of this doctoral thesis.

In chapter 2, basic concepts of developed CVD system using direct plasma generated near AP are explained in detail.[77] As a Zn source material, *β*-diketonate complexes: Bis-2,4octanedionato zinc [$Zn(C_8H_{13}O_2)_2$ denoted as $Zn(OD)_2$] was selected, and low temperature formation of ZnO films around 200 ºC was demonstrated using O_2-based N_2/O_2 direct plasma. In order to assess the growth process of ZnO films from

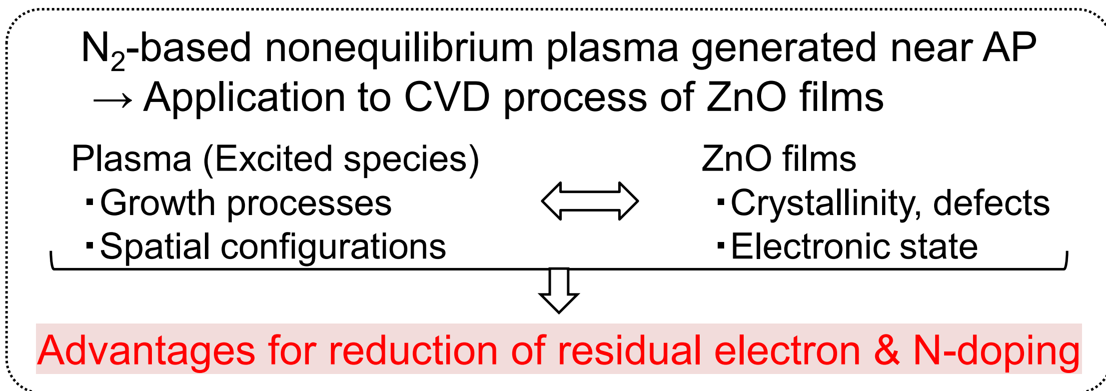

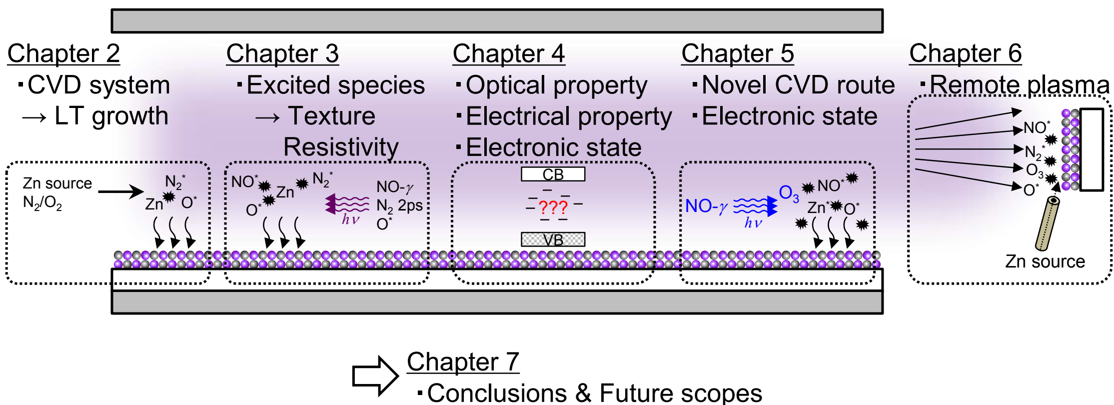

Fig. 1-4. Overall picture of this thesis. The composition of this thesis is also schematically illustrated.

a macroscopic point of view, growth rate was evaluated at various growth conditions. Moreover, from the change of growth rate against the gas flow direction, potential application for low-temperature growth of ZnO is discussed.

In chapter 3, the author focuses on the effects of radiative excited species in N_2/O_2 plasma on the crystallinity and electrical property of low temperature grown ZnO films on glass substrates.[78] Although a high temperature growth is effective for the enhancement of crystallinity, low temperature growth enables the evaluation of intrinsic effect of plasma on the properties of films. Finally, highly (0001)-oriented ZnO films were successfully obtained by adjusting the O_2 concentration in N_2/O_2 and the gas flow velocity, while keeping a constant growth temperature of as low as 200 ºC. Despite such a low growth temperature, ZnO films showed quite high specific resistivity exceeding 10^6 Ωcm at room temperature. Texture control and formation mechanism of highly resistive ZnO films are discussed.

In chapter 4, the electronic states of highly resistive ZnO films are discussed in order to elucidate the origin of high resistivity. In addition to the improvement of crystal quality by the control of excited species proposed in chapter 3, epitaxial growth was introduced to approach the further intrinsic effects of plasma on the formation of highly resistive ZnO films. Photoluminescence (PL) measurement revealed that the existence of radiative recombination center around the midgap of ZnO, which is possibly originate from acceptor-type intrinsic defects. Temperature-dependent Hall effect together with secondary ion mass spectroscopy (SIMS) and Raman spectroscopy suggested that nonequilibrium AP plasma is effective to reduce shallow donor in ZnO. Based on the experimental results, the electronic states of highly resistive epitaxial ZnO

films are discussed in comparison with ZnO films grown by the conventional vacuum processes.

In chapter 5, the author proposes a novel chemical vapor deposition (CVD) route of ZnO films involving a nonequilibrium N_2 plasma generated near atmospheric pressure with small O_2 concentration (O_2%) below 1%, where is expected to be effective region for the reduction of residual donors and nitrogen doping to ZnO films. In the optical emission (OE) spectra of the plasma, OE lines corresponding to the NO-γ system ($A^2\Sigma^+ \longrightarrow X^2\Pi_\gamma^+$) are observed, despite the only introduced gases being N_2 and O_2; these vanish at an O_2% of more than 1%. This plasma generated some highly reactive oxidant and leaded to the formation of ZnO films with excellent (0001) preferred orientation and high transmittance in the visible region. Based on the analyses of the plasma and the exhaust gases, the decomposition, oxidation and crystallization processes are analyzed in detail. Moreover, this plasma is able to form ZnO films with quite high specific resistivity of 4×10^6 Ωcm in a wide process window, which is difficult to be formed by conventional vacuum processes. Thus, the electronic states are investigated by thermally stimulated current (TSC) measurement to elucidate the origin of high resistivity. Finally the author refers to a few directions in which this technique can be extended.

In chapter 6, remote plasma CVD system is newly developed in order to improve the crystal quality and extend a degree of freedom for deposition such as deposition onto metal or flexible substrates. According to the finding obtained in chapter 5, nonequilibrium N_2 plasma generated near atmospheric pressure with small O_2 concentration was employed. OES at remote region revealed that metastable $N_2(A^3\Sigma_u^+)$

with remarkably long lifetime of 2 s [79,80] played a key role in the generation of remote plasma. Separate injection of zinc source material and oxidant was employed to avoid unintentional parasitic reactions before arriving at the substrate which often degraded the crystal quality.[28,29,45] As a result, epitaxial growth of ZnO films was realized with high deposition rate and material yield.

In chapter 7, the author comprehensively summarizes the results obtained throughout this doctoral thesis and refers to the future scopes of this plasma CVD technique.

References

1) B. E. Deal, and A. S. Grove, General Relationship for the Thermal Oxidation of Silicon, *J. Appl. Phys.* **36**, 3770 (1965).
2) G. D. Wilk, R. M. Wallace, and J. M. Anthony, High-k gate dielectrics: Current status and materials properties considerations, *J. Appl. Phys.* **89**, 5243 (2001).
3) Riikka L. Puurunen, Surface chemistry of atomic layer deposition: A case study for the trimethylaluminum/water process, *J. Appl. Phys.* **97**, 121301 (2005).
4) M. Imada, A. Fujimori, and Y. Tokura, Metal-insulator transitions, *Rev. Mod. Phys.* **70**, 1039 (1998).
5) H. Hosono, Recent progress in transparent oxide semiconductors: Materials and device application, *Thin Solid Films* **515**, 6000 (2007).
6) H. J. Kim, U. Kim, T. H. Kim, J. Kim, H. M. Kim, B.-G. Jeon, W.-J. Lee, H. S. Mun, K. T. Hong, J. Yu, K. Char, and K. H. Kim, Physical properties of transparent perovskite oxides $(Ba,La)SnO_3$ with high electrical mobility at room temperature, *Phys. Rev. B* **86**, 165205 (2012).
7) H. Maeda, Y. Tanaka, M. Fukutomi, and T. Asano, A New High-T_c Oxide Superconductor without a Rare Earth Element, *Jpn. J. Appl. Phys.* **27**, L209 (1988).
8) David Larbalestier, Alex Gurevich, D. Matthew Feldmann, and Anatoly Polyanskii, High-T_c superconducting materials for electric power applications, *Nature* **414**, 368 (2001).
9) A. D. Caviglia, S. Gariglio, N. Reyren, D. Jaccard, T. Schneider, M. Gabay, S. Thiel, G. Hammerl, J. Mannhart, and J.-M. Triscone, Electric field control of the $LaAlO_3/SrTiO_3$ interface ground state, *Nature* **456**, 624 (2008).
10) K. Ueno, S. Nakamura, H. Shimotani, H. T. Yuan, N. Kimura, T. Nojima, H. Aoki, Y. Iwasa, and M. Kawasaki, Discovery of superconductivity in $KTaO_3$ by electrostatic carrier doping, *Nat. Nanotech.* **6**, 408 (2011).
11) M. W. J. Prins, S. E. Zinnemers, J. F. M. Cillessen, and J. B. Giesbers, Depletion-type thin-film transistors with a ferroelectric insulator, *Appl. Phys. Lett.* **70**, 458 (1997).
12) K. J. Choi, M. Biegalski, Y. L. Li, A. Sharan, J. Schubert, R. Uecker, P. Reiche, Y. B. Chen, X. Q. Pan, V. Gopalan, L.-Q. Chen, D. G. Schlom, and C. B. Eom, Enhancement of Ferroelectricity in Strained $BaTiO_3$ Thin Films, *Science* **306**, 1005 (2004).
13) T. Miyasako, M. Senoo, and E. Tokumitsu, Ferroelectric-gate thin-film transistors

using indium-tin-oxide channel with large charge controllability, *Appl. Phys. Lett.* **86**, 162902 (2005).

14) T. S. Böscke, J. Müller, D. Bräuhaus, U. Schröder, and U. Böttger, Ferroelectricity in hafnium oxide thin films, *Appl. Phys. Lett.* **99**, 102903 (2011).

15) J.-H. Park, E. Vescovo, H.-J. Kim, C. Kwon, R. Ramesh, and T. Venkatesan, Direct evidence for a half-metallic ferromagnet, *Nature* **392**, 794 (1998).

16) Y. Yamada, K. Ueno, T. Fukumura, H. T. Yuan, H. Shimotani, Y. Iwasa, L. Gu, S. Tsukimoto, Y. Ikuhara, and M. Kawasaki, Electrically Induced Ferromagnetism at Room Temperature in Cobalt-Doped Titanium Dioxide, *Science* **332**, 1065 (2011).

17) M. Kitano, S. Kanbara, Y. Inoue, N. Kuganathan, P. V. Sushko, T. Yokoyama, M. Hara, and H. Hosono, Electride support boosts nitrogen dissociation over ruthenium catalyst and shifts the bottleneck in ammonia synthesis, *Nat. Commn.* **6**, 1 (2015).

18) J. Heber, Enter the oxides, *Nature* **459**, 28 (2009).

19) J. G. Bednorz, and K. A. Müller, Possible High T_c Superconductivity in the Ba-La-Cu-O System, *Z. Phys. B* **64**, 189 (1986).

20) A. Ohtomo, D. A. Muller, J. L. Grazul, and H. Y. Hwang, Artificial charge-modulation in atomic-scale perovskite titanate superlattices, *Nature* **419**, 378 (2002).

21) M. Kawasaki, K. Takahashi, T. Maeda, R. Tsuchiya, M. Shinohara, O. Ishiyama, T. Yonezawa, M. Yoshimoto, and H. Koinuma, Atomic Control of the $SrTiO_3$ Crystal Surface, *Science* **266**, 1540 (1994).

22) T. Kamiya, K. Nomura, and H. Hosono, Present status of amorphous In-Ga-Zn-O thin-film transistors, *Sci. Technol. Adv. Mater.* **11**, 044305 (2010).

23) M. Higashiwaki, K. Sasaki, A. Kuramata, T. Masui, and S. Yamakoshi, Development of gallium oxide power devices, *Phys. Stat. Sol. A* **211**, 21 (2014).

24) A. N. Mariano, and R. E. Hanneman, Crystallographic Polarity of ZnO Crystals, *J. Appl. Phys.* **34**, 384 (1963).

25) T. Yamamoto (ed.), *State-of-the-Art Research and Prospective of Zinc Oxide* (CMC shuppan, Tokyo, 2011) p. 1 [in Japanese].

26) H. Nakahata, K. Higaki, A. Hachigo, S. Shikata, N. Fujimori, Y. Takahashi, T. Kajihara, and Y. Yamamoto, High Frequency Surface Acoustic Wave Filter Using ZnO/Diamond/Si Structure, *Jpn. J. Appl. Phys.* **33**, 324 (1994).

27) N. W. Emanetoglu, C. Gorla, Y. Liu, S. Liang, and Y. Lu, Epitaxial ZnO piezoelectric thin films for saw filters, *Mater. Sci. Semicond. Process.* **2**, 247

(1999).

28) C. R. Gorla, N. W. Emanetoglu, S. Liang, W. E. Mayo, Y. Lu, M. Wraback, and H. Shen, Structural, optical, and surface acoustic wave properties of epitaxial ZnO films grown on $(01\bar{1}2)$ sapphire by metalorganic chemical vapor deposition, *J. Appl. Phys.* **85**, 2595 (1999).

29) J. Ye, S. Gu, S. Zhu, T. Chen, L. Hu, F. Qin, R. Zhang, Y. Shi, Y. Zheng, The growth and annealing of single crystalline ZnO films by low-pressure MOCVD, *J. Cryst. Growth* **243**,151 (2002).

30) Ü. Özgür, D. Hofstetter, and H. Morkoç, ZnO Devices and Applications: A Review of Current Status and Future Prospects, *Proc. IEEE* **98**, 1255 (2010).

31) L. Qian, C. Li, M. Li, F. Wang, and B. Yang, Theoretical investigation of surface acoustic wave propagation characteristics in periodic $(AlN/ZnO)_N$/diamond multilayer structures, *Appl. Phys. Lett.* **105**, 183501 (2014),

32) Y. Kozuka, A. Tsukazaki, and M. Kawasaki, Challenges and opportunities of ZnO-related single crystalline heterostructures, *Appl. Phys. Rev.* **1**, 011303 (2014).

33) K. Maeda, M. Sato, I. Niikura, and T. Fukuda, Growth of 2 inch ZnO bulk single crystal by the hydrothermal method, *Semicond. Sci. Tech.* **20**, S49 (2005).

34) S. Akasaka, K. Nakahara, H. Yuji, A. Tsukazaki, A. Ohtomo, and M. Kawasaki, Preparation of an Epitaxy-Ready Surface of a ZnO(0001) Substrate, *Appl. Phys. Express* **4**, 035701 (2011).

35) T. Nakamura, and N. Fujimura, The Difference of Surface Treatment Mothod for ZnO Single Crystals and the Epitaxial Growth Process Occurred by the Difference in the Surface Polarity, *Zairyo* **60**, 983 (2013).

36) D. M. Bagnall, Y. F. Chen, Z. Zhu, T. Yao, M. Y. Shen, and T. Goto, High temperature excitonic stimulated emission from ZnO epitaxial layers, *Appl. Phys. Lett.* **73**, 1038 (1998).

37) B. Gil, D. Felbacq, and S. F. Chichibu, Exciton binding energies in chalcopyrite semiconductors, *Phys. Rev. B* **85**, 075205 (2012).

38) A. Tsukazaki, A. Ohtomo T. Onuma, M. Ohtani, T. Makino, M. Sumiya, K. Ohtani, S. F. Chichibu, S. Fuke, Y. Segawa, H. Ohno, H. Koinuma, and M. Kawasaki, Repeated temperature modulation epitaxy for p-type doping and light-emitting diode based on ZnO, *Nat. Mater.* **4**, 42 (2005).

39) O. Maksimov, Recent advances and novel approaches of p-type doping of zinc oxide, *Rev. Adv. Mater. Sci.* **24**, 26 (2010).

40) K. Nakahara, S. Akasaka, H. Yuji, K. Tamura, T. Fujii, Y. Nishimoto, D. Takamizu, A. Sasaki, T. Tanabe, H. Takasu, H. Amaike, T. Onuma, S. F. Chichibu, A. Tsukazaki, A. Ohtomo, and M. Kawasaki, Nitrogen doped $Mg_xZn_{1-x}O$/ZnO single heterostructure ultraviolet light-emitting diodes on ZnO substrates, *Appl. Phys. Lett.* **97**, 013501 (2010).

41) J. Falson, Y. Kozuka, J. H. Smet, T. Arima, A. Tsukazaki, and M. Kawasaki, Electron scattering times in ZnO based polar heterostructures, *Appl. Phys. Lett.* **107**, 082102 (2015).

42) J. Falson, Y. Kozuka, A. Tsukazaki, and M. Kawasaki, Two-dimensional quantum transport in high-quality ZnO heterointerfaces, *OYO BUTURI* **84**, 984 (2015) [in Japanese].

43) J. D. Albrecht, P. P. Ruden, S. Limpijumnong, W. R. L. Lambrecht, and K. F. Brennan, High field electron transport properties of bulk ZnO, *J. Appl. Phys.* **86**, 6864 (1999).

44) Ü. Özgür, Ya. I. Alivov, C. Liu, A. Teke, M. A. Reshchikov, S. Doğan, V. Avrutin, S.-J. Cho, and H. Morkoç, A comprehensive review of ZnO materials and devices, *J. Appl. Phys.* **98**, 041301 (2005).

45) R. Triboulet, J. Perriere, Epitaxial growth of ZnO films, *Prog. Cryst. Growth Charact.* **47**, 65 (2003).

46) E. Tokumitsu, Correlation between Fermi Level Stabilization Positions and Maximum Free Carrier Concentrations in III-V Compound Semiconductors, *Jpn. J. Appl. Phys.* **29**, L698 (1990).

47) A. Zunger, Practical doping principles, *Appl. Phys. Lett.* **83**, 57 (2003).

48) E.-C. Lee, Y.-S. Kim, Y.-G. Jin, and K. J. Chang, Compensation mechanism for N acceptors in ZnO, *Phys. Rev. B* **64**, 085120 (2001).

49) T. Tamamoto, and H. Katayama-Yoshida, Solution Using a Codoping Method to *Unipolarity* for the Fabrication of p-Type ZnO, *Jpn. J. Appl. Phys.* **38**, L166 (1999).

50) Y. Yan, and S.-H. Wei, Doping asymmetry in wide-bandgap semiconductors: Origins and solutions, *Phys. Stat. Sol. B* **245**, 641 (2008).

51) J. L. Lyons, A. Janotti, and C. G. Van de Walle, Why nitrogen cannot lead to p-type conductivity in ZnO, *Appl. Phys. Lett.* **95**, 252105 (2009).

52) J. C. Fan, K. M. Sreekanth, Z. Xie, S. L. Chang, and K. V. Rao, p-Type ZnO materials: Theory, growth, properties and devices, *Prog. Mater. Sci.* **58**, 874 (2013).

53) J. L. Lyons, A. Janotti, and C. G. Van de Walle, Effects of hole localization on

limiting p-type conductivity in oxide and nitride semiconductors, *J. Appl. Phys.* **115**, 012014 (2014).

54) M. C. Tarun, M. Z. Iqbal, and M. D. McCluskey, Nitrogen is a deep acceptor in ZnO, *AIP Advances* **1**, 022105 (2011).

55) S. Fujita, Wide-bandgap semiconductor materials: For their full bloom, *Jpn. J. Appl. Phys.* **54**, 030101 (2015).

56) A. Janotti, and C. G. Van de Walle, Native point defects in ZnO, *Phys. Rev. B* **76**, 165202 (2007).

57) T. Yao, Growth of p-type ZnO, *OYO BUTURI* **82**, 852 (2013) [in Japanese].

58) M. A. L. Johnson, S. Fujita, W. H. Rowland, Jr., W. C. Hughes, J. W. Cook, Jr., and J. F. Schetzina, MBE growth and properties of ZnO on sapphire and SiC substrates, *J. Electron. Mater.* **25**, 855 (1996).

59) T. Kawaharamura, H. Nishinaka, and S. Fujita, Growth of Crystalline Zinc Oxide Thin Films by Fine-Channel-Mist Chemical Vapor Deposition, *Jpn. J. Appl. Phys.* **47**, 4669 (2008).

60) K. Kaneko, T. Nomura, I. Kakeya, and S. Fujita, Fabrication of Highly Crystalline Corundum-Structured α-$(Ga_{1-x}Fe_x)_2O_3$ Alloy Thin Films on Sapphire Substrates, *Appl. Phys. Express* **2**, 075501 (2009).

61) H. Tanoue, T. Taniguchi, S. Wada, S. Yamamoto, S. Nakamura, Y. Naka, H. Yoshikawa, M. Munekata, S. Nagaoka, and Y. Nakamura, Uniform ZnO epitaxial films formed at atmospheric pressure by high-speed rotation-type mist chemical vapor deposition, *Appl. Phys. Express* **8**, 125502 (2015).

62) M. Iwasaki, H. Inui, Y. Matsudaira, H. Kano, N. Yoshida, M. Ito, and M. Hori, Nonequilibrium atmospheric pressure plasma with ultrahigh electron density and high performance for glass surface cleaning, *Appl. Phys. Lett.* **92**, 081503 (2008).

63) D. Merche, N. Vandencasteele, and F. Reniers, Atmospheric plasmas for thin film deposition: A critical review, *Thin Soild Films* **520**, 4219 (2012).

64) S. Kanazawa, M. Kogoma, T. Moriwaki, and S. Okazaki, Stable glow plasma at atmospheric pressure, *J. Phys. D: Appl. Phys.* **21**, 838 (1988).

65) H. Kakiuchi, H. Ohmi, and K. Yasutake, Atmospheric-pressure low-temperature plasma processes for thin film deposition, *J. Vac. Sci. Tech.* A, **32**, 030801 (2014).

66) H. Tanaka, M. Mizuno, K. Ishikawa, K. Nakamura, H. Kajiyama, H. Kano, F. Kikkawa, and M. Hori, Plasma-Activated Medium Selectively Kills Glioblastoma Brain Tumor Cells by Down-Regulating a Survival Signaling Molecule, AKT

Kinase, *Plasma Medicine* **1**, 265 (2011).
67) S. Iseki, K. Nakamura, M. Hayashi, H. Tanaka, H. Kondo, H. Kajiyama, H. Kano, F. Kikkawa, and M. Hori, Selective killing of ovarian cancer cells through induction of apoptosis by nonequilibrium atmospheric pressure plasma, *Appl. Phys. Lett.* **100**, 113702 (2012).
68) W. J. Nuttall, R. H. Clarke, and B. A. Glowacki, Stop squandering helium, *Nature* **485**, 573 (2012).
69) S. Okazaki, M. Kogoma, M. Uehara, and Y. Kimura, Appearance of stable glow discharge in air, argon, oxygen and nitrogen at atmospheric pressure using a 50 Hz source, *J. Phys. D: Appl. Phys.* **26**, 889 (1993).
70) M. Yuasa, and T. Yara, *Japan Patent* 3040358 (1997).
71) M. Yuasa, Application of Mass Production for Electric Devices Using Atmospheric Pressure Plasma, *Hyomen Gijutsu* **60**, 390 (2009) [in Japanese].
72) R. Hayakawa, Dr. Thesis, Novel Nitridation Technique Using Atmospheric Pressure Plasma –Formation Mechanism of Ultrathin Silicon Nitride Film and the Dielectric Property–, Faculty of engineering, Osaka Prefecture University, Osaka, 2006.
73) Y. Suzaki, S. Ejima, T. Shikama, S. Azuma, O. Tanaka, T. Kajitani, and H. Koinuma, Deposition of ZnO film using an open-air cold plasma generator, *Thin Solid Films* **506-507**, 155 (2006).
74) M. D. Barankin, E. Gonzalez II, A. M. Ladwig, and R. F. Hicks, Plasma-enhanced chemical vapor deposition of zinc oxide at atmospheric pressure and low temperature, *Sol. Energy Mater. Sol. Cells* **91**, 924 (2007).
75) Y. Ito, O. Sakai, and K. Tachibana, Study of plasma enhanced chemical vapor deposition of ZnO films by non-thermal plasma jet at atmospheric pressure, *Thin Solid Films* **518**, 3513 (2010).
76) Y. Suzaki, A. Kawaguchi, T. Murase, T. Yuji, T. Shikama, D.-B. Shin, and Y.-K. Kim, Effect of substrate temperature on ZnO thin film fabrication by using an atmospheric pressure cold plasma generator, *Phys. Status Solidi C* **8**, 503 (2011).
77) Y. Nose, T. Yoshimura, A. Ashida, T. Uehara, and N. Fujimura, Low temperature growth of ZnO thin films by non-equilibrium atmospheric pressure N_2/O_2 plasma and the growth morphology of the films, *Zairyo* **61**, 756 (2012) [in Japanese].
78) Y. Nose, T. Nakamura, T. Yoshimura, A. Ashida, T. Uehara, and N. Fujimura, Orientation Control of ZnO Films Deposited Using Nonequilibrium Atmospheric Pressure N_2/O_2 Plasma, *Jpn. J. Appl. Phys.* **52**, 01AC03 (2013).

79) A. Lofthus and P. H. Krupenie, The spectrum of molecular nitrogen, *J. Phys. Chem. Ref. Data* **6**, 113 (1977).

80) Y. Horikawa, T. Hayashi, and K. Sasaki, Lifetime of Molecular Nitrogen at Metastable $A^3\Sigma_u^+$ State in Afterglow of Inductively-Coupled Nitrogen Plasma, *Jpn. J. Appl. Phys.* **51**, 126301 (2012).

Chapter 2: Development of chemical vapor deposition system using nonequilibrium N_2/O_2 plasma generated near atmospheric pressure

2-1 Introduction

Nonequilibrium plasma have played indispensable role in the manufacturing process of electronic devices such as cleaning, deposition, etching, ashing and surface modification etc.[1] Regarding the crystal growth technique, sputtering [2] has been widely used for the deposition because of their advantage of the capability of wide and uniform deposition. However, the electronics industry is now looking to fabricate structures on a larger scale, and would prefer to use flexible substrates that would have a lower profile and lighter weight and be more rugged than silicon substrates.[3-5] Their use would also offer manufacturers the potential for continuous, high-throughput printing on large rolls rather than batch processing using small 12” wafers. To realize the economical huge size deposition such as a roll-to-roll processing, low-temperature CVD operated at near atmospheric pressure (AP) is studied.[6-8] In particular, AP plasma-enhanced CVD has an advantage for the low-temperature growth of ZnO films. Regarding the AP plasma enhanced CVD of ZnO films, although a few reports exist,[9-12] their processes require the use of expensive rare gas (He) as a dilution gas to maintain arcless, nonequilibrium, stable discharge near AP. From the industrial point of view, He-less processes are desirable. Therefore, we have focused on the stabilization of N_2-based plasma near AP,[13] and applied to the CVD process of ZnO films.

In this chapter, at first, basic concepts of developed CVD system using direct plasma are explained including Zn source materials. Using this system, low temperature formation of ZnO films around 200 ºC is demonstrated using O_2-based direct plasma generated near AP. Secondly, the growth process of ZnO films is evaluated from macroscopic viewpoint. Finally, potential application for low-temperature growth of ZnO is discussed.

2-2 Experimental

2-2-1 Source materials for CVD

In case of CVD, the choice of source material is one of the most important criteria, because the growth rate, crystal quality, impurity incorporation etc. are directly affected by the selection. Their purity, safety, toxicity, reactivity and vapor pressure must be comprehensively taken into account. Among various CVD source materials, metal organic (MO) compounds including metal-alkyl bond and metal organic complexes such as β-diketonate have been widely used. MO has long been used for the MOCVD of GaAs [14] or GaN [15-17] and their family alloys since the early stage of MOCVD.[18,19] Since the development of atomic layer deposition, trimethylaluminum (TMAl) has been widely used in the formation of AlO_x dielectric or passivation layer and the reaction scheme with water (H_2O) has been studied deeply.[20] Although the MO precursors have excellent purity and property, most of them have a spontaneous combustibility, which requires utmost attention to the sealing of system and the treatment of the waste gases.[19] The latter has a relatively short history, however, complexes with moderately high vapor pressure suitable for CVD are able to synthesize even for a variety of transition metals.[20,21] Therefore, these complexes have been used in the deposition of high-k dielectric,[22] ferroelectrics,[23] superconductor [24] etc.

Regarding the CVD of ZnO films, MO compounds: diethyl zinc (DEZn) and dimethyl zinc (DMZn) has been the most popular source materials.[25] They have also been used as acceptor dopant source in GaAs films.[26] However, these materials have an explosive reactivity with oxidants such as O_2 and H_2O, which result in the premature reaction before arriving at the substrate.[25,27] To avoid this problem, some researchers proposed separate injection of DEZn and oxidant [25,28,29] or use of less-reactive oxidants such as CO_2,[29] NO_x,[30-33] ketone [33] and alcohol [33-35] and so on.

The use of solid β-diketonate complexes is examined for the growth of ZnO.[36,37] In case of thermal CVD from β-diketonate and O_2, a relatively high growth temperature above 300 ºC is required due to its thermal stability.[38]

In this thesis, metal organic compound: Diethyl zinc [$Zn(C_2H_5)_2$ (Tri Chemical Laboratories Inc.) denoted as DEZn] [27] and β-diketonate complexes: Bis-2,4octanedionato zinc [$Zn(C_8H_{13}O_2)_2$ (Adeka Corp.) denoted as $Zn(OD)_2$] [12] were selected as source materials of Zn.

The chemical structural formulas and the vapor pressure curves for these Zn source materials are shown in **Fig. 2-1** and **Fig. 2-2**, respectively. Vapor pressure curves of dimethyl zinc (DMZn) and other liquid β-diketonate complexes (Zn-MOPD,[10] Zn-TD) are also written in dashed lines. In general, vapor pressure required for CVD is around 100 mTorr – 1 Torr, which is easily obtained for DEZn even around room temperature. Therefore DEZn is supplied by bubbling method in this study. Detail explanation on DEZn will be presented in chapter 6. Although the vapor pressure of $Zn(OD)_2$ is rather smaller than that of DEZn, this material is suitable for the constant supply using vaporizer, because it is liquid at room temperature and at ambient pressure.[12] The handling is easier than DEZn due to the stability, which is desirable for the growth near AP sometimes in open (chamber-less) system. From chapter 2 to 5, the results using $Zn(OD)_2$ is discussed.

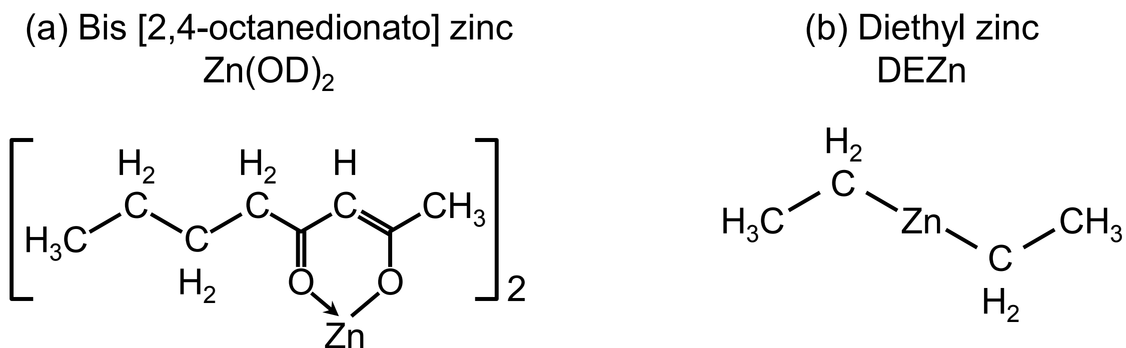

Fig. 2-1. Chemical structural formula of organic Zn source materials used in this study: Bis [2,4-octanedionato] zinc [$Zn(C_8H_{13}O_2)_2$ denoted as $Zn(OD)_2$] **(a)** [12] and Diethyl zinc [$Zn(C_2H_5)_2$ denoted as DEZn] **(b)**.

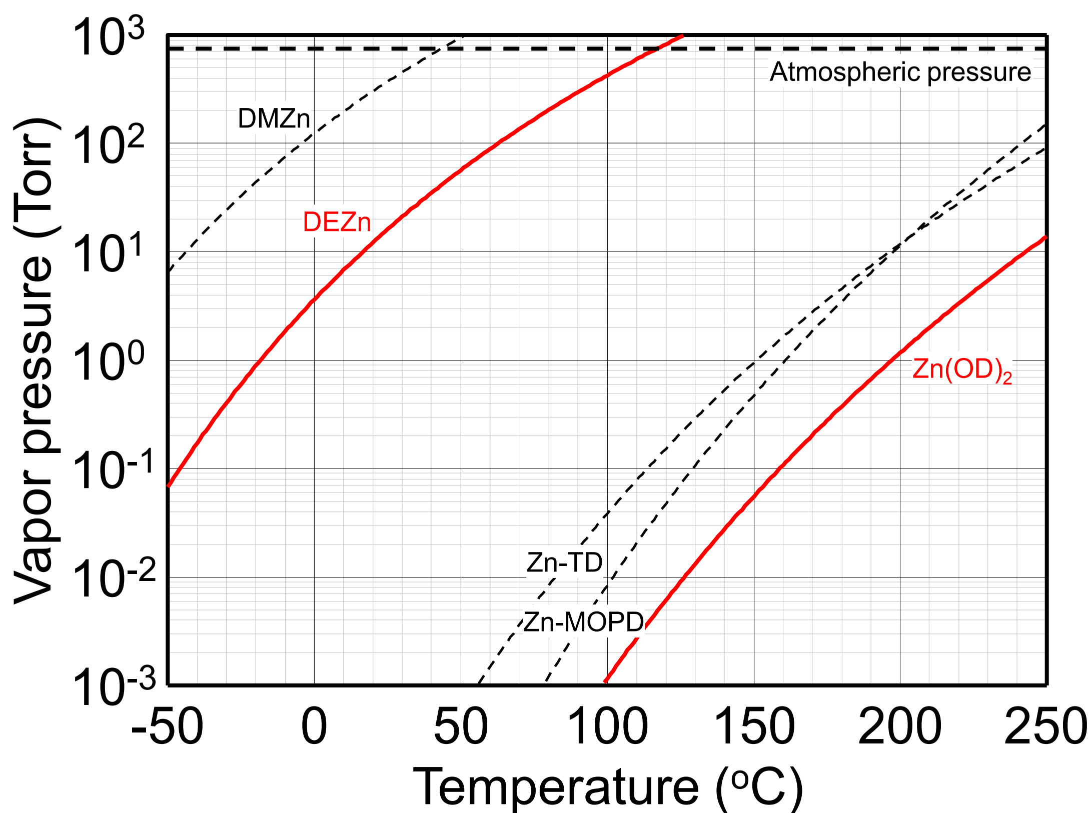

Fig. 2-2. Vapor pressure curves for various organic Zn source materials calculated from Clausius-Clapeyron equation. Those for $Zn(OD)_2$ and DEZn are written in red solid lines.

2-2-2 CVD system using N_2/O_2 direct plasma generated near atmospheric pressure

A schematic illustration of CVD system is illustrated in **Fig. 2-3 (a)**. Bis-2,4octanedionato zinc [$Zn(C_8H_{13}O_2)_2$ (Adeka Corp.) denoted as $Zn(OD)_2$] is stored in a stainless cylinder with two different length tubes. The liquid surface of $Zn(OD)_2$ is statically pushed by He of 0.4 MPa from shorter tube to transport it through longer dip tube as liquid state. The flow rate of $Zn(OD)_2$ is controlled at 0.01 g/min by liquid mass flow controller (LMFC). $Zn(OD)_2$ is splashed by the irradiation of surrounding N_2 gas (denoted as Top gas) of 1 slm (standard liter per minute) to ease its vaporization, vaporized by thermal vaporizer maintained at 190 °C and transported by preheated N_2 gas (denoted as Carrier gas) of 3 slm. Net N_2 gas of 4 slm is reduced to 20 - 100 ml/min ($F_{Carrier}$) by vent line, and the reduced one is mixed with additional N_2 and O_2 (F_{O2}) controlled by mass flow controller (MFC). The mixed gases are introduced into plasma. Most of the gas lines are heated at 190 - 230 °C by ribbon heaters and temperature controllers so as not to condensate the vaporized $Zn(OD)_2$. O_2-based Nonequilibrium N_2/O_2 plasma is generated between two parallel plate electrode separated by uniform gap of 1.1 mm and covered with dielectric aluminum nitride (AlN) based on dielectric barrier discharge as shown in **Fig. 2-3 (b)**. The thicknesses of AlN dielectric plates are 0.8 mm (Top electrode side) and 0.9 mm (Bottom electrode side). Applied alternating voltage and frequency are 6.0 – 6.7 kV (peak-to-peak) and 180 kHz (close to resonance frequency), respectively. The typical discharge current is around 200 mA.

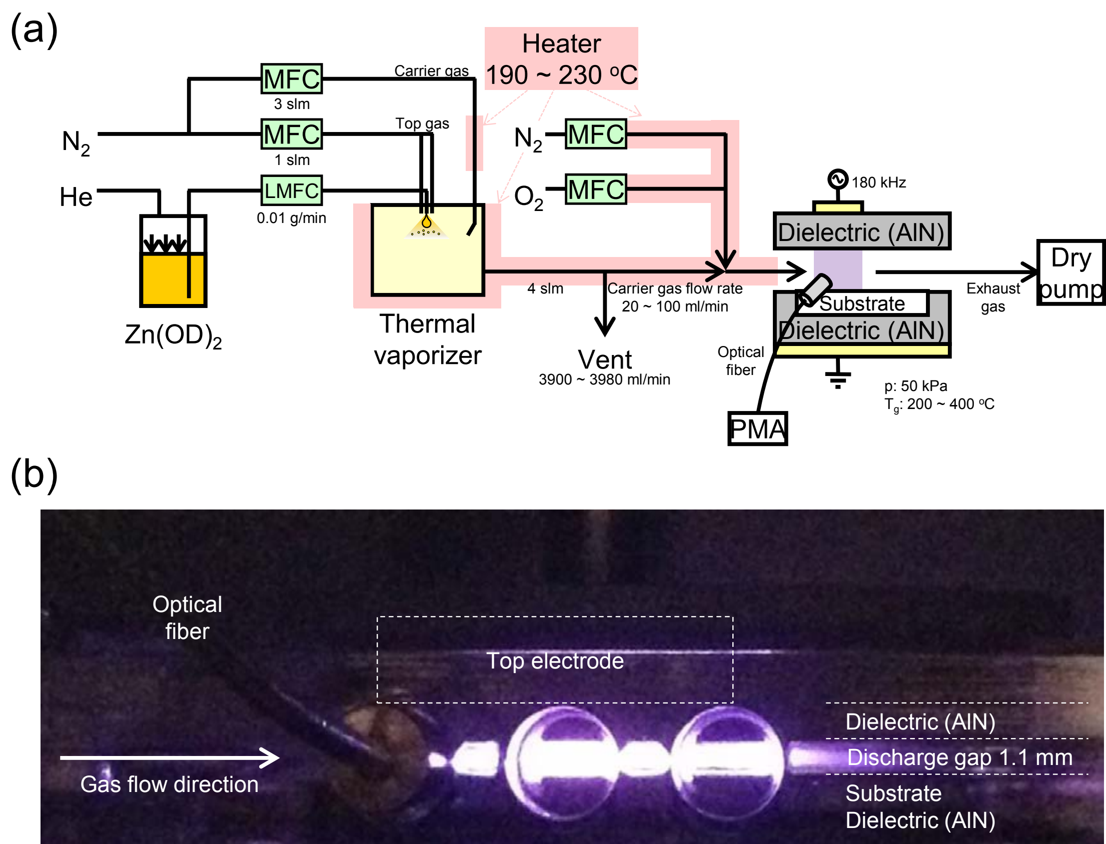

Fig. 2-3. A schematic illustration of CVD system using N_2/O_2 direct plasma generated near atmospheric pressure for the deposition of ZnO films **(a)** and a photograph of the discharging region taken from cross-sectional direction. **(b)** Although the plasma seems to be discontinuous along the gas glow direction, this is due to the holes on the side of quartz susceptor to fix the edge of optical fiber adjacent to the direct plasma.

ZnO films are grown on glass (Borosilicate glass, D263, 25×25×0.5*t*, Matsunami Glass Ind., Ltd.) or sapphire (0001) substrate (One-side polished, 10×10×0.33*t*, Shinkosha Co., Ltd.) mounted in the plasma so called direct configuration. The growth pressure and the growth temperature (T_g) are 50 kPa and 200 - 400 °C, respectively. During the growth, the total pressure is kept constant by adjusting a needle valve located at the exhaust gas line. In order to investigate excited species in the plasma, optical emission of the plasma is guided into photonic multichannel spectral analyzer (PMA-C7473, Hamamatsu Photonics) with the wavelength resolution of < 2 nm. Quartz optical fiber is attached adjacent to the plasma to analyze the excited species just above the deposition area. Detail information on the CVD system is reported elsewhere.[39)]

2-2-3 Film characterization

After CVD, deposited films were characterized by several methods. The crystal structure was investigated by X-ray diffraction (XRD: X'pert MRD, Philips) using Cu-Kα radiation. The optical configuration of XRD is 2θ-ω. Optical transmittance, optical bandgap and thickness of the deposited films were simultaneously obtained using a UV-vis spectrophotometer (V-650, JASCO) assuming that the refractive index of ZnO in range of UV-vis is 1.95. For some samples, film thickness was measured using a field-emission-type scanning electron microscope (FE-SEM; S-4500, Hitachi Co Ltd) in cross-sectional view after cleaving the sample parallel to the gas flow direction.

2-3 Results and discussions

2-3-1 Analysis of plasma by optical emission spectroscopy

The growth conditions of ZnO films are summarized in **Table 2-1**. In order to get information on the excited species in the plasma, optical emission spectroscopy (OES) was carried out at first. **Fig. 2-4** shows OE spectrum of the O_2-based plasma generated at the O_2% of 90%. Weak OEs corresponding to N_2 second positive system (N_2 2ps: $C^3\Pi_u^+ \longrightarrow B^3\Pi_u^+$) are observed at the wavelengths ranging from 300 to 450 nm. Although N_2 2ps is reported to be the strongest OE lines in nonequilibrium N_2 plasma generated near AP,[40] the intensity is suppressed in O_2-based N_2/O_2 plasma. On the other hand, OE lines attributed to atomic oxygen (Atomic O^*) are predominantly observed at the wavelengths of 777 nm ($3p^5P \rightarrow 3s^5S$), 843 nm ($3p^3P \rightarrow 3s^3S$), and 927 nm ($3d^5D \rightarrow 3p^5P$), which are often observed in O_2 plasma generated at low pressure.[41,42] The OE intensity of Atomic O^* with introducing $Zn(OD)_2$ (during deposition) was 30 – 70% weaker than that of without introducing $Zn(OD)_2$, suggesting that the active Atomic O* contribute to the decomposition of $Zn(OD)_2$ and subsequent oxidation of ZnO similar to low pressure plasma processes of oxide films.[43,44] The growth of ZnO films were performed using this plasma.

Table. 2-1. Typical growth condition of ZnO films by O_2-based N_2/O_2 direct plasma generated near atmospheric pressure.

Vaporizer temperature T_V	190 °C
Vaporizer pressure p_V	100 kPa
O_2 flow rate F_{O2}	550 sccm
Carrie gas flow rate $F_{Carrier}$	60 sccm
Gas flow velocity v	0.7 m/s
Growth pressure p	50 kPa
Growth temperature T_g	200 °C
AC voltage V_{pp}	6.0 kV (Peak to peak)
AC frequency f	180 kHz

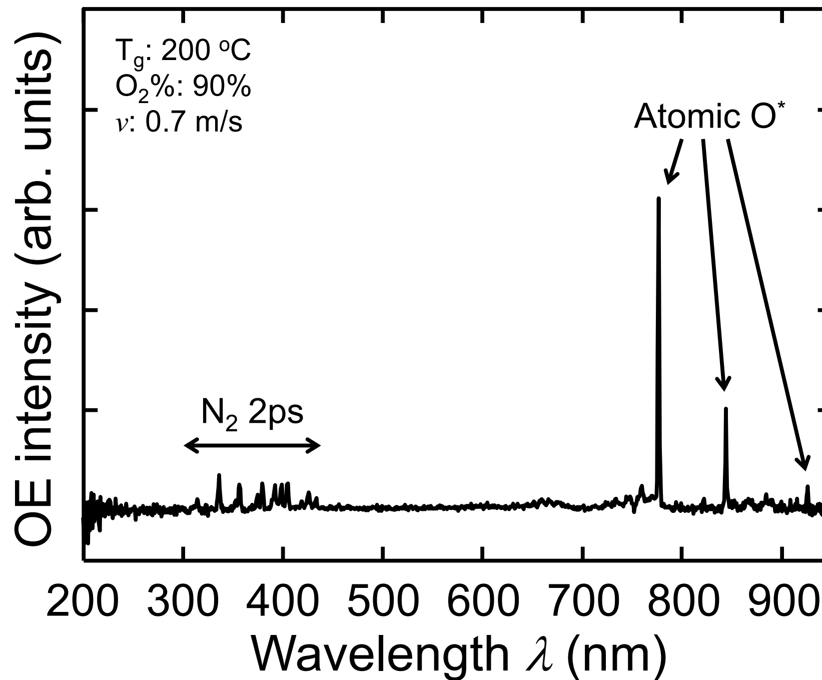

Fig. 2-4. OE spectrum of the N_2/O_2 plasma generated at the O_2% of 90%.

2-3-2 Characterization of ZnO films

Fig. 2-5 shows XRD profile of the deposited film taken by the optical configuration of 2θ-ω. Strong 0002 and relatively weak $10\bar{1}1$ diffractions of ZnO are clearly observed without any secondary phase, indicating that (0001)-oriented ZnO film is successfully obtained on a glass substrate at the T_g of as low as 200 °C.

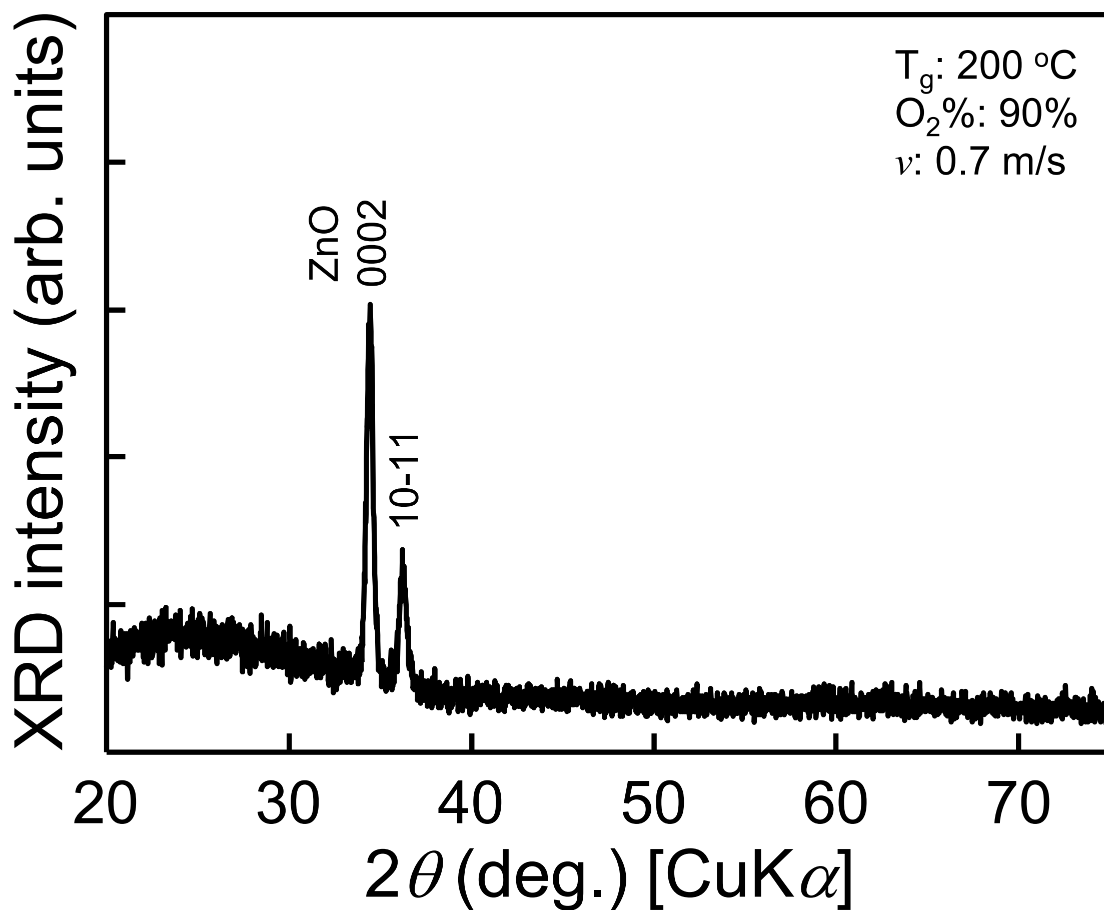

Fig. 2-5. 2θ-ω scanned XRD profile of the sample grown at the substrate temperature and O_2% of 200 ºC and 90%, respectively.

Fig. 2-6 shows optical transmittance spectrum of ZnO film shown in **Fig. 2-5**. ZnO film show high transmittance above 90% in visible region with no noticeable in-gap absorption and sharp basic absorption edge. The direct optical bandgap was calculated to be 3.31 eV from Tauc plot derived from this spectrum,[45] which is close to the bandgap of ZnO at room temperature.[46,47] The film thickness was also determined to be approximately 300 nm from the oscillation period assuming that the refractive index of ZnO in visible region of 1.95, which corresponds to the growth rate of 10 nm/min.

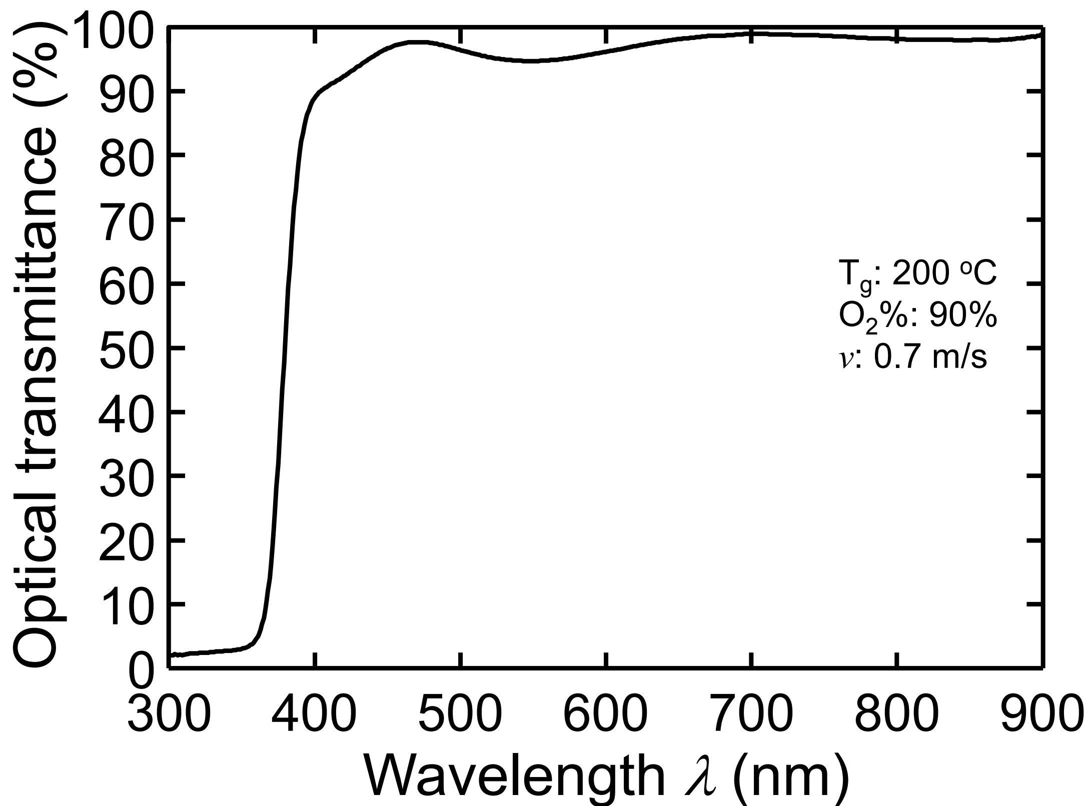

Fig. 2-6. Optical transmittance spectrum of ZnO film grown at the substrate temperature and O_2% of 200 ºC and 90%, respectively.

2-3-3 Position dependence of growth rate

In general, substrate is rotated during CVD to improve the uniformity of film thickness. However, thickness distribution without substrate rotation gives important information on the reaction process of source materials along gas flow direction. **Fig. 2-7** shows photograph of the plasma **(a)**, cross-section of horizontal reactor **(b)** and thickness distribution along the gas flow direction **(c)**. Although the plasma in **Fig. 2-7 (a)** seems to be discontinuous along the gas glow direction, that is due to the holes on the quartz susceptor to fix the edge of optical fiber adjacent to the direct plasma. Note that the lateral position $x = 0$ mm in **Fig. 2-7 (b)** and **(c)** corresponds to the upstream edge of the "top electrode", where high voltage is applied. At the lateral position $x < -2$ mm, plasma is not observed due to the low electric field at this section. In this section, the growth of ZnO is not recognized at all despite the precursor concentration itself should be the highest in all region. This result indicates the important finding that we cannot deposit ZnO films at 200 °C by thermal CVD process (without plasma), and ZnO films are grown by the contribution of excited species in the O_2-based N_2/O_2 plasma at 200 °C. At the lateral position of $-2 \leq x < -1$, the growth of ZnO suddenly starts and the film thickness reaches to the maximum despite the plasma density should be lower than that of $x \geq 0$. On the other hand, the film thickness recovers at $-1 \leq x < 0$ probably due to the increase of plasma density in this region, and becomes almost constant at $0 \leq x < 1.5$ and then monotonically decreases at $x \geq 1.5$ due to the decrease of precursor concentration. CVD processes using horizontal reactor as in our case, film thickness distribution along the gas flow direction should have a single peak at the most upstream region, and then monotonically decrease against the increase of lateral

position x, due to the decrease of precursor concentration along the gas flow.[48,49] In our case, however, that has two peaks. This finding suggest that the growth mechanism at the left side ($x < 0$) of boundary position ($x = 0$) is different from the right side ($x > 0$). In the following discussion (from chapter 2 to 5), we focus on the result of $x > 0$, where the CVD process is certainly performed by the excited species in "direct" plasma.

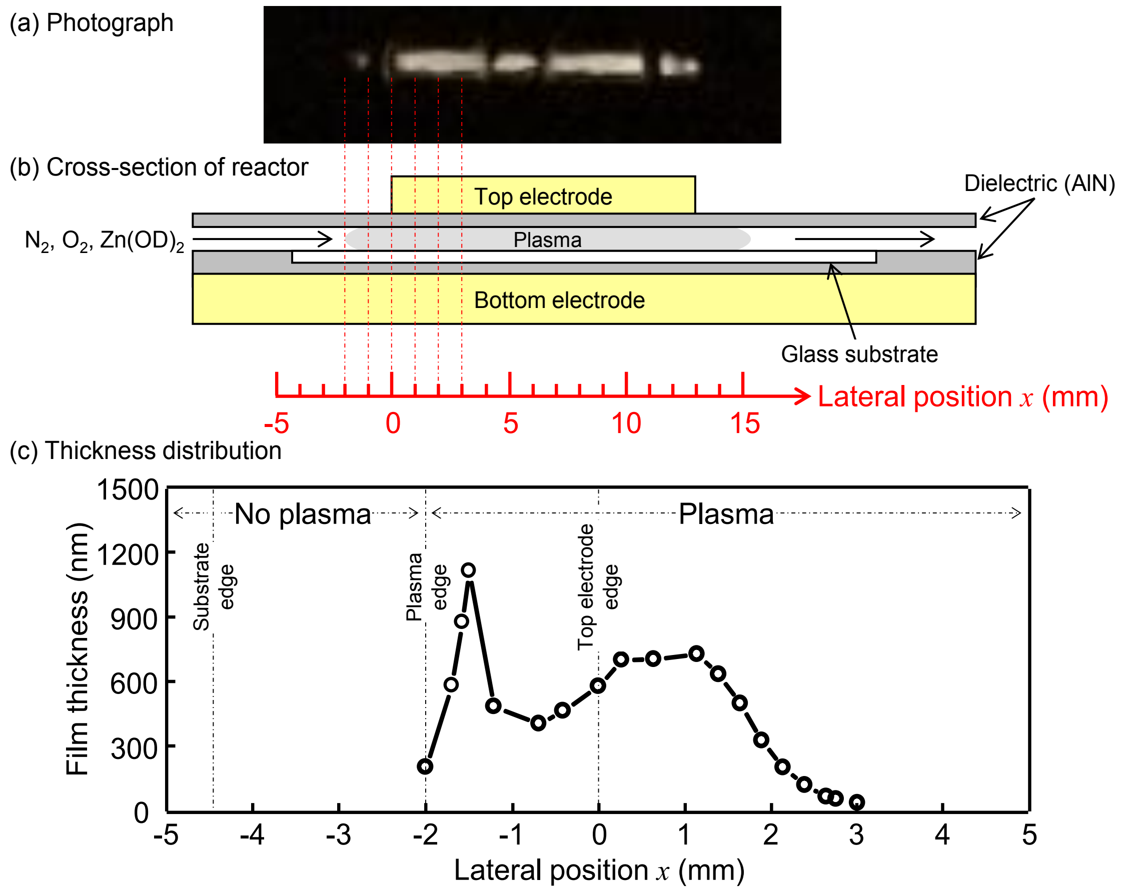

Fig. 2-7. Photograph of the O_2-based N_2/O_2 plasma generated near AP taken from the cross sectional direction **(a)**, schematic illustration of the reactor **(b)** and the distribution of film thickness **(c)**.

2-3-4 Analysis of the limiting factor of CVD

In general, CVD growth can be described by chemical reaction formula. In case of $Zn(OD)_2$ and O_2, following formula can be described after taking the constant into account:

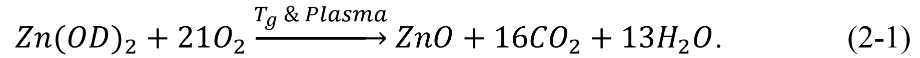

$$Zn(OD)_2 + 21O_2 \xrightarrow{T_g\ \&\ Plasma} ZnO + 16CO_2 + 13H_2O. \qquad (2\text{-}1)$$

According to this equation, the limiting factor of the CVD of ZnO films can be estimated from the change of the growth rate of ZnO films against the change of the flow rate of source gases ($F_{Carrier}$, F_{O2}) or the driving force of chemical reaction (T_g) in eq. (2-1).

In order to estimate the macroscopic growth mechanisms of ZnO films from the viewpoint of limiting factor, $F_{Carrier}$, F_{O2} and T_g were varied as summarized in **Table 2-2**. **Fig. 2-8** shows $F_{Carrier}$ **(a)**, F_{O2} **(b)** and T_g **(c)** dependence of the growth rate of ZnO films. Note that the film thickness is measured at $0 < x < 1.5$, where the films are certainly grown by direct plasma. The growth rate of ZnO films is almost proportional to the $F_{Carrier}$ at constant F_{O2} and T_g (a), while that is insensitive to the change of F_{O2} at constant $F_{Carrier}$ and T_g (b). That is not increase with increasing the T_g at every F_{O2} (c). These results indicate that the growth of ZnO is supply limited in this experimental condition, which is an ideal state for industrial device fabrication by CVD.[50,51)]

Table. 2-2. Summary of the growth condition of ZnO films discussed in **Fig. 2-8**.

Vaporizer temperature T_V	190 °C
Vaporizer pressure p_V	100 kPa
O_2 flow rate F_{O2}	50 ~ 550 sccm
Carrie gas flow rate $F_{Carrier}$	30 ~ 100 sccm
Gas flow velocity v	0.7 m/s
Growth pressure p	50 kPa
Growth temperature T_g	200 ~ 400 °C
AC voltage V_{pp}	6.0 kV (Peak to peak)
AC frequency f	180 kHz
Substrate	Glass, Sapphire (0001)

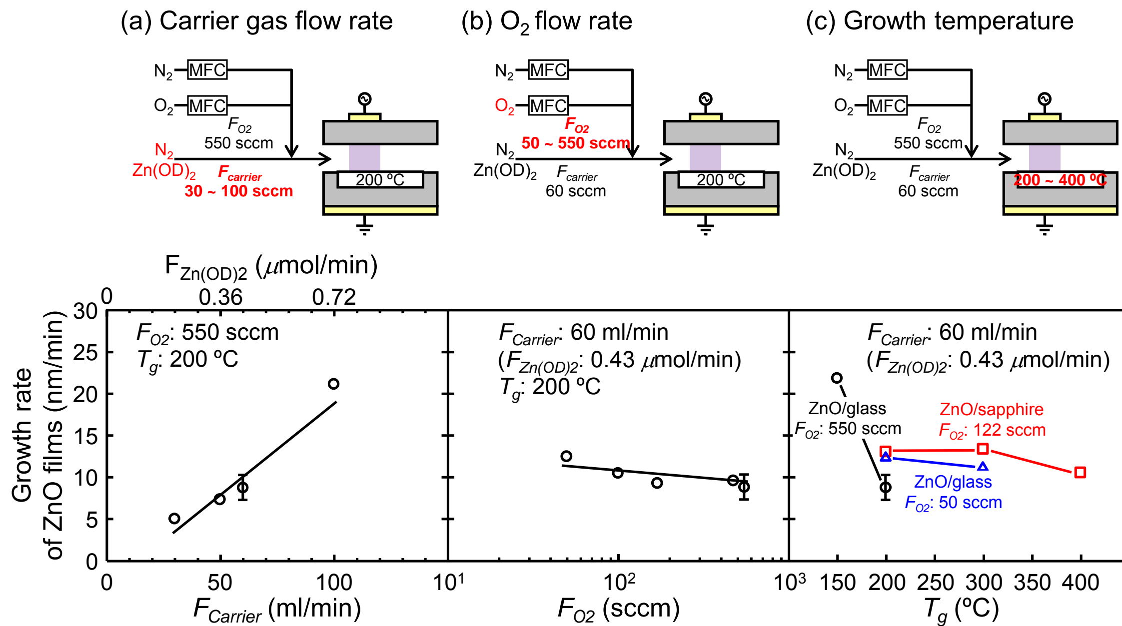

Fig. 2-8. Change of the growth rate of ZnO films against the change of $F_{Carrier}$ **(a)**, F_{O2} **(b)** and T_g **(c)**. Flow rate of each gases are written in the schematics of CVD system. Error bars indicate the maximum and minimum growth rate in three different samples deposited at the same condition.

2-4 Conclusions

The chemical vapor deposition system using non-equilibrium N_2/O_2 plasma was developed for the low temperature growth of ZnO films. As Zn source material, β-diketonate complexes: Bis-2,4octanedionato zinc [$Zn(C_8H_{13}O_2)_2$ (Adeka Corp.) denoted as $Zn(OD)_2$] was selected which is free from spontaneous combustibility. By introducing vaporized $Zn(OD)_2$ into O_2-based N_2/O_2 plasma generated near AP, ZnO films was successfully obtained on glass substrates at the substrate temperature of as low as 200 °C without using He dilution of mixed gases. From XRD measurement, it was found that the film was well crystallized with (0001) preferred orientation. The film also showed high transmittance above 90% in visible region and sharp absorption edge at 3.31 eV corresponding to the optical band-gap of ZnO. The film thickness distribution profile showed two thickness peaks located at remote and direct position. According to the chemical reaction formula, the growth rate of ZnO films at the direct position were evaluated and found that the growth of ZnO films is limited by Zn supply, which is an ideal state of CVD. Considering the fact that ZnO films were not grown by thermal CVD around this temperature, our plasma is effective for the low temperature formation of ZnO films near AP.

References

1) Y. Ichikawa, T. Sasaki, and S. Teii, *Purazuma handōta purosesu kōga u: Seimaku to etchingu nyū on* (Uchidarokakuho shuppan, Tokyo, 2003) p. 1 [in Japanese].
2) K. Ellmer, Magnetron sputtering of transparent conductive zinc oxide: relation between the sputtering parameters and the electronic properties, *J. Phys. D: Appl. Phys.* **33**, R17 (2000).
3) S. U. Lee, J.-H. Boo, and B. Hong, Structural, Electrical, and Optical Properties of SnO_2:Sb Films Prepared on Flexible Substrate at Room Temperature, *Jpn. J. Appl. Phys.* **50** (2011) 01AB10.
4) M. Kasuya, S. Yasui, and M. Noda, Deposition of SiO_2 Thin Films on Polycarbonate by Atmospheric-Pressure Plasma, *Jpn. J. Appl. Phys.* **51** (2012) 01AC01.
5) Y.-S. Lin, and J.-Y. Lai, Low Temperature Plasma Enhanced Chemical Vapor Deposition-Synthesized Electrochromic MoO_xC_y Thin Films for Flexible Electrochromic Devices, *Jpn. J. Appl. Phys.* **51**, 01AC03 (2012).
6) K. Haga, F. Katahira, and H. Watanabe, Preparation of ZnO films by atmospheric pressure chemical-vapor deposition using zinc acetylacetonate and ozone, *Thin Solid Films* **343-344**, 145 (1999).
7) J. Nishino and Y. Nosaka, Preparation of ZnO by a nearby vaporizing chemical vapor deposition method, *J. Mater. Res.* **18**, 2029 (2003).
8) J. G. Lu, T. Kawaharamura, H. Nishinaka, Y. Kamada, T. Ohshima, and S. Fujita, ZnO-based thin films synthesized by atmospheric pressure mist chemical vapor deposition, *J. Cryst. Growth* **299**, 1 (2007).
9) Y. Suzaki, S. Ejima, T. Shikama, S. Azuma, O. Tanaka, T. Kajitani, and H. Koinuma, Deposition of ZnO film using an open-air cold plasma generator, *Thin Solid Films* **506-507**, 155 (2006).
10) Y. Suzaki, A. Kawaguchi, T. Murase, T. Yuji, T. Shikama, D.-B. Shin, and Y.-K. Kim, Effect of substrate temperature on ZnO thin film fabrication by using an atmospheric pressure cold plasma generator, *Phys. Status Solidi C* **8**, 503 (2011).
11) M. D. Barankin, E. Gonzalez II, A. M. Ladwig, and R. F. Hicks, Plasma-enhanced chemical vapor deposition of zinc oxide at atmospheric pressure and low temperature, *Sol. Energy Mater. Sol. Cells* **91**, 924 (2007).

12) Y. Ito, O. Sakai, and K. Tachibana, Study of plasma enhanced chemical vapor deposition of ZnO films by non-thermal plasma jet at atmospheric pressure, *Thin Solid Films* **518**, 3513 (2010).
13) M. Yuasa, and T. Yara, *Japan Patent* 3040358 (2000).
14) D. H. Reep, and S. K. Ghandi, Deposition of GaAs Epitaxial Layers by Organometallic CVD, *J. Electrochem. Soc.* **130**, 675 (1983).
15) H. Amano, N. Sawaki, I. Akasaki, and Y. Toyoda, Metalorganic vapor phase epitaxial growth of a high quality GaN film using an AlN buffer layer, *Appl. Phys. Lett.* **48**, 353 (1986).
16) S. Nakamura, Y. Harada, and M. Seno, Novel metalorganic chemical vapor deposition system for GaN growth, *Appl. Phys. Lett.* **58**, 2021 (1991).
17) J. R. Creighton, W. G. Breiland, M. E. Coltrin, and R. P. Pawlowski, Gas-phase nanoparticle formation during AlGaN metalorganic vapor phase epitaxy, *Appl. Phys. Lett.* **81**, 2626 (2002).
18) H. M. Manasevit, Single-crystal Gallium Arsenide on Insulating Substrates, *Appl. Phys. Lett.* **12**, 156 (1968).
19) K. L. Choy, Chemical vapour deposition of coatings, *Prog. Mater. Sci.* **48**, 57 (2003).
20) Riikka L. Puurunen, Surface chemistry of atomic layer deposition: A case study for the trimethylaluminum/water process, *J. Appl. Phys.* **97**, 121301 (2005).
21) M. Leskelä, and M. Ritala, Atomic layer deposition (ALD): from precursors to thin film structures, *Thin Solid Films* **409**, 138 (2002).
22) Richard W. Johnson, Adam Hultqvist, and Stacey F. Bent, A brief review of atomic layer deposition: From fundamentals to applications, *Mater. Today* **17**, 236 (2014).
23) A. C. Jones, Molecular design of improved precursors for the MOCVD of electroceramic oxides, *J. Mater. Chem.* **12**, 2576 (2002).
24) T. Sugimoto, M. Yoshida, K. Yamaguchi, Y. Yamada, K. Sugawara, Y. Shinohara, and S. Tanaka, Fabrication and characterization of Bi-Sr-Ca-Cu-O MOCVD thin films, *J. Cryst. Growth* **107**, 692 (1991).
25) R. Triboulet, J. Perriere, Epitaxial growth of ZnO films, *Prog. Cryst. Growth Charact.* **47**, 65 (2003).
26) T. Lin, L. Jiang, X. Wei, G. H. Wang, G. Z. Zhang, and X. Y. Ma, Growth of heavily Zn-doped InGaAs at low temperature by LP-MOCVD, *J. Cryst. Growth* **261**, 490 (2004).

27) S. M. Smith, and H. B. Schlegal, Molecular Orbital Studies of Zinc Oxide Chemical Vapor Deposition: Gas-Phase Hydrolysis of Diethyl Zinc, Elimination Reactions, and Formation of Dimers and Tetramers, *Chem. Mater.* **15**, 162 (2003).
28) C. R. Gorla, N. W. Emanetoglu, S. Liang, W. E. Mayo, Y. Lu, M. Wraback, and H. Shen, Structural, optical, and surface acoustic wave properties of epitaxial ZnO films grown on $(01\bar{1}2)$ sapphire by metalorganic chemical vapor deposition, *J. Appl. Phys.* **85**, 2595 (1999).
29) J. Ye, S. Gu, S. Zhu, T. Chen, L. Hu, F. Qin, R. Zhang, Y. Shi, Y. Zheng, The growth and annealing of single crystalline ZnO films by low-pressure MOCVD, *J. Cryst. Growth* **243**,151 (2002).
30) K, Maejima, and S. Fujita, Chemical vapor reactions of ZnO growth by metal-organic vapor phase epitaxy, *J. Cryst. Growth* **293**, 305 (2006).
31) Xiaonan. Li, Sally E. Asher, Sukit Limpijumnong, S. B. Zhang, Su-Huai Wei, Teresa M. Barnes, Timothy J. Coutts, and Rommel Noufi, Unintentional doping and compensation effects of carbon in metal-organic chemical-vapor deposition fabricated ZnO thin films, *J. Vac. Sci. Tech. A* **24**, 1213 (2006).
32) I. Bisotto, C. Granier, S. Brochen, A. Ribeaud, P. Ferret, G. Chicot, J. Rothman, J. Pernot, and G. Feuillet, Residual Doping in Homoepitaxial Zinc Oxide Layers Grown by Metal Organic Vapor Phase Epitaxy, *Appl. Phys. Express* **3**, 095802 (2010).
33) N. Oleynik, M. Adam, A. Krtschil, J. Bläsing, A. Dadgar, F. Bertram, D. Forster, A. Diez, A. Greiling, M. Seip, J. Christen, and A. Krost, Metalorganic chemical vapor phase deposition of ZnO with different O-precursors, *J. Cryst. Growth* **248**, 14 (2003).
34) A. Krost, J. Christen, N. Oleynik, A. Dadgar, S. Deiter, J. Bläsing, A. Krtschil, D. Forster, F. Bertram, and A. Diez, Ostwald ripening and flattening of epitaxial ZnO layers during in situ annealing in metalorganic vapor phase epitaxy, *Appl. Phys. Lett.* **85**, 1496 (2004).
35) D. A. Lamb, and S. J. C. Irvine, Growth properties of thin film ZnO deposited by MOCVD with *n*-butyl alcohol as the oxygen precursor, *J. Cryst. Growth* **273**, 111 (2004).
36) H. Sato, T. Minami, T. Miyata, S. Takata, and M. Ishii, Transparent conducting ZnO thin films prepared on low temperature substrates by chemical vapour deposition using $Zn(C_5H_7O_2)_2$, *Thin Solid Films* **246**, 65 (1994).

37) Y. Kashiwaba, F. Katahira, K. Haga, T. Sekiguchi, and H. Watanabe, Hetero-epitaxial growth of ZnO thin films by atmospheric pressure CVD method, *J. Cryst. Growth* **221**, 431 (2000).
38) H. Asahara, A. Inokuchi, K. Watanuki, M. Hirayama, A. Teramoto, and T. Ohmi, Characterization of zinc oxide films grown by a newly developed plasma enhanced metal organic chemical vapor deposition employing microwave excited high density plasma, *Jpn. J. Appl. Phys.* **47**, 2994 (2008).
39) Y. Nose, T. Yoshimura, A. Ashida, T. Uehara, and N. Fujimura, Low temperature growth of ZnO thin films by non-equilibrium atmospheric pressure N_2/O_2 plasma and the growth morphology of the films, *Zairyo* **61**, 756 (2012).
40) R. Hayakawa, T. Yoshimura, A. Ashida, N. Fujimura, H. Kitahata, and M. Yuasa, Analysis of nitrogen plasma generated by a pulsed plasma system near atmospheric pressure, *J. Appl. Phys.* **96**, 6094 (2004).
41) Yefan Chen, D. M. Bagnall, Hang-jun Koh, Ki-tae Park, Kenji Hiraga, Ziqiang Zhu, and Takafumi Yao, Plasma assisted molecular beam epitaxy of ZnO on c-plane sapphire: Growth and characterization, *J. Appl. Phys.* **84**, 3912 (1998).
42) K. Nakahara, T. Tanabe, H. Takasu, P. Fons, K. Iwata, A. Yamada, K. Matsubara, R. Hunger, and S. Niki, Growth of undoped ZnO films with improved electrical properties by radical source molecular beam epitaxy, *Jpn. J. Appl. Phys.* **40**, 250 (2001).
43) A. Morita, I. Watanabe, N. Ohta, and H. Shirai, Chemical Activity of Oxygen Atoms in Magnetron Sputter-Deposited ZnO Films during Film Growth, *Jpn. J. Appl. Phys.* **50**, 08JD02 (2011).
44) T. Oshio, K. Masuko, A. Ashida, T. Yoshimura, and N. Fujimura, Effect of Mn doping on the electric and dielectric properties of ZnO epitaxial films, *J. Appl. Phys.* **103**, 093717 (2008).
45) M. Fox, *Optical Properties of Solids* (Oxford Univ. Press, 2001) p. 58.
46) T. Yamamoto, *State-of-the-Art Research and Prospective of Zinc Oxide*, (CMC shuppan, Tokyo, 2011) p. 5 [in Japanese].
47) V. Srikant, and D. R. Clarke, On the optical band gap of zinc oxide, *J. Appl. Phys.* **83**, 5447 (1998).
48) K. Matsumoto, and A. Tachibana, Growth mechanism of atmospheric pressure MOVPE of GaN and its alloys: gas phase chemistry and its impact on reactor design, *J. Cryst. Growth* **272**, 360 (2004).

49) K. Yasutake, H. Ohmi, H. Kakiuchi, T. Wakamiya, and H. Watanabe, Characterization of Epitaxial Si Films Grown by Atmospheric Pressure Plasma Chemical Vapor Deposition Using Cylindrical Rotary Electrode, *Jpn. J. Appl. Phys.* **45**, 3592 (2006).
50) K. Nakajima, *Epitaxial Growth Mechanisms. Crystal Growth Dynamics Series, Vol. 3* (Kyoritsu shuppan, Tokyo, 2002) p. 109 [in Japanese].
51) H. Tanoue, T. Taniguchi, S. Wada, S. Yamamoto, S. Nakamura, Y. Naka, H. Yoshikawa, M. Munekata, S. Nagaoka, and Y. Nakamura, Uniform ZnO epitaxial films formed at atmospheric pressure by high-speed rotation-type mist chemical vapor deposition, *Appl. Phys. Express* **8**, 125502 (2015).

Chapter 3: Orientation control of low temperature grown ZnO films and the electrical property

3-1 Introduction

Zinc oxide (ZnO) has been intensively studied because of its potential for various applications such as transparent conductive films,[1-5] thin-film transistors,[6,7] high-electron mobility transistors [8,9] and piezoelectric devices [10-12] and so on. Although ZnO have a lot of attractive material properties for these applications such as high exciton binding energy,[13] high electron saturation velocity [14] and large electromechanical coupling coefficient among semiconductors,[15] ZnO and its related alloys are not put into practical use well mainly due to the large number of residual electron concentration.[7] To solve this chronic problem, we propose chemical vapor deposition (CVD) using nonequilibrium plasma generated near atmospheric pressure (AP) which is potentially able to supply rather dense and oxidative excited species to ZnO films compared with low pressure processes represented by sputtering.[16] Regarding the AP plasma enhanced CVD of ZnO films, although a few reports exist,[17-20] their processes require the use of expensive rare gas (He) as a dilution gas to maintain arc-less, nonequilibrium and stable discharge near AP. From the industrial point of view, He-less process is desirable.[21] Therefore, we have developed nonequilibrium plasma source operated near AP, and demonstrated the formation of ZnO films at a substrate temperature as low as 200 °C using O_2-based plasma. Although the film showed (0001) preferred orientation, X-ray diffraction from $(10\bar{1}1)$ which

has the largest structural factor [22] was also observed in XRD pattern.[23] Additionally, the electrical property was not discussed in chapter 2.

In this chapter, we access the effects of radiative activated species in N_2/O_2 plasma generated at various gas compositions on the crystallinity and electrical property of low temperature grown ZnO films.[24]

3-2 Experimental

Bis-2,4octanedionato zinc [$Zn(C_8H_{13}O_2)_2$ (Adeka Corp.) denoted as $Zn(OD)_2$] was used as the Zn source material that was free from spontaneous combustibility in atmosphere and was also suitable for constant supply because it was liquid at room temperature and at AP. **Fig. 3-1** shows a schematic illustration of the AP plasma-enhanced ZnO-CVD system.[23,24] Vaporized $Zn(OD)_2$ is transported with N_2 carrier gas at the constant flow rate of 60 ml/min. The source and N_2 carrier gases are mixed with N_2 and O_2 controlled by the mass flow controller (MFC). The O_2 concentration in the total mixed gas flow rate (O_2%) is varied from 0.1 to 90% to change the composition of the N_2/O_2 mixed gas. The mixed gases heated at 190 °C are introduced into the growth chamber. The total pressure of the chamber during deposition is maintained at 50 kPa. The deposition of ZnO films is performed on glass substrates at the growth temperature (T_g) of 150 - 300 °C. The substrates are mounted in direct plasma generated between two parallel-plate electrodes covered with dielectric materials (AlN). The applied AC voltage and frequency are 6.0 - 6.5 kV and 180 kHz, respectively. Growth conditions of ZnO films are summarized in **Table 3-1**. The excited species in the plasma during deposition are evaluated by optical emission spectroscopy (OES) using a photonic multichannel spectral analyzer (PMA-C7473, Hamamatsu Photonics). After deposition, crystal structure of the films is investigated by X-ray diffraction (XRD: X'pert MRD, Philips). The specific resistivity of ZnO layer was evaluated by van der Pauw's method using Hall-effect measurement system (TOYO-Corp., ResiTest 8310). Prior to the electrical measurement, indium dot was soldered onto the four corners of sample as Ohmic electrodes.

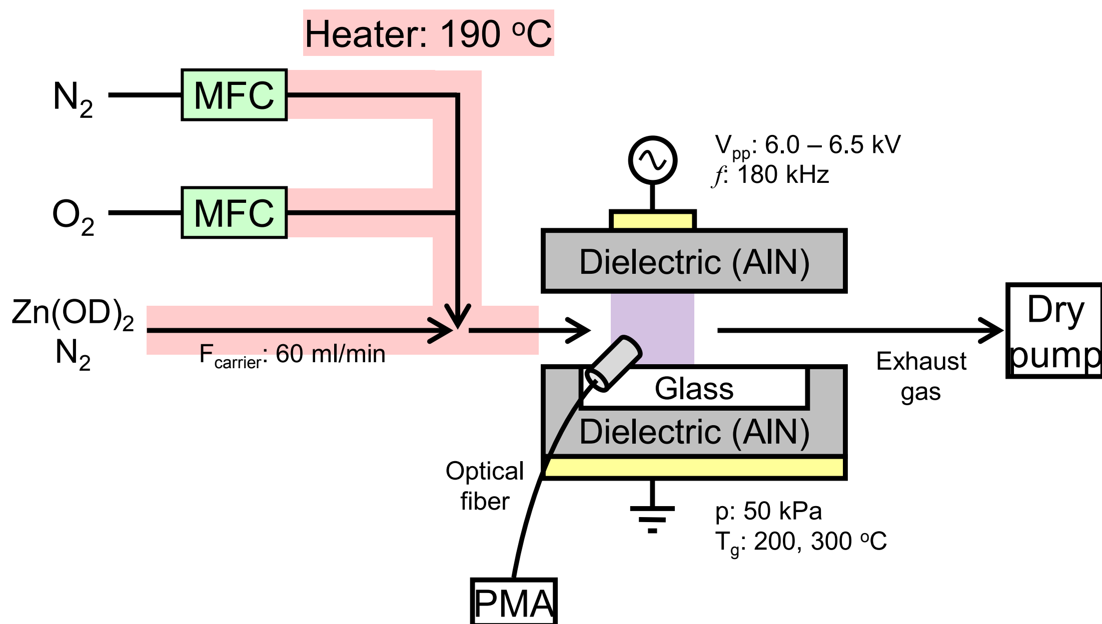

Fig. 3-1. A schematic illustration of CVD system using N_2/O_2 direct plasma generated near atmospheric pressure.

Table. 3-1. Growth condition of ZnO films for the control of (0001) preferred orientation.

Carrie gas flow rate $F_{Carrier}$	60 sccm
O_2%	0.1 ~ 90%
Gas flow velocity v	0.7, 3.8 m/s
Growth pressure p	50 kPa
Growth temperature T_g	150 ~ 300 °C
AC voltage V_{pp}	6.0 - 6.5 kV (Peak to peak)
AC frequency f	180 kHz

3-3 Results and discussions

3-3-1 Growth temperature dependence on the crystallinity

ZnO films were grown on glass substrate heated at 150, 200 and 300 °C at the constant O_2% of 90% under observation of Atomic O^* (777, 843 and 927 nm) as shown in chapter 2. After the deposition, the crystal structure of the obtained films was evaluated by XRD. **Fig. 3-2** shows 2θ-ω scanned XRD profiles for the samples deposited at the substrate temperatures of 150, 200 and 300 °C. With increasing the growth temperature, relative XRD intensity of ZnO $000l$ increases, whereas that of another plane decreases. Since the ZnO (0001) plane has the lowest surface free energy density of 0.099 eV/Å^2, ZnO films prefer (0001) orientation. Therefore, ZnO films with strong (0001) preferred orientation can be easily obtained without the effect of epitaxy (self-texture) such as on a glass substrate.[25)] In general, the crystallinity of thin films is improved by increasing T_g mainly due to the enhancement of decomposition and surface migration of precursors. In this chapter, however, we attempted to fabricate strongly (0001)-oriented ZnO films at 200 °C by optimizing other deposition parameters in order to access the effects of radiative activated species in N_2/O_2 plasma generated at various gas compositions on the crystallinity to discuss intrinsic nature of plasma on the crystallinity of ZnO films.

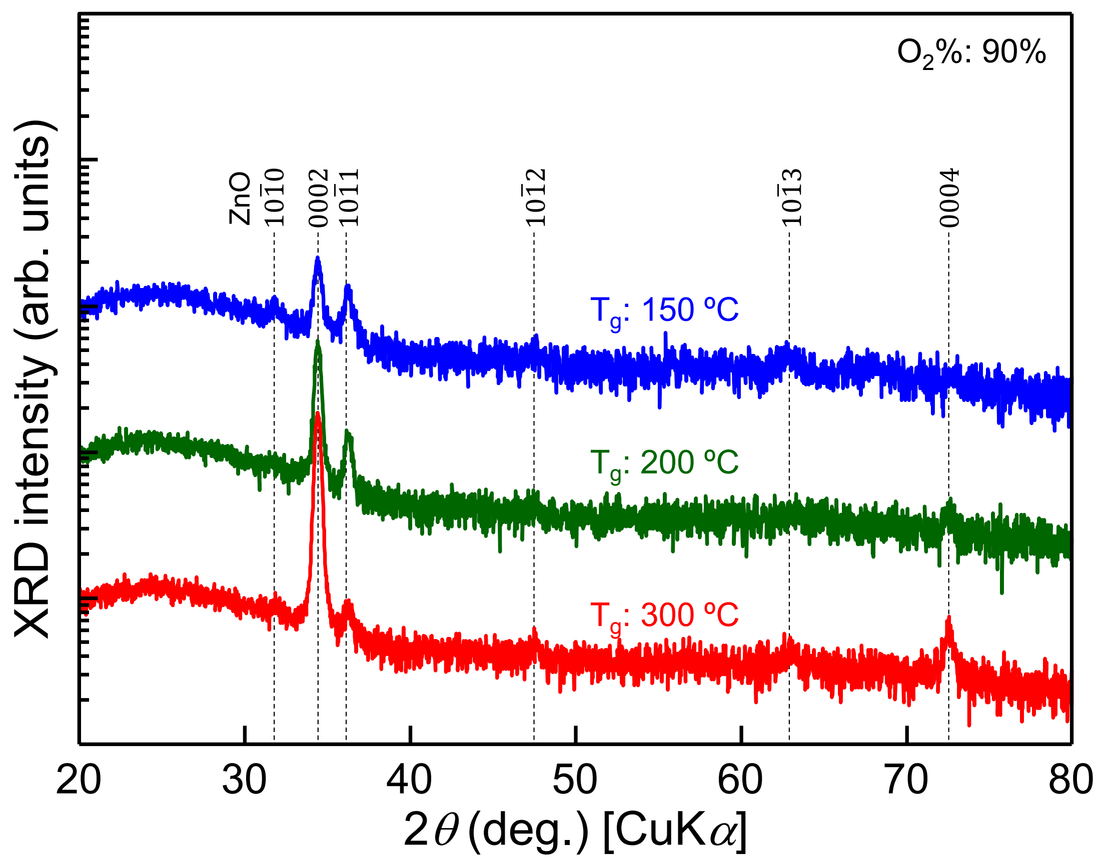

Fig. 3-2. 2θ-ω scanned XRD profiles of the sample grown at the substrate temperature of 150, 200 and 300 ºC. In this experiment, O_2% is fixed at 90%.

3-3-2 Orientation control and the kinetics

We have reported that the N_2 second positive system (N_2 2ps: $C^3\Pi_u^+ \longrightarrow B^3\Pi_u^+$) was predominantly observed in N_2 plasma generated near AP and it retained a reactivity high enough to accomplish room-temperature nitridation of a silicon wafer.[26-28] There is quite a high potential energy state of above 10 eV from the ground state in the reaction process of N_2 2ps,[29,30] which might supply precursors a high energy to form highly (0001)-oriented ZnO films. Therefore, we investigated the change in the optical emission spectra by varying the O_2% systematically from N_2-rich to O_2-rich gas composition.

Fig. 3-3 (a) shows the change in the optical emission (OE) intensities of predominantly observed radiative transitions, NO-γ system (NO-γ: $A^2\Sigma^+ \longrightarrow X^2\Pi_\gamma^+$), N_2 2ps and atomic oxygen (Atomic O^*: $3p^5P \rightarrow 3s^5S$), as a function of the O_2%. NO-γ is observed only at the O_2% of below 1%. The generation processes of NO will be discussed in chapter 5. N_2 2ps is observed in all O_2% except 100%. The OE is rapidly quenched by the addition of O_2, and tends to decrease against the increase of O_2% due to the decrease of electron density by the strong electronegativity of O_2 [31] or quenching reaction of $N_2(C^3\Pi_u^+)$ with O_2.[32] The OE of Atomic O^* appears at the O_2% of more than 20%, and the intensity is gradually increases with increasing the O_2%. This result suggests that the dominant excited species can be selectively used for deposition by adjusting the O_2%.

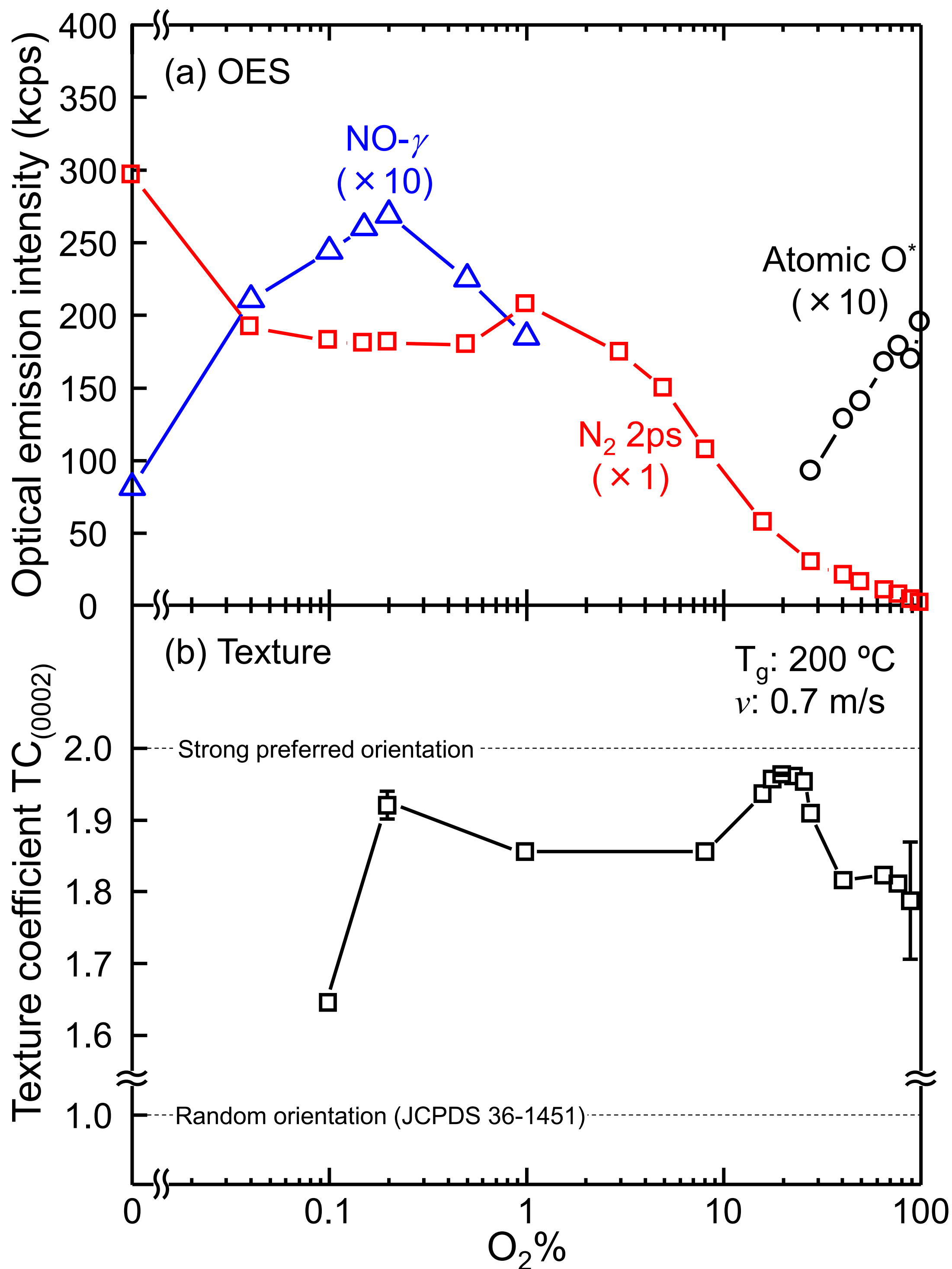

Fig. 3-3. Change of the OE intensity of NO-γ, N_2 2ps and Atomic O^* against the change of the O_2%. Magnification of the OE intensity is indicated. **(a)** Plot of texture coefficient $TC_{(0002)}$ as a function of the O_2%. Error bars at 0.2, 20 and 90% indicates maximum and minimum value for several samples deposited at the same condition. **(b)**

The crystal structure of the deposited films fabricated under various O_2% was analyzed by 2θ-ω scanned XRD measurement. The strongest diffraction peak originates from ZnO 0002 in all samples discussed here, indicating that the films have (0001) preferred orientation regardless of the O_2%; however, diffraction intensity from another plane depended on O_2%, suggesting that the texture of ZnO films is affected by excited species in the plasma. The texture coefficient (*TC*) used in the quantitative characterization of preferred orientation for thin films can be described according to the following formula: [33,34]

$$TC_{(hklm)} = \frac{I_{m(kklm)}/I_{0(kklm)}}{(1/n)\sum I_{m(kklm)}/I_{0(kklm)}}, \tag{3-1}$$

where $I_{m(hklm)}$ is measured relative XRD intensity of $hklm$ plane, $I_{0(hklm)}$ is that of standard reference data (e.g. JCPDS 36-1451) and n is the number of diffraction peaks. In our sample, $TC_{(0002)}$ should be between 1 (random orientation) and 2 (strong preferred orientation), because ZnO 0002 and $10\bar{1}1$ both of which have relatively large structural factor are dominantly observed in 2θ-ω scanned XRD profiles for all sample discussed here. **Fig. 3-3 (b)** shows plot of $TC_{(0002)}$ of ZnO films as a function of the O_2%. $TC_{(0002)}$ is less than 1.85 at the O_2% of 0.1%, 1 – 10% and 40 – 90%. The value specifically increases at around the O_2% of 0.2 and 20%. At the O_2% of around 20%, $TC_{(0002)}$ is almost equal to 2, indicating that highly (0001)-oriented ZnO films were successfully obtained by adjusting the O_2% without increasing the growth temperature. Regarding the O_2% of around 0.2%, NO-γ seems to play important roles in the enhancement of texture. We will focus on the mechanism of this region in chapter 5. On the other hand, O_2% of 20%, where only a relatively weak OE of N_2 2ps is observed,

shows the highest $TC_{(0002)}$. From this result, the texture control mechanism cannot attribute to single radiative excited species (N_2 2ps). Another non-radiative species [25,35] or plasma parameter [36,37] might be responsible for the enhancement of self-texture on glass substrate.

3-3-3 Electrical properties of ZnO films

This section focuses on the resistivity of our low temperature grown ZnO films. In the last section (3-3-2), the crystallinity of ZnO films from viewpoint of self-texture was found to be affected by the excited species in the direct plasma. At the specific O_2% of 0.2%, radiative excited species (NO-γ) seemed to be responsible for the crystallinity. On the other hand, at the O_2% of 20%, where the highest $TC_{(0002)}$ was obtained, the texture enhancement mechanism was not able to attribute to single radiative species (N_2 2ps or Atomic O^*), and the texture might be affected by some plasma parameter. However, the analysis of plasma parameters in direct region using Langmuir probe is almost impossible due to the quite small gap of 1.1 mm and the destruction of dielectric barrier discharge. Instead of that, discharge current was measured during deposition by an oscilloscope in combination with a current probe to evaluate the change of plasma parameters as represented by the electron concentration. As a result, peak-to-peak value of the discharge current was approximately 200 mA, which was almost independent on the O_2% at around the O_2%s in the vicinity of 20%. This fact suggests that the electron concentration in the plasma does not show a drastic change near the O_2% of 20%.

As described in chapter 2 (see **Fig. 2-7** again), the deposition area was limited to near the edge of top electrode, suggesting that the most of the Zn source material reacts with oxidant as soon as the mixed gases are introduced into the plasma, which might cause an unintentional parasitic reaction at the vapor phase. Therefore, the gas flow velocity (denoted as v_{gas}) was increased from 0.7 to 3.8 m/s by increasing total gas flow rate in order to reduce the effect of vapor-phase reaction.[38-40]

Fig. 3-4 (a) shows O_2% dependence of the $TC_{(0002)}$ for ZnO films grown at the gas flow velocity of 0.7 [already shown in **Fig. 3-3 (b)**] and 3.8 m/s. With increasing the v_{gas}, $TC_{(0002)}$ approaches to 2, indicating the enhancement of crystallinity by the increase of v_{gas}. This result suggests that the use of fast gas velocity is effective for the enhancement of crystallinity possibly due to the reduction of vapor-phase reactions. Subsequently, the specific resistivity was evaluated for several samples by van der Pauw's method using indium Ohmic electrodes. [**Fig. 3-4 (b)**] Note that all samples show high resistivity exceeding 10^3 Ωcm at room temperature, which is rather higher than nominally un-doped ZnO films grown by vacuum processes such as molecular beam epitaxy (MBE) and pulsed laser deposition (PLD). At the v_{gas} of 0.7 m/s, the specific resistivity changes from 10^3 to 10^6 Ωcm against the change of the O_2%. On the other hand, the specific resistivity shows quite high value of 10^6 – 10^7 Ωcm and smaller O_2% dependence when the v_{gas} is increased from 0.7 to 3.8 m/s, while enhancing the $TC_{(0002)}$. Although the microscopic growth mechanism of ZnO films is not clearly understood, it is clear that the high resistivity is not due to the degradation of crystallinity such as the incorporation of undecomposed residues, but the intrinsic nature in the CVD processes using N_2/O_2 direct plasma generated near AP, suggesting that the advantage of this plasma for the formation of ZnO films with low residual electron concentration.

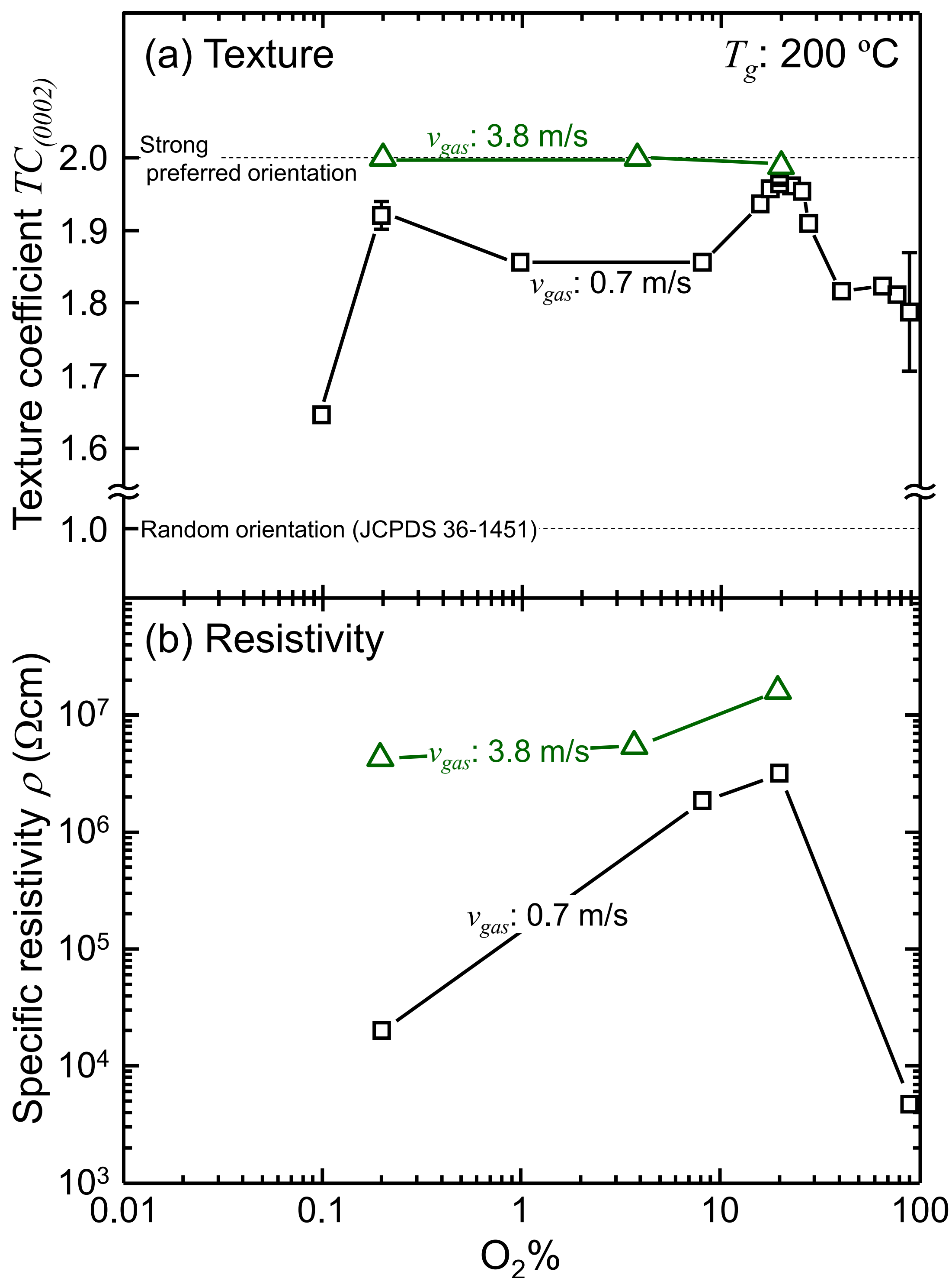

Fig. 3-4. Plot of $TC_{(0002)}$ for the samples grown at the gas flow velocity v_{gas} of 0.7 and 3.8 m/s as a function of the O_2%. **(a)** Change of the specific resistivity of the samples grown at the various O_2% and v_{gas}. **(b)**

3-4 Conclusions

In summary, we applied nonequilibrium N_2/O_2 plasma generated near AP to the low-temperature formation of ZnO films. In the optical emission spectra of plasma during deposition, optical emission peaks corresponding to the NO-γ system, N_2 second positive system and atomic O were observed, and the emission intensities of those transitions could be controlled by varying the O_2%. ZnO films with strong (0001) preferred orientation were successfully obtained on the glass substrate at a deposition temperature of 200 °C by systematically optimizing the O_2% and gas flow velocity without increasing the substrate temperature, suggesting that the control of radiative excited species and efficient use of direct plasma are the important factors for the improving the crystallographic quality of low temperature grown ZnO films. Despite such a low growth temperature, ZnO films showed quite high specific resistivity exceeding 10^6 Ωcm at room temperature while keeping the crystallinity, suggesting that the potential ability of our direct plasma for the formation of ZnO films with low residual carrier concentration even at small amount of O_2. This finding is very important for nitrogen doping to ZnO films.

References

1) K.-H. Kim, K.-C. Park, and D.-Y. Ma, Structural, electrical and optical properties of aluminum doped zinc oxide films prepared by radio frequency magnetron sputtering, *J. Appl. Phys.* **81**, 7764 (1997).
2) H. Agura, A. Suzuki, T. Matsushita, T. Aoki, and M. Okuda, Low resistivity transparent conducting Al-doped ZnO films prepared by pulsed laser deposition, *Thin Solid Films* **445**, 263 (2003).
3) C. Jeong, H. S. Kim, D. R. Chang, and K. Kamisako, Effect on Al_2O_3 Doping Concentration of RF Magnetron Sputtered ZnO:Al Films for Solar Cell Applications, *Jpn. J. Appl. Phys.* **47**, 5656 (2008).
4) H. Makino, H. Song, and T. Yamamoto, Influences of oxygen gas flow rate on electrical properties of Ga-doped ZnO thin films deposited on glass and sapphire substrates, *Thin Solid Films* **559**, 78 (2014).
5) A. Hongsingthong, T. Krajangsang, I. A. Yunaz, S. Miyajima, and M. Konagai, ZnO Films with Very High Haze Value for Use as Front Transparent Conductive Oxide Films in Thin-Film Silicon Solar Cells, *Appl. Phys. Express* **3**, 051102 (2010).
6) T. Hirao, M. Furuta, T. Hiramatsu, T. Matsuda, C. Li, H. Furuta, H. Hokari, M. Yoshida, H. Ishii, and M. Kakegawa, Bottom-Gate Zinc Oxide Thin-Film Transistors (ZnO TFTs) for AM-LCDs, *IEEE Trans. Electron Devices* **55**, 3136 (2008).
7) H. Hosono, Recent progress in transparent oxide semiconductors: Materials and device application, *Thin Solid Films* **515**, 6000 (2007).
8) H. Tampo, H. Shibata, K. Matsubara, A. Yamada, P. Fons, S. Niki, M. Yamagata, and H. Kanie, Two-dimensional electron gas in Zn polar ZnMgO/ZnO heterostructures grown by radical source molecular beam epitaxy, *Appl. Phys. Lett.* **89**, 132113 (2006).
9) J. D. Ye, S. Pannirselvam, S. T. Lim, J. F. Bi, X. W. Sun, G. Q. Lo, and K. L. Teo, Two-dimensional electron gas in Zn-polar ZnMgO/ZnO heterostructure grown by metal-organic vapor phase epitaxy, *Appl. Phys. Lett.* **97**, 111908 (2010).
10) H. Nakahata, K. Higaki, A. Hachigo, S. Shikata, N. Fujimori, Y. Takahashi, T. Kajihara, and Y. Yamamoto, High Frequency Surface Acoustic Wave Filter Using ZnO/Diamond/Si Structure, *Jpn. J. Appl. Phys.* **33**, 324 (1994).
11) J. G. E. Gardeniers, Z. M. Rittersma, and G. J. Burger, Preferred orientation and piezoelectricity in sputtered ZnO films, *J. Appl. Phys.* **83**, 7844 (1998).

12) T. Yoshimura, H. Sakiyama, T. Oshio, A. Ashida, and N. Fujimura, Direct Piezoelectric Properties of Mn-Doped ZnO Epitaxial Films, *Jpn. J. Appl. Phys.* **49**, 021501 (2010).

13) B. Gil, D. Felbacq, and S. F. Chichibu, Exciton binding energies in chalcopyrite semiconductors, *Phys. Rev. B* **85**, 075205 (2012).

14) J. D. Albrecht, P. P. Ruden, S. Limpijumnong, W. R. L. Lambrecht, and K. F. Brennan, High field electron transport properties of bulk ZnO, *J. Appl. Phys.* **86**, 6864 (1999).

15) Ü. Özgür, D. Hofstetter, and H. Morkoç, ZnO Devices and Applications: A Review of Current Status and Future Prospects, *Proc. IEEE* **98**, 1255 (2010).

16) K. Ellmer, Magnetron sputtering of transparent conductive zinc oxide: relation between the sputtering parameters and the electronic properties, *J. Phys. D: Appl. Phys.* **33**, R17 (2000).

17) Y. Suzaki, S. Ejima, T. Shikama, S. Azuma, O. Tanaka, T. Kajitani, and H. Koinuma, Deposition of ZnO film using an open-air cold plasma generator, *Thin Solid Films* **506-507**, 155 (2006).

18) M. D. Barankin, E. Gonzalez II, A. M. Ladwig, and R. F. Hicks, Plasma-enhanced chemical vapor deposition of zinc oxide at atmospheric pressure and low temperature, *Sol. Energy Mater. Sol. Cells* **91**, 924 (2007).

19) Y. Ito, O. Sakai, and K. Tachibana, Study of plasma enhanced chemical vapor deposition of ZnO films by non-thermal plasma jet at atmospheric pressure, *Thin Solid Films* **518**, 3513 (2010).

20) Y. Suzaki, A. Kawaguchi, T. Murase, T. Yuji, T. Shikama, D.-B. Shin, and Y.-K. Kim, Effect of substrate temperature on ZnO thin film fabrication by using an atmospheric pressure cold plasma generator, *Phys. Status Solidi C* **8**, 503 (2011).

21) W. J. Nuttall, R. H. Clarke, and B. A. Glowacki, Stop squandering helium, *Nature* **485**, 573 (2012).

22) O. Garcia-Martinez, R. M. Rojas, and E. Vila, Microstructural characterization of nanocrystals of ZnO and CuO obtained from basic salts, *Solid State Ionics* **63-65**, 442 (1993).

23) Y. Nose, T. Yoshimura, A. Ashida, T. Uehara, and N. Fujimura, Low temperature growth of ZnO thin films by non-equilibrium atmospheric pressure N_2/O_2 plasma and the growth morphology of the films, *Zairyo* **61**, 756 (2012) [in Japanese].

24) Y. Nose, T. Nakamura, T. Yoshimura, A. Ashida, T. Uehara, and N. Fujimura,

Orientation Control of ZnO Films Deposited Using Nonequilibrium Atmospheric Pressure N_2/O_2 Plasma, *Jpn. J. Appl. Phys.* **52**, 01AC03 (2013).

25) N. Fujimura, T. Nishihara, S. Goto, J. Xu, and T. Ito, Control of preferred orientation for ZnO_x films: control of self-texture, *J. Cryst. Growth* **130**, 269 (1993).

26) R. Hayakawa, T. Yoshimura, A. Ashida, T. Uehara, and N. Fujimura, Reaction of Si with excited nitrogen species in pure nitrogen plasma near atmospheric pressure, *Thin Solid Films* **506-507**, 423 (2006).

27) R. Hayakawa, M. Nakae, T. Yoshimura, A. Ashida, N. Fujimura, T. Uehara, M. Tagawa, and Y. Teraoka, Detailed structural analysis and dielectric properties of silicon nitride film fabricated using pure nitrogen plasma generated near atmospheric pressure, *J. Appl. Phys.* **100**, 073710 (2006).

28) M. Nakae, R. Hayakawa, T. Yoshimura, A. Ashida, N. Fujimura, S. Kunugi, and T. Uehara, The comparison of the growth models of silicon nitride ultrathin films fabricated using atmospheric pressure plasma and radio frequency plasma, *J. Appl. Phys.* **101**, 023513 (2007).

29) F. R. Gilmore, R. R. Laher, and P. J. Espy, Franck-Condon Factors, *r*-Centroids, Electronic Transition Moments, and Einstein Coefficients for Many Nitrogen and Oxygen Band Systems, *J. Phys. Chem. Ref. Data* **21**, 1005 (1992).

30) Y. Horikawa, K. Kurihara, and K. Sasaki, Effective Species in Inductively Coupled Nitrogen Plasma for Silicon Nitriding, *Appl. Phys. Express* **4**, 086201 (2011).

31) M. Iwasaki, Y. Matsudaira, K. Takeda, M. Ito, E. Miyamoto, T. Yara, T. Uehara, and M. Hori, Roles of oxidizing species in a nonequilibrium atmospheric-pressure pulsed remote O_2/N_2 plasma glass cleaning process, *J. Appl. Phys.* **103**, 023303 (2008).

32) E. Suetomi, T. Mizukoshi, K. Fukazawa, and A. Saito, Simulation of Atmospheric Pressure Glow Discharge Plasmas in Nitrogen-Oxygen Mixtures, *Konika Minolta Technology Report* **3**, 80 (2006) [in Japanese].

33) S. Lemlikchi, S. Abdelli-Messaci, S. Lafane, T. Kerdja, A. Guittoum, and M. Saad, Study of structural and optical properties of ZnO films grown by pulsed laser deposition, *Appl. Surf. Sci.* **256**, 5650 (2010).

34) M. Zhao, F. Shang, J. Lv, Y. Song, F. Wang, Z. Zhou, G. He, M. Zhang, X. Song, Z. Sun, Y. Wei, and X. Chen, Influence of water content in mixed solvent on surface

morphology, wettability, and photoconductivity of ZnO thin films, *Nanoscale Res. Lett.* **9**, 485 (2014).

35) C. R. Aita, A. J. Purdes, R. J. Lad, and P. D. Funkenbusch, The effect of O_2 on reactively sputtered zinc oxide, *J. Appl. Phys.* **51**, 5533 (1980).

36) J. R. Williams, H. Furukawa, Y. Adachi, S. Grachev, E. Søndergård, and N. Ohashi, Polarity control of intrinsic ZnO films using substrate bias, *Appl. Phys. Lett.* **103**, 042107 (2013).

37) B. B. Sahu, J. G. Han, M. Hori, and K. Takeda, Langmuir probe and optical emission spectroscopy studies in magnetron sputtering plasmas for Al-doped ZnO film deposition, *J. Appl. Phys.* **117**, 023301 (2015).

38) H. Amano, N. Sawaki, I. Akasaki, and Y. Toyoda, Metalorganic vapor phase epitaxial growth of a high quality GaN film using an AIN buffer layer, *Appl. Phys. Lett.* **48**, 353 (1986).

39) J. R. Creighton, W. G. Breiland, M. E. Coltrin, and R. P. Pawlowski, Gas-phase nanoparticle formation during AlGaN metalorganic vapor phase epitaxy, *Appl. Phys. Lett.* **81**, 2626 (2002).

40) K. Yasutake, H. Ohmi, H. Kakiuchi, T. Wakamiya, and H. Watanabe, Characterization of Epitaxial Si Films Grown by Atmospheric Pressure Plasma Chemical Vapor Deposition Using Cylindrical Rotary Electrode, *Jpn. J. Appl. Phys.* **45**, 3592 (2006).

Chapter 4: Evaluation of the electronic state for highly resistive ZnO epitaxial films

4-1 Introduction

Zinc oxide (ZnO) and its related alloys have been intensively studied for their excellent optical, electrical, and magnetic properties.[1–10] Recent advances regarding crystal growth and peripheral technology of ZnO films have drastically improved the quality and purity of ZnO films,[10] and have established their position as one of the purest semiconductors.[11,12] Although ZnO have many inherent advantages in terms of its material properties compared with III-V semiconductors such as gallium nitride (GaN),[13–15] the control and suppression of its "high residual electron concentration" has still remained one of the biggest issues toward the practical application of ZnO-based devices in various aspects [16] such as thin-film transistors,[17] piezoelectric devices,[18] and light emitting devices,[7] despite enormous efforts have been devoted to the problem and the various crystal growth techniques proposed and assessed.[19] Recent theoretical research predicted that nonequilibrium growth at an oxygen-rich environment is effective in suppressing representative donor-type defects such as zinc interstitials (Zn_i) and oxygen vacancies (V_O).[20,21] From an experimental point of view, the use of a reactive oxygen source is also important for the suppression of donor-type defects in oxide films.[22–25] The history regarding crystal growth of ZnO films implicitly recommends that nonequilibrium processes near atmospheric pressure (AP) using active species with high oxidizability is the promising approach in suppressing residual electron in ZnO [22] and its related compounds.[25] Therefore, we focused on

nonequilibrium plasma generated near atmospheric pressure (AP), which has an extremely high plasma density exceeding 10^{15} cm^{-3},[26] and a sufficiently high reactivity to achieve Si [27,28] and Ge [29] nitridation even at ambient temperatures. We have also found that small amounts of O_2 added to N_2 plasma (~ 250 ppm) significantly enhances the oxidation of Si, which led to the formation of a dense silicon oxynitride layer with a low leakage current density of 1.4×10^{-4} A/cm^2 at 5 MV/cm.[30]

Although ZnO films grown by conventional vacuum processes tend to show low resistivity due to a large number of residual electrons, those grown by our plasma exhibit quite high specific resistivity exceeding 10^6 Ωcm at ambient temperature while keeping high crystallinity, suggesting its low residual electron concentration.[31,32] However, the origin of this high resistivity was not elucidated directly in chapter 3. In this chapter, therefore, we focus on the electrical property of highly resistive ZnO films with a considerably higher crystal quality than poly-crystal ZnO films discussed in the last chapter. Using high-quality epitaxial films, we discuss the advantages of N_2-based nonequilibrium N_2/O_2 plasma for the reduction of “shallow donor” and “residual electron” in ZnO films.

4-2 Experimental

A single crystal of sapphire (0001) was used as a substrate. Prior to deposition, the substrate was degreased by ultrasonic cleaning in acetone and ethanol each for 5 min, and subsequently annealed at 1000 °C for 10 h in air to obtain a well-defined/atomically-flat step and terrace structure with a single step height of 0.23 nm, reported by Yoshimoto *et al.*[33] [**Fig. 4-3 (a)**]. Bis-2,4octanedionato zinc [$Zn(C_8H_{13}O_2)_2$, Adeka Corp.] was selected for CVD as the Zn source material being free from spontaneous combustibility and liquid at standard conditions. $Zn(C_8H_{13}O_2)_2$ was vaporized at 190 ºC by thermal vaporizer, transported at a constant flow rate of 0.4 μmol/min together with N_2 carrier gas at a flow rate of 60 ml/min and mixed with additional N_2 at 428 ml/min and O_2 at 122 ml/min for a total mixed gas flow rate of 610 ml/min. These conditions correspond to the O_2 concentration in the N_2/O_2 mixture (O_2%) of 20%, which was found to optimal in chapter 3.[31] N_2-based nonequilibrium N_2/O_2 plasma was generated between two parallel plate electrodes covered with aluminum nitride dielectrics based on dielectric barrier discharge by applying an alternating voltage with the peak-to-peak value and frequency of 5.7 – 6.0 kV and 180 kHz, respectively. Growth pressure and gas flow velocity were set to 50 kPa and 0.7 m/s, respectively. Detailed information of the CVD system is reported elsewhere.[31,32,34] In this chapter, growth temperature (denoted as T_g) is set to 200, 300 and 400 °C to improve the crystal quality. For comparison, ZnO film was deposited by pulsed laser deposition (PLD) system using KrF excimer laser and ZnO ceramic target at the T_g and O_2 partial pressure of 600 °C and $1{\times}10^{-4}$ Torr, respectively. Hydrothermally (HYD) grown resistive ZnO single crystal supplied by OPTOSTAR Ltd.

(n_{300K} ~ 3×10^{14} cm^{-3}) was also prepared as a control sample for optical measurement. After deposition, the crystal structure and epitaxial relationship were evaluated through X-ray diffraction (XRD: X'pert MRD, Philips) using the optical geometry for 2θ-ω and ϕ, respectively. The surface morphology was investigated by dynamic force microscope (DFM) mode of scanning probe microscope (SPM: NanoNaviReal, Hitachi High-Tech Science Corp.). Optical transmittance, optical bandgap and thickness of the films were simultaneously evaluated using UV-vis spectrophotometer (V-650, JASCO). Photoluminescence (PL) measurement was performed using He-Cd laser (IK3802R-G, Kimmon Koha) and photonic multichannel spectral analyzer (PMA-C7473, Hamamatsu Photonics) as an excitation source and a detector, respectively. Electrical properties (specific resistivity, carrier concentration, and Hall mobility) were evaluated using Hall-effect measurement system (Resitest 8310, Toyo Corp.) at measurement temperatures (T) ranging from 340 to 400 K using a sinusoidal alternating magnetic field with a root mean square and frequency of 0.54 T and 100 mHz, respectively. The applied current was optimized within a range of 10^{-8} to 10^{-7} A, depending on the inter-terminal resistivity and signal/noise (S/N) ratio of Hall voltage for each T. The impurity concentration was evaluated by secondary ion mass spectroscopy (SIMS: PHI ADEPT1010, ULVAC-Phi). Finally, micro Raman scattering measurements were carried out in backscattering geometry (RAMAN-11, Nanophoton). ZnO film grown at the T_g of 400 °C was cleaved and one of the pieces was annealed by rapid thermal annealing system (RTA: MILA-3000, Ulvac-Riko, Inc.) at 700 °C for 10 min in O_2 atmosphere to evaluate the effect of thermal treatment on the resistivity and the chemical bonding state of nitrogen in ZnO.

4-3 Results and discussions

4-3-1 Crystallinity and morphology of epitaxial ZnO films

To investigate the crystal structure and epitaxial relationships, XRD measurement was performed in the optical geometry of 2θ-ω and ϕ as shown in **Fig. 4-1 (a)** and **(b)**, respectively. The 2θ-ω scanned XRD profile (a) shows only ZnO $000l$ diffraction peaks, indicating the strong (0001) preferred orientation of ZnO films on sapphire (0001) substrates. The ϕ-scanned XRD profiles (b) show the six-fold symmetric diffraction peaks of ZnO $10\bar{1}1$, which are rotated by 30° from the three-fold symmetric diffraction peaks of sapphire $10\bar{1}4$, indicating that ZnO films are epitaxially grown on the sapphire substrates with the epitaxial relationships of (0001) $[11\bar{2}0]$ ZnO // (0001) $[10\bar{1}0]$ sapphire as illustrated in the inset of (b). The incorporation of a 30° rotation domain, $[10\bar{1}0]$ ZnO // $[10\bar{1}0]$ sapphire,[35,36] is suppressed in our epitaxial films. Additionally, the magnitudes of orientation were evaluated by the full width at the half maximum (FWHM) value of ω- and ϕ-scanned XRD profiles. (**Fig. 4-2**) Regarding ω-scan, ZnO 0002 and $10\bar{1}1$ plane are selected for tilt and twist measurement, respectively, because the lattice plane inclination (ψ) of these two planes is much different from each other.[37] The FWHM values of rocking curve and ϕ-scan decrease with increasing the T_g signaling the improvement of crystallinity at higher T_g growth, probably due to the enhancement of surface migration of adatoms or Ostwald ripening.[38]

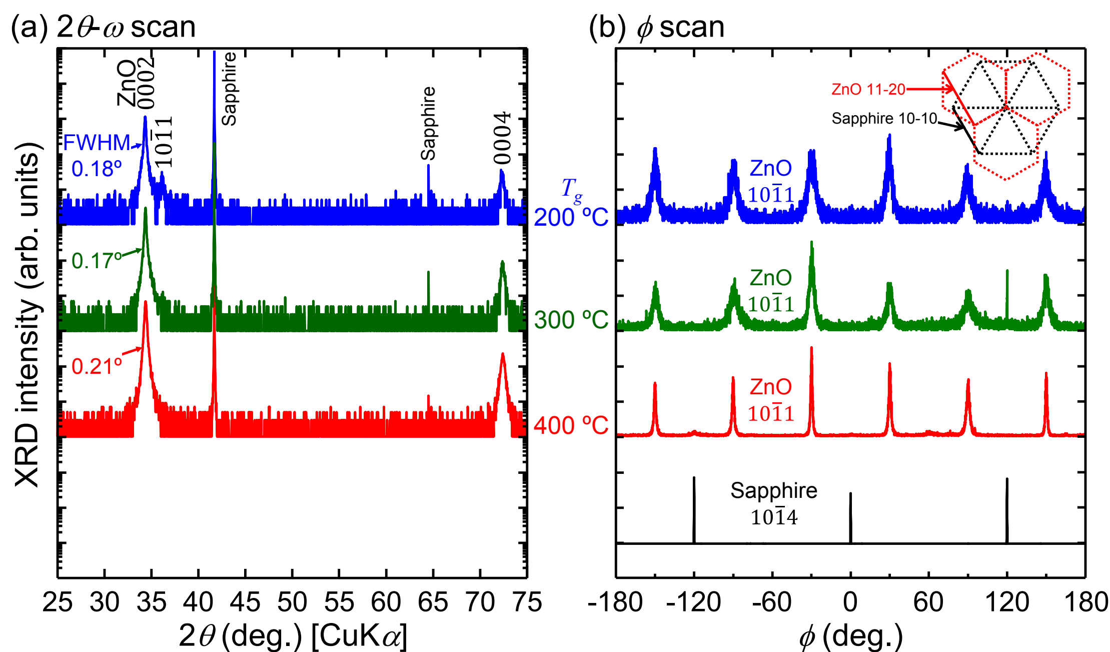

Fig. 4-1. 2θ-ω scanned **(a)** and φ scanned **(b)** XRD profiles for ZnO epitaxial films on sapphire (0001) substrate grown at various T_g. Epitaxial relationships are (0001) $[11\bar{2}0]$ ZnO // (0001) $[10\bar{1}0]$ sapphire as shown in the inset of **(b)**.

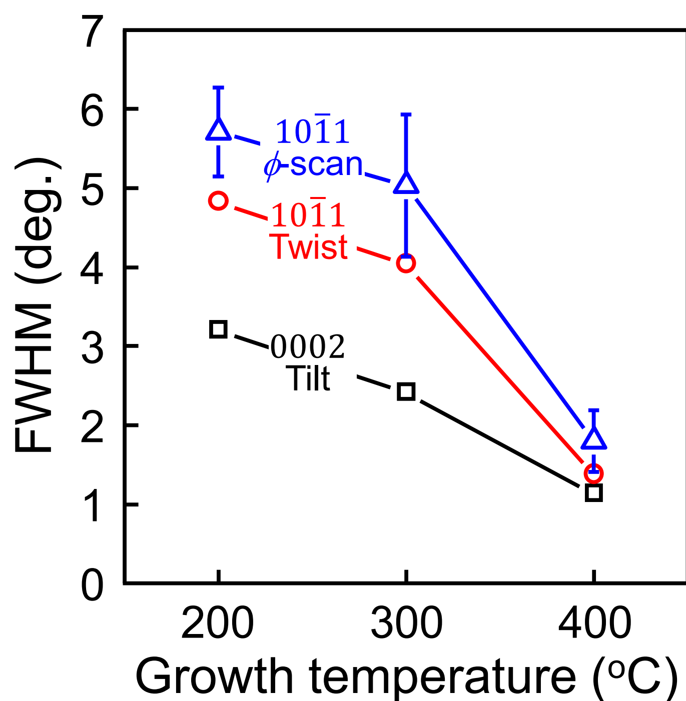

Fig. 4-2. Plot of FWHM values for ω and φ scanned XRD profiles as a function of the T_g. Error bar in $10\bar{1}1$ φ-scan indicates the standard deviation (±σ) of six-folded equivalent diffraction peaks.

Fig. 4-3 (b) – (d) show surface morphologies of ZnO epitaxial films grown on atomically flat sapphire (0001) single crystal substrates. **(a)** Although the growth mode seems to be a typical three-dimensional grain growth mode, the diameter of grain for 400 °C-grown film is approximately 100 nm, which is apparently larger than that of 200 °C- and 300 °C-grown ones (~ 50 nm). These observations support the results described above. (**Fig. 4-2**) Root mean square (RMS) values for 400 °C-grown film is slightly larger than those of other ones despite the film thicknesses are almost the same. This is possibly due to the expansion of grain size.

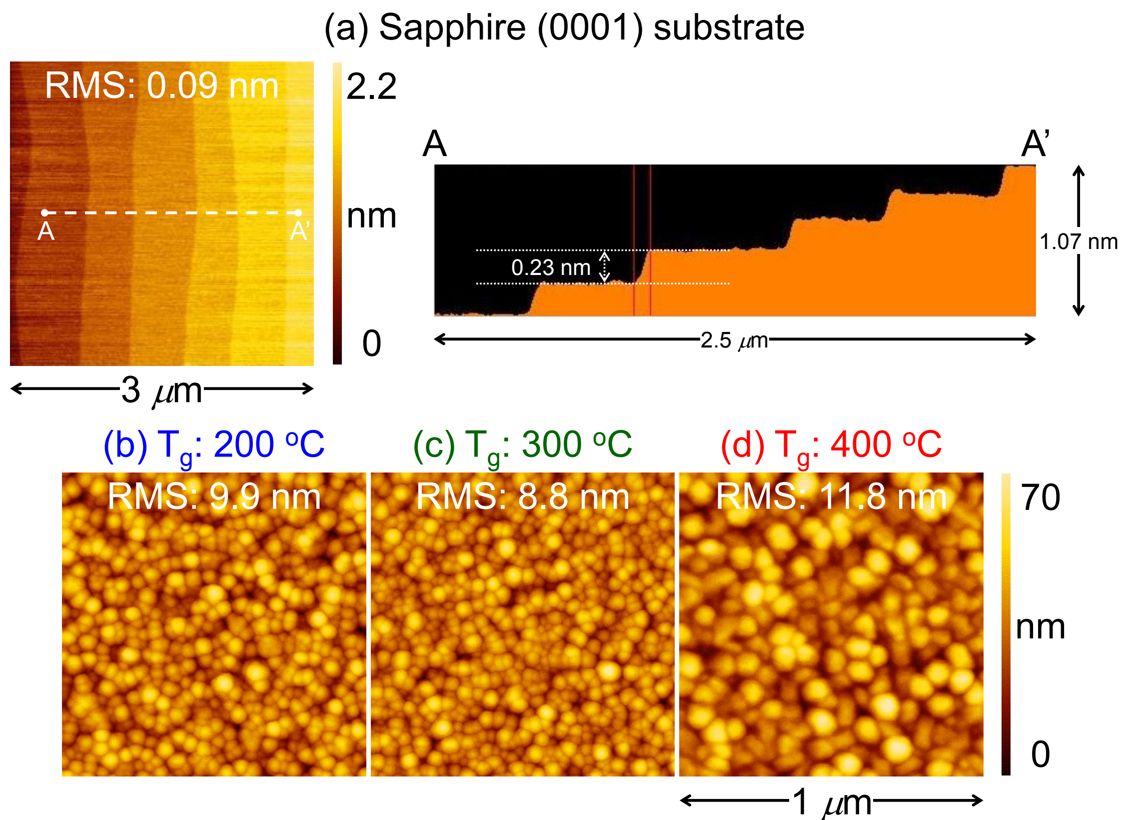

Fig. 4-3. DFM image of sapphire (0001) single crystal substrate after optimum annealing treatment.[33)] **(a)** Single step height of 0.23 nm corresponds to one sixth of c-axis length of sapphire. DFM images of ZnO films grown on the substrate at various T_g. **(b) - (d)**

4-3-2 Optical properties of epitaxial ZnO films

The optical properties of the ZnO epitaxial films were investigated using optical transmittance measurements at wavelengths ranging from 300 to 900 nm (**Fig. 4-4**). The ZnO films show high transmittance above 85% at wavelengths ranging from 400 to 900 nm with no noticeable in-gap absorption, and a sharp basic absorption edge near the bandgap of ZnO. From the oscillation period of the spectrum and the assumed refractive index of 1.95, the film thicknesses of 200 ºC-, 300 ºC- and 400 ºC-grown ZnO films can be determined to be approximately 390, 400 and 350 nm, respectively, which shows good agreement with observations using a cross-sectional scanning electron microscope (SEM) after cleaving the samples. The corresponding growth rate is calculated to be 11 ~ 13 nm/min, which shows small change against the increase of T_g because the CVD is performed in a supply limited region as described in chapter 2. The direct optical bandgap (E_g) is estimated using the following formula (the so-called Tauc plot): [39)]

$$(\alpha E)^2 = A(E - E_g), \tag{4-1}$$

where α, E, and A are the absorption coefficient, photon energy, and constant, respectively. By linear extrapolating the line (inset of **Fig. 4-4**), the values of E_g for 200 ºC-, 300 ºC- and 400 ºC-grown ZnO films are determined to be 3.29, 3.30 and 3.27 eV, respectively, which are close to the bandgap of ZnO at ambient temperature and pressure.[40)] From the above results, the ZnO epitaxial films with good crystallographic and optical transmittance properties were successfully formed by N_2-based nonequilibrium N_2/O_2 plasma generated near AP.

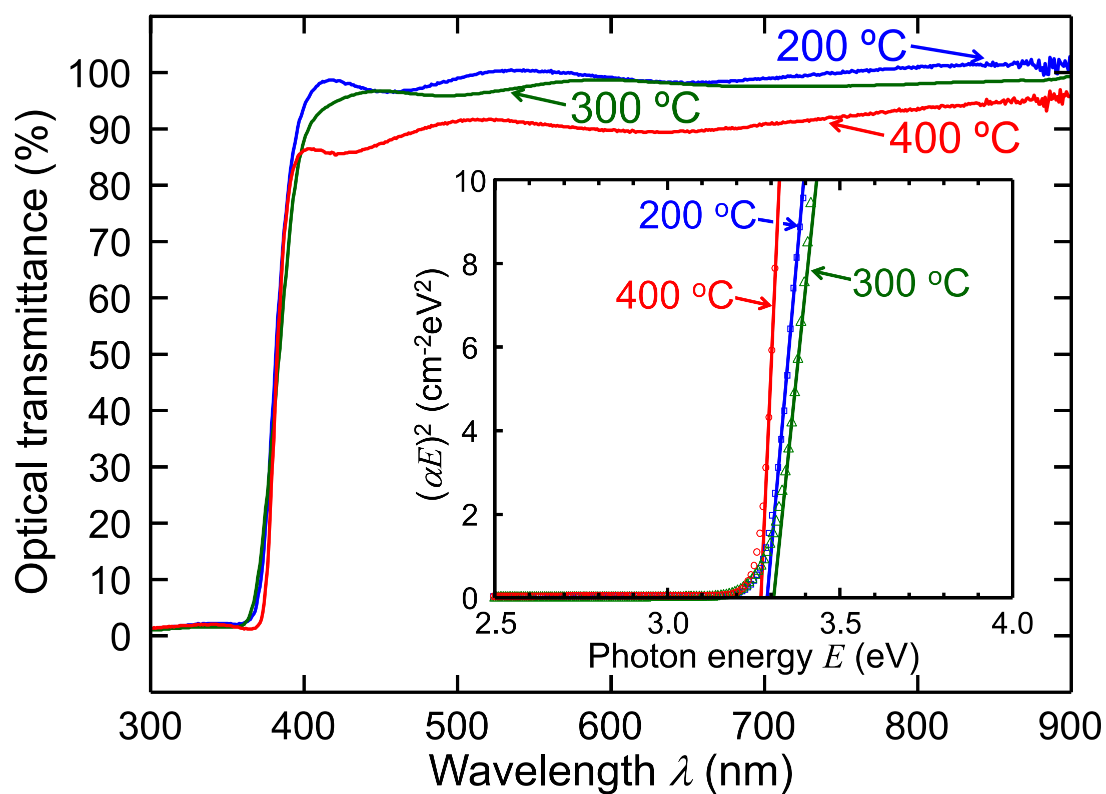

Fig. 4-4. Optical transmittance spectra for ZnO epitaxial films grown at various T_gs. The inset gives the Tauc plot derived from the transmittance spectra.

As a more defect-sensitive method, PL measurement was also carried out. (**Fig. 4-5**) At 300 K (a), PL spectrum of ZnO film grown at 400 °C is dominated by red luminescence (RL) around its mid-gap centered at 1.8 eV (~ 680 nm) with a relatively weak near band edge luminescence (NBL), while those of PLD-grown ZnO film and HYD-grown resistive ZnO single crystal are dominated by green luminescence (GL) and yellow luminescence (YL). GL in ZnO centered at 2.4 eV (~ 520 nm) is generally assigned as oxygen vacancy (V_O)-related emission, which is often observed in nominally un-doped ZnO regardless of the growth methods.[16,20,41] Compared to that, RL in ZnO is poorly understood. Although a few reports exist, RL does not seem to exist naturally, but seems to be created artificially during harsh treatments such as high temperature annealing [42] or electron beam irradiation.[42,43] Knutsen *et al*. have associated the RL centered at 1.75 meV with zinc vacancy (V_{Zn}) acceptor. They performed high energy electron beam irradiation to ZnO single crystal to find that the drastic decrease of residual electron concentration from ~ 10^{16} cm^{-3} to ~ 10^{13} cm^{-3} as well as the enhancement of RL intensity with increasing irradiation energy, supporting that the RL have a nature of acceptor-type intrinsic defects.[42] At a cryogenic temperature of 8.4 K (b), PL measurement was performed again. RL is still predominantly observed for all CVD-grown samples. These results indicate that ZnO epitaxaial films grown by N_2-based nonequilibrium N_2/O_2 plasma generated near AP naturally include V_{Zn} acceptor at as-deposited states, which behaves as efficient radiative recombination center in our CVD-grown ZnO epitaxial films.

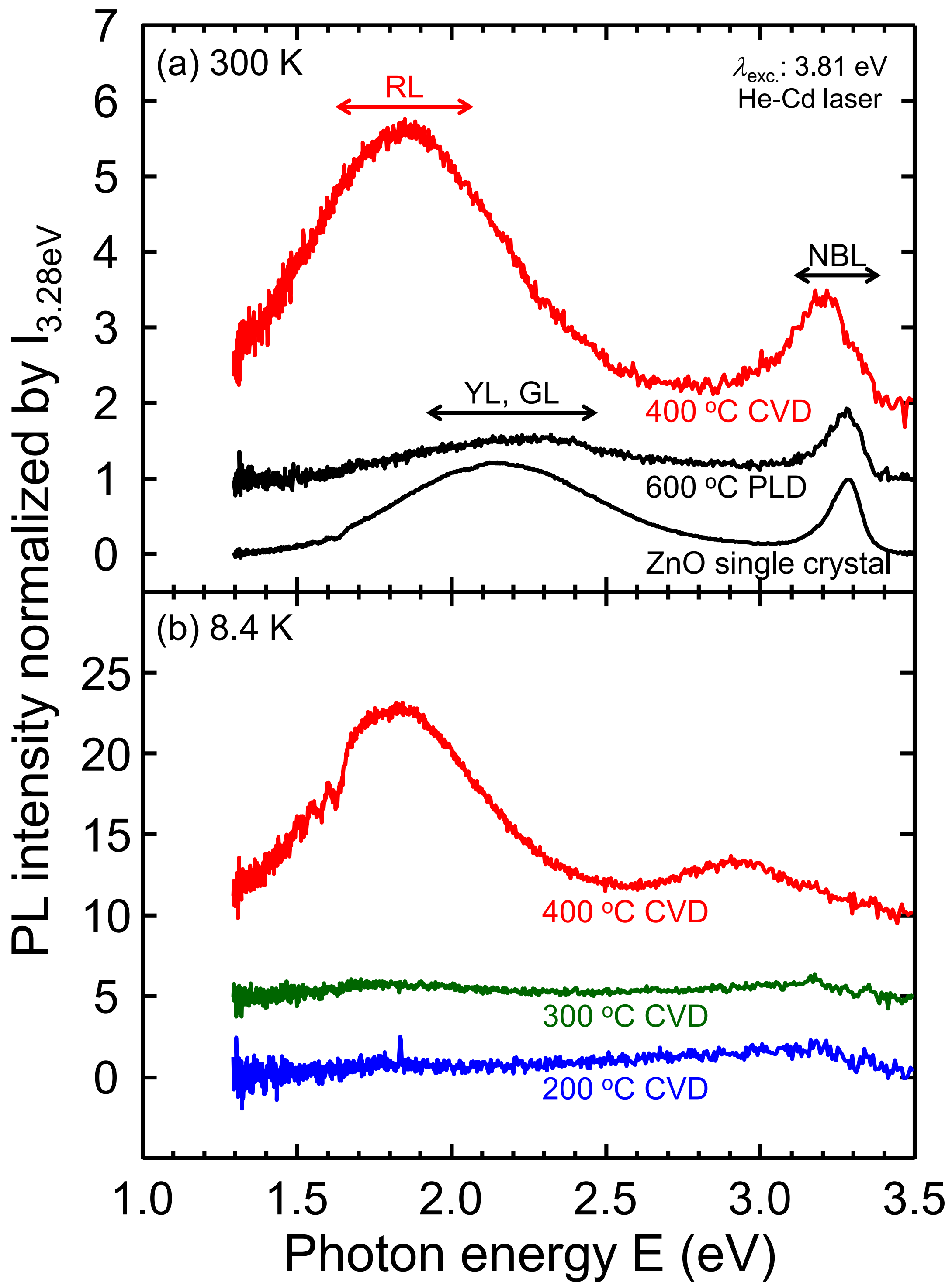

Fig. 4-5. PL spectra of ZnO epitaxial films and single crystal taken at 300 K **(a)** and 8.4 K **(b)**. All spectra are normalized by the PL intensity at 3.28 eV.

4-3-3 Electrical property of ZnO epitaxial films

Hall-effect measurements were performed for ZnO epitaxial films to electrically investigate the electronic states. Prior to the measurement, the samples were processed into Hall-bar structures with a channel length and width of 200 μm and 150 μm, respectively, through standard photolithography consisting of chemical etching of the ZnO films (ITO-02, Kanto Kagaku, 0.1 wt.% for 1 min), electron beam (EB) deposition of Ti(5 nm)/Au(200 nm) Ohmic electrodes (EBG-303, Biemtron Co., Ltd.), and subsequent lift-off techniques in the remover (AZ Products, AZ-700, 80°C). All samples exhibited n-type conduction independent on the T. **Fig. 4-6** shows T dependence of the specific resistivity ρ **(a)**, electron concentration n **(b)** and Hall mobility μ_{Hall} **(c)**. An optical microscope image of a Hall-bar structure and the measurement configurations are also inserted in **Fig. 4-6 (b)**. A PLD-grown sample measured by van der Pauw's method shows low resistivity (~ 2×10^{-1} Ωcm) regardless of the T, due to the high residual shallow donors concentration above 10^{18} cm^{-3}, whereas all CVD-grown samples show high resistivity exceeding 10^{3} Ωcm even at 400 K. The resistivity was too high to obtain a reliable Hall voltage near 300 K. Although the μ_{Hall}s themselves are not so high (0.8 - 4 $cm^2V^{-1}s^{-1}$ at 400 K) probably due to the grain boundary scattering,[44] n are quite low values on the order of 10^{13} to 10^{15} cm^{-3} even at 400 K. It is clear that our process is able to obtain ZnO films with quite low n, which has still been a major challenging issue for the device application of ZnO. From another viewpoint, carrier compensation by acceptors as represented by V_{Zn} must be taken into account. To reveal the origin of such a low residual electron concentration, the T dependence of n was analyzed in detail based on the charge neutral formula.

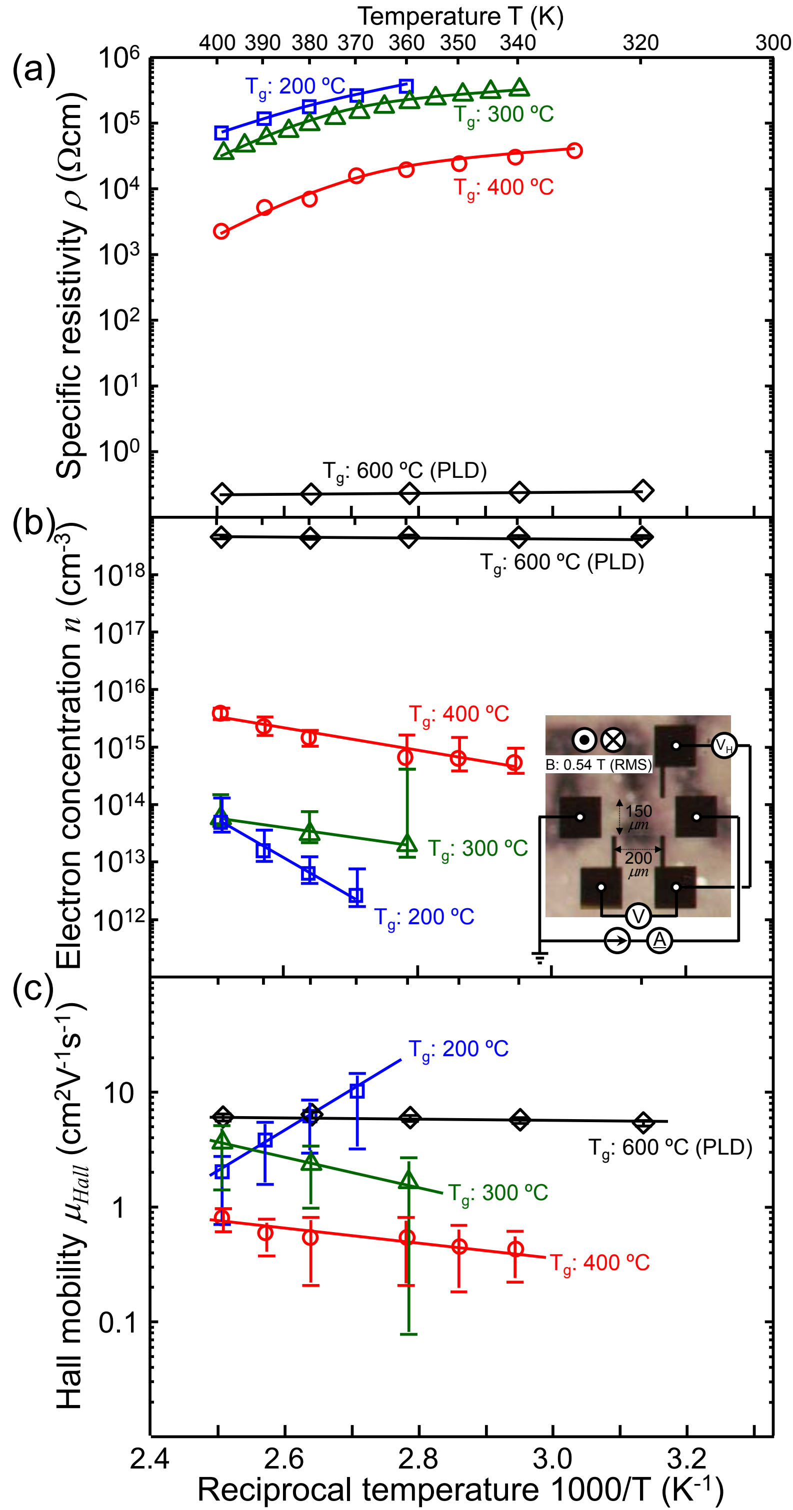

Fig. 4-6. T dependence ρ **(a)**, n **(b)**, and μ_{Hall} **(c)**. Error bars in n **(b)** and μ_{Hall} **(c)** indicate the maximum and minimum value for each temperature measured at an optimized applied current. Optical microscope image and measurement configurations of a five-terminal Hall-bar structure are also shown in **(b)**.

For non-degenerated n-type semiconductors with a single dominant donor level and a negligible free hole concentration, the charge neutral formula can be expressed as:[45,46)]

$$\frac{n(n+N_A^{net})}{N_D-N_A^{net}-n} = \frac{N_C}{2} exp(-\frac{E_C-E_D}{k_B T}), \tag{4-2}$$

where n, N_A^{net}, N_D, $E_C - E_D$, k_B, and T are the free electron concentration, net compensating acceptors concentration, dominant donor concentration, activation energy of the donor level, Boltzmann constant, and absolute temperature, respectively. Here, N_C is an effective density of states of the conduction band:

$$N_C = 2(\frac{2\pi m_e^* m_0 k_B T}{h^2})^{3/2}, \tag{4-3}$$

where $m_e^* m_0$, and h are the effective electron mass and the Planck constant, respectively. In the following calculation, 0.21 m_0 (parallel to the c-axis) is used as an effective mass of the electron.[47)] Also, our n-type ZnO films on sapphire (0001) substrates have quite low n of the order of $10^{13} \sim 10^{15}$ cm^{-3} even at 400 K, which is obtained in a wide process window. These values are lower than that of high quality epitaxial films on sapphire $(11\bar{2}0)$ substrates with smaller lattice mismatch,[48,49)] homoepitaxial films,[50)] and lattice-matched heteroepitaxial films,[51)] despite all of which are obtained as a result of their continuous efforts toward a reduction of the n. Such situations enable the use of an additional approximation:

$$n \ll N_A^{net},\ N_D. \tag{4-4}$$

From Eqs. (4-2) – (4-4), the following equation can be derived.[45,52,53)]

$$nT^{-3/2} = \left(\frac{N_D}{N_A^{net}} - 1\right)\left(\frac{2\pi m_e^* m_0 k_B}{h^2}\right)^{3/2} exp(-\frac{E_C-E_D}{k_B T}). \tag{4-5}$$

According to Eq. (4-5), $nT^{-3/2}$ is plotted against the reciprocal temperature $1000/T$ (**Fig. 4-7**). From the slope and intercept of the solid fitted lines, the activation energy of the dominant donor level (E_D) and the compensation ratio (N_A^{net}/N_D) for each samples are deduced. Although the sample grown at 200 °C is not able to get a reliable fitting result to calculate its compensation ratio, only the donor level is calculated to be (1.19±0.08) eV from the conduction band (E_c). On the other hand, samples grown at 300 and 400 °C show almost the same activation energy of (0.29±0.04) and (0.34±0.05) eV from the E_c, respectively, suggesting that the free electron of these samples come from

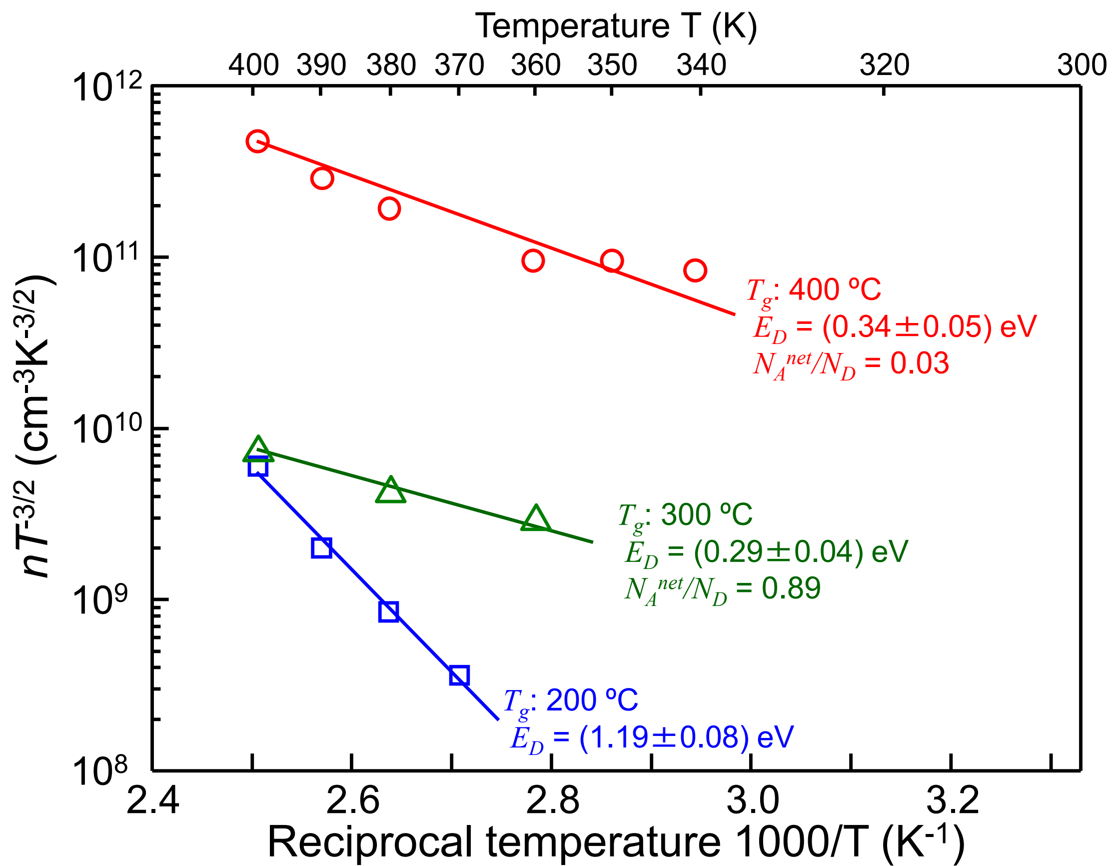

Fig. 4-7. Temperature dependence of the $nT^{-3/2}$ in highly resistive ZnO epitaxial films. Activation energy of the dominant donor level (E_D) and the compensation ratio (N_A^{net}/N_D) are deduced from the slope and intercept of the solid fitted lines, respectively.

the same donor level around E_c − 0.3 eV. In the conventional growth techniques performed in a vacuum such as molecular beam epitaxy (MBE), pulsed laser deposition (PLD), such deep donor is hardly confirmed in Hall-effect measurement unless an introduction of counter (acceptor) dopants due to a large amount of shallow donors in ZnO films. Even in single crystals of ZnO, such deep donor is hardly observed in Hall-effect measurement unless the compensation of shallow donors by Li acceptor.[54,55] Moreover, n at 300 K (n_{300K}) for 400 °C-grown sample is estimated to be as low as 7×10^{13} cm^{-3} by the extrapolation of the fitted line despite its low N_A^{net}/N_D for semiconductor materials.[54)] These results indicates that nonequilibrium N_2/O_2 plasma generated near AP is effective for the suppression of not only residual electron but also shallow donors in ZnO, which still has been the most critical issue for the practical application of ZnO-based devices. For 400 °C-grown sample, the slope seems to change at the T around 370 K, suggesting that the change of dominant donor level should be taken into account just in case. Assuming the existence of two dominant donor levels, those activation energies (E_{D1} and E_{D2}) are calculated to be 70 and 590 meV, respectively, both of which are apparently larger than the thermal energy of measurement temperature (k_BT, T = 340 ~ 400 K). Moreover, their compensation ratios (N_A^{net}/N_{D1} and N_A^{net}/N_{D2}) are calculated to be 0.996 and 2×10^{-5}, respectively. These fitting results support the former discussion that nonequilibrium N_2/O_2 plasma generated near AP is effective for the suppression of not only residual electron but also shallow donors in ZnO.

To return to Eq. (4-2), numerical calculation was performed as N_D variable, and as E_D and N_A^{net}/N_D constants.[46)] Although we could not get a higher limit of N_D due to the absence of Hall-effect measurements more than 400 K, lower limit of N_D could be estimated: $N_D \gtrsim 10^{16}$ cm^{-3} for 300 °C-grown film and $N_D \gtrsim 10^{18}$ cm^{-3} for 400 °C-grown film. Additionally, the compensation ratio N_A^{net}/N_D tends to increase with decreasing the T_g, signaling the change of defect or impurity concentration. That for 300 °C-grown sample is close to unity, indicating a nearly full compensation. However, the carrier type conversion from n-type to p-type against the decrease of T_g from 300 to 200 °C is not confirmed, which can be explained by the appearance of additional deeper donor located at E_c - 1.2 eV.

4-3-4 Extrinsic impurities and nitrogen acceptors

SIMS measurement was performed to get information on the extrinsic impurities in ZnO film, those are possible candidates of donor and acceptor. Cesium ion (Cs^+) was used as a primary ion. **Fig. 4-8** shows depth profiles of hydrogen (H), carbon (C), nitrogen (N) and silicon (Si) in ZnO films. H (m/z = 1), C (m/z = 12), NO (m/z = 30) and Si (m/z = 28) is used as secondary ions for the quantification of H, C, N and Si, respectively. Isotope ratio (^{28}Si : ^{29}Si : ^{30}Si) is taken into account in the quantification of N to eliminate the interference effects between ^{30}NO and ^{30}Si. For all impurities, their concentrations naturally tend to decrease with increasing the T_g. Note that the depth profile and concentration of 200 °C- and 300 °C-grown ZnO films are similar to each other despite the activation energies of dominant donor are obviously different between these samples, suggesting that the dominant deep donors in our samples are not extrinsic impurities such as carbon [56,57] or silicon,[58,59] but an intrinsic defects. Recently, H has believed to be the origin of shallow donor in ZnO,[20,60] it does not seem to behave as a shallow donor, because dominant donor supplying free electron to the conduction band is "deep donor" in our case. On the other hand, nitrogen, a representative candidate of compensating acceptor, uniformly distributes along depth direction regardless of the T_g. In order to clarify the contribution of nitrogen to carrier compensation, chemical bonding state of nitrogen must be investigated for the epitaxial films discussed here.

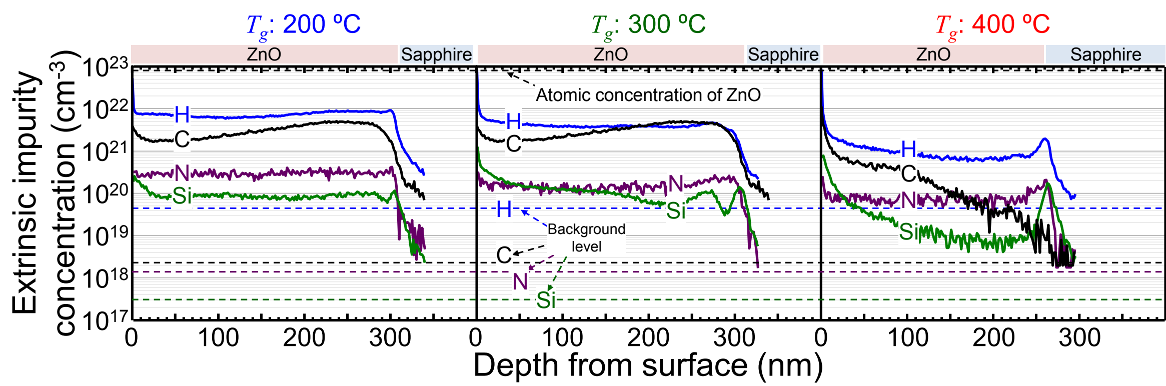

Fig. 4-8. SIMS profiles for ZnO epitaxial films grown at various T_g. Cs^+ is used as a primary ion. Background levels of each element are determined using standard ZnO film.

Fig. 4-9 (a) shows Micro Raman spectra for ZnO films grown at various T_g. As a host vibration mode, ZnO E_2(high) is predominantly observed at 438 cm^{-1} for all samples, because our Raman measurement is performed for ZnO films with (0001) preferred orientation using backscattering configuration.[16)] In addition to the vibration modes of host ZnO and sapphire substrate, local vibration modes (LVMs) are observed at 275 and 582 cm^{-1}, both of which are not confirmed at all in PLD-grown nominally nitrogen-free ZnO films. These LVMs are generally attributed to nitrogen substituting oxygen site (N_O) acceptor.[16)] Kaschner *et al*. proposed non-destructive and quantitative evaluation of nitrogen concentration using linear relationship between nitrogen concentration and intensity ratio, $I_{LVM} / I_{E2(high)}$.[61)] **Fig. 4-9 (b)** is change in the integrated intensity ratio, $I_{LVM} / I_{E2(high)}$, as a function of nitrogen concentration determined by SIMS measurements according to their proposal. Voigt function was used for the peak fitting and separation after the removal of linear background. $I_{LVM} / I_{E2(high)}$ for both LVMs of 275 and 582 cm^{-1} show linear relationship against the change of nitrogen concentration, and their magnitude relation [$I_{275} / I_{E2(high)} < I_{582} / I_{E2(high)}$] agree with the report given by Kaschner *et al.*,[61)] indicating that N_O acceptor certainly exist in our ZnO films. However, the slopes in **Fig. 4-9 (b)** [3.0×10^{-21} /cm^{-3} for $I_{582} / I_{E2(high)}$ and 4.8×10^{-22} /cm^{-3} for $I_{275} / I_{E2(high)}$] are approximately 0.065 and 0.028 times smaller than Kaschner's report despite the nitrogen concentration of our ZnO films are one or two order of magnitude higher than their ZnO:N films,[61)] suggesting that only a small portion of nitrogen behaves as N_O acceptor in our sample thus they are not a dominant compensating acceptor.

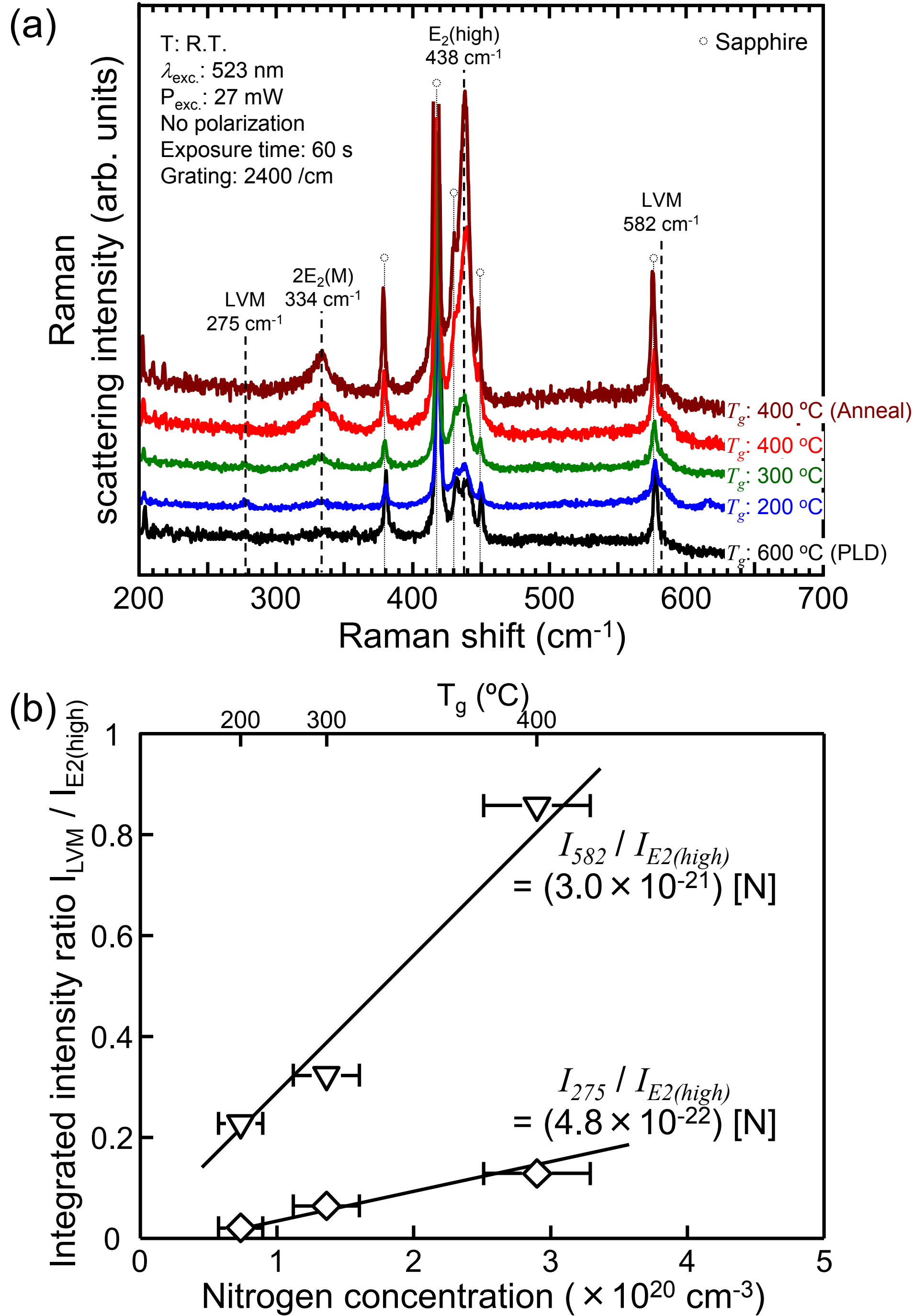

Fig. 4-9. Micro Raman spectra of epitaxial ZnO films on sapphire (0001) substrate grown at various T_g **(a)**. PDA (700 ºC, 10 min, O_2 flow) was performed for 400 ºC grown sample. Change in the integrated intensity ratio, I_{LVM} / $I_{E2(high)}$, as a function of nitrogen concentration determined by SIMS measurements, **(b)**. Error bars along the horizontal axis indicate standard deviation of nitrogen concentration at the depth of 100 – 200 nm from the surface.

In fact, we performed post deposition annealing (PDA) using rapid thermal annealing (RTA) system (700 °C, under O_2 flow for 10 min) for another piece of 400 °C-grown ZnO epitaxial film after cleaving the sample. [**Fig. 4-9 (a)**] The LVMs of N_O acceptor are observed in the as-grown state, whereas those disappear after the PDA treatment. On the other hand, van der Pauw's method revealed that this piece had a high specific resistivity of 1.5×10^5 Ωcm at 300 K even after the PDA treatment, which is almost equal to the extended line of **Fig. 4-6 (a)**. Although it has also reported that nitrogen-related complex defects are easily formed in N-doped ZnO such as NC [62,63] or NN,[62,64-67] such signal was not detected at all in Raman spectra taken over a wide wavenumber before and after PDA,[68] and in synchrotron radiation photoemission spectrum (SR-PES) of N1s orbital for as deposited sample.[69] Considering the flat distribution of nitrogen concentration regardless of the T_g as shown in **Fig. 4-8**, most of the nitrogen might exist in the lattice of host ZnO as some stable state.

4-3-5 Electronic state of highly resistive ZnO films

Based on PL measurement (**Fig. 4-5**), Hall-effect measurement (**Fig. 4-6** and **Fig. 4-7**), SIMS measurement (**Fig. 4-8**) and Micro Raman spectroscopy (**Fig. 4-9**), the electronic states of our highly resistive ZnO films can be illustrated as **Fig. 4-10**. In case of ZnO film grown by vacuum processes (PLD) and HYD-grown ZnO single crystal, V_O-related deep radiative recombination center (GL and YL) exists close to the conduction band (CB) side.[20] On the other hand, our highly resistive ZnO films contain V_{Zn}-related one around its mid-gap, which act as an efficient recombination center (RL).[42] At a quasi-equilibrium state (low electric field) such as Hall-effect measurement, shallow donors (Zn_i or H etc.) dominate the conductivity of ZnO film with low resistivity grown by vacuum processes (PLD), whereas they do not dominate the conductivity of our highly resistive ZnO films. Partially filled deep donors around 1.2 eV and 0.3 eV from the conduction band minimum should play important roles in the generation of free electron and contribute to their low conductivities. On the other hand, representative deep acceptors such as V_{Zn} and N_O should compensate residual donors and completely be filled by electron from the donors. Even assuming that shallow donors coexist in the highly resistive ZnO films, it is considered that the shallow donors should be preferentially and fully compensated to reduce the entire energy (Fermi energy). Such a complex situation with multiple donors is schematically illustrated and discussed in several literatures.[70-73] [In case of ZnO, see Fig. 1 in ref.[73]] In our highly resistive ZnO films, free electron from shallow donors should never exist because the concentration of n-type carrier is as low as 10^{13} - 10^{15} cm^{-3} even at 400 K. Therefore, the concentration of shallow donors should be less than N_A^{net} (~ $0.89E_D$ and ~ $0.03E_D$

for 300 ºC- and 400 ºC-grown ZnO films, respectively). These results suggest that N_2-based nonequilibrium N_2/O_2 plasma generated near AP is effective in suppressing not only residual electron but also shallow donors in ZnO.

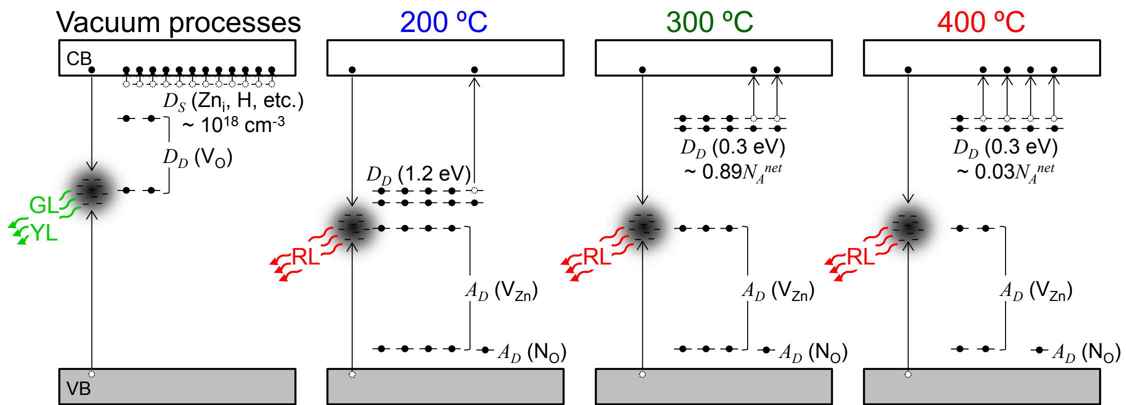

Fig. 4-10. Schematic illustrations of the electronic states for ZnO films discussed here. The words CB, VB, D_S, D_D, A_D, Zn_i, H, V_O, V_{Zn}, N_O, GL, YL and RL in this figure denote the conduction band, valence band, shallow donor, deep donor, deep acceptor, zinc interstitial, hydrogen, oxygen vacancy, zinc vacancy, nitrogen substituting oxygen site, green luminescence, yellow luminescence and red luminescence, respectively.

4-4 Conclusions

In conclusions, we have successfully grown ZnO epitaxial films on sapphire (0001) substrate free from the incorporation of noticeable 30° rotational domain using N_2-based nonequilibrium N_2/O_2 plasma generated near AP with the specific O_2% of 20% that is discovered in chapter 3.[31)] The ZnO epitaxial films exhibited high transmittance above 85% at the wavelengths ranging from 400 to 900 nm, and a sharp basic absorption edge corresponding to the optical bandgap of ZnO.[40)] On the other hand, PL spectra of our films are dominated by red luminescence (RL) centered at 1.8 eV possibly originate from zinc vacancy (V_{Zn}) acceptor acting as an efficient radiative recombination center, which does not exist naturally but artificially created by some intentional damage.[42)] Hall-effect measurement revealed that these films are highly resistive because of an extremely low residual electron concentration originate from the suppression of shallow donors. As a result, extremely low free electron concentration of 10^{13} - 10^{15} cm^{-3} was achieved even at 400 K. Although temperature-dependent Hall-effect measurement involving SIMS measurement and Raman measurement revealed carrier compensation by acceptors possibly originate from V_{Zn} or N_O, the concentration of shallow donors should be less than N_A^{net} (~ $0.89E_D$ and ~ $0.03E_D$ for 300 ºC- and 400 ºC-grown samples, respectively). These results indicate that N_2-based nonequilibrium N_2/O_2 plasma near AP is the effective method to suppress not only the residual electron but also the shallow donors in ZnO, which had been the most critical issue for practical applications of ZnO-based devices.

References

1) D. C. Reynolds, D. C. Look, and B. Jogai, Optically pumped ultraviolet lasing from ZnO, *Solid State Commun.* **99**, 873 (1996).
2) D. M. Bagnall, Y. F. Chen, Z. Zhu, T. Yao, M. Y. Shen, and T. Goto, High temperature excitonic stimulated emission from ZnO epitaxial layers, *Appl. Phys. Lett.* **73**, 1038 (1998).
3) T. Dietl, H. Ohno, F. Matsukura, J. Cibert, and D. Ferrand, Zener Model Description of Ferromagnetism in Zinc-Blende Magnetic Semiconductors, *Science* **287**, 1019 (2000).
4) T. Edahiro, N. Fujimura, and T. Ito, Formation of two-dimensional electron gas and the magnetotransport behavior of ZnMnO/ZnO heterostructure, *J. Appl. Phys.* **93**, 7673 (2003).
5) S. Ghosh, V. Sih, W. H. Lau, D. D. Awschalom, S.-Y. Bae, S. Wang, S. Vaidya, and G. Chapline, Room-temperature spin coherence in ZnO, *Appl. Phys. Lett.* **86**, 232507 (2005).
6) M. Nakano, T. Makino, A. Tsukazaki, K. Ueno, A. Ohtomo, T. Fukumura, H. Yuji, Y. Nishimoto, S. Akasaka, D. Takamizu, K. Nakahara, T. Tanabe, A. Kamisawa, and M. Kawasaki, $Mg_xZn_{1-x}O$-Based Schottky Photodiode for Highly Color-Selective Ultraviolet Light Detection, *Appl. Phys. Express* **1**, 121201 (2008).
7) K. Nakahara, S. Akasaka, H. Yuji, K. Tamura, T. Fujii, Y. Nishimoto, D. Takamizu, A. Sasaki, T. Tanabe, H. Takasu, H. Amaike, T. Onuma, S. F. Chichibu, A. Tsukazaki, A. Ohtomo, and M. Kawasaki, Nitrogen doped $Mg_xZn_{1-x}O$/ZnO single heterostructure ultraviolet light-emitting diodes on ZnO substrates, *Appl. Phys. Lett.* **97**, 013501 (2010).
8) K. Sato, L. Bergqvist, J. Kudrnovsky, P. H. Dederichs, O. Eriksson, I. Turek, B. Sanyal, G. Bouzerar, H. Katayama-Yoshida, V. A. Dinh, T. Fukushima, and H. Kizaki, First-principles theory of dilute magnetic semiconductors, *Rev. Mod. Phys.* **82**, 1633 (2010).
9) Aleksandra B. Djurisic, Xinyi Chen, Yu Hang Leung, and Alan Man Ching Ng, ZnO nanostructures: growth, properties and applications, *J. Mater. Chem.* **22**, 6526 (2012).
10) Y. Kozuka, A. Tsukazaki, and M. Kawasaki, Challenges and opportunities of ZnO-related single crystalline heterostructures, *Appl. Phys. Rev.* **1**, 011303 (2014).
11) J. Falson, Y. Kozuka, J. H. Smet, T. Arima, A. Tsukazaki, and M. Kawasaki,

Electron scattering times in ZnO based polar heterostructures, *Appl. Phys. Lett.* **107**, 082102 (2015).

12) J. Falson, Y. Kozuka, A. Tsukazaki, and M. Kawasaki, Two-dimensional quantum transport in high-quality ZnO heterointerfaces, *OYO BUTURI* **84**, 984 (2015) [in Japanese].

13) J. D. Albrecht, P. P. Ruden, S. Limpijumnong, W. R. L. Lambrecht, and K. F. Brennan, High field electron transport properties of bulk ZnO, *J. Appl. Phys.* **86**, 6864 (1999).

14) K. Maeda, M. Sato, I. Niikura, and T. Fukuda, Growth of 2 inch ZnO bulk single crystal by the hydrothermal method, *Semicond. Sci. Tech.* **20**, S49 (2005).

15) B. Gil, D. Felbacq, and S. F. Chichibu, Exciton binding energies in chalcopyrite semiconductors, *Phys. Rev. B* **85**, 075205 (2012).

16) Ü. Özgür, Ya. I. Alivov, C. Liu, A. Teke, M. A. Reshchikov, S. Doğan, V. Avrutin, S.-J. Cho, and H. Morkoç, A comprehensive review of ZnO materials and devices, *J. Appl. Phys.* **98**, 041301 (2005).

17) H. Hosono, Recent progress in transparent oxide semiconductors: Materials and device application, *Thin Solid Films* **515**, 6000 (2007).

18) N. W. Emanetoglu, J. Zhu, Y. Chen, J. Zhong, Y. Chen, and Y. Lu, Surface acoustic wave ultraviolet photodetectors using epitaxial ZnO multilayers grown on r-plane sapphire, *Appl. Phys. Lett.* **85**, 3702 (2004).

19) R. Triboulet, J. Perriere, Epitaxial growth of ZnO films, *Prog. Cryst. Growth Charact.* **47**, 65 (2003).

20) M. D. McCluskey, and S. J. Jokela, Defects in ZnO, *J. Appl. Phys.* **106**, 071101 (2009).

21) A. Janotti, and C. G. Van de Walle, Native point defects in ZnO, *Phys. Rev. B* **76**, 165202 (2007).

22) T. Kawaharamura, H. Nishinaka, and S. Fujita, Growth of Crystalline Zinc Oxide Thin Films by Fine-Channel-Mist Chemical Vapor Deposition, *Jpn. J. Appl. Phys.* **47**, 4669-4675 (2008).

23) S. Akasaka, K. Nakahara, A. Tsukazaki, A. Ohtomo, and M. Kawasaki, $Mg_xZn_{1-x}O$ Films with a Low Residual Donor concentration (<10^{15} cm^{-3}) Grown by Molecular Beam Epitaxy, *Appl. Phys. Express* **3**, 071101 (2010).

24) K. Sasaki, A. Kuramata, T. Masui, E. G. Villora, K. Shimamura, and S. Yamakoshi, Device-Quality β-Ga_2O_3 Epitaxial Films Fabricated by Ozone Molecular Beam

Epitaxy, *Appl. Phys. Express* **5**, 035502 (2012).

25) T. Kawaharamura, T. Uchida, D. Wang, M. Sanada, and M. Furuta, Enhancing carrier mobility of IGZO TFT fabricated by non-vacuum mist CVD with O_3 assistance, *Phys. Stat. Sol. C* **10**, 1565 (2013).

26) M. Iwasaki, H. Inui, Y. Matsudaira, H. Kano, N. Yoshida, M. Ito, and M. Hori, Nonequilibrium atmospheric pressure plasma with ultrahigh electron density and high performance for glass surface cleaning, *Appl. Phys. Lett.* **92**, 081503 (2008).

27) R. Hayakawa, T. Yoshimura, A. Ashida, T. Uehara, and N. Fujimura, Reaction of Si with excited nitrogen species in pure nitrogen plasma near atmospheric pressure, *Thin Solid Films* **506-507**, 423 (2006).

28) R. Hayakawa, M. Nakae, T. Yoshimura, A. Ashida, N. Fujimura, T. Uehara, M. Tagawa, Y. Teraoka, Detailed structural analysis and dielectric properties of silicon nitride film fabricated using pure nitrogen plasma generated near atmospheric pressure, *J. Appl. Phys.* **100**, 073710 (2006).

29) R. Hayakawa, M. Yoshida, K. Ide, Y. Yamashita, H. Yoshikawa, K. Kobayashi, S. Kunugi, T. Uehara, and N. Fujimura, Structural analysis and electrical properties of pure Ge_3N_4 dielectric layers formed by an atmospheric-pressure nitrogen plasma, *J. Appl. Phys.* **110**, 064103 (2011).

30) R. Hayakawa, T. Yoshimura, A. Ashida, H. Kitahata, M. Yuasa, and N. Fujimura, Formation of Silicon Oxynitride Films with Low Leakage Current Using N_2/O_2 Plasma near Atmospheric Pressure, *Jpn. J. Appl. Phys.* **43**, 7853 (2004).

31) Y. Nose, T. Nakamura, T. Yoshimura, A. Ashida, T. Uehara, and N. Fujimura, Orientation Control of ZnO Films Deposited Using Nonequilibrium Atmospheric Pressure N_2/O_2 Plasma, *Jpn. J. Appl. Phys.* **52**, 01AC03 (2013).

32) Y. Nose, T. Yoshimura, A. Ashida, T. Uehara, and N. Fujimura, submitted to *Thin Solid Films*.

33) M. Yoshimoto, T. Maeda, T. Ohnishi, H. Koinuma, O. Ishiyama, M. Shinohara, M. Kubo, R. Miura, and A. Miyamoto, Atomic-scale formation of ultrasmooth surfaces on sapphire substrates for high-quality thin-film fabrication, *Appl. Phys. Lett.* **67**, 2615 (1995).

34) Y. Nose, T. Yoshimura, A. Ashida, T. Uehara, and N. Fujimura, Low Temperature Growth of ZnO Thin Films by Non-Equilibrium Atmospheric Pressure N_2/O_2 Plasma and the Growth Morphology of the Films, *Zairyo* **61**, 756 (2012).

35) B. Zhang, L. Manh, K. Wakatsuki, K. Tamura, T. Ohnishi, M. Lippmaa, N. Usami, M. Kawasaki, H. Koinuma, and Y. Segawa, In-Plane Orientation and Polarity of ZnO Epitaxial Films on As-Polished Sapphire (α-Al_2O_3) (0001) Substrates Grown by Metal Organic Chemical Vapor Deposition, *Jpn. J. Appl. Phys.* **42**, L264 (2003).
36) S. Akiyama, K. Minegishi, T. Tanaka, H. Ogawa, and M. Kasuga, Effects of Sapphire Substrate Preparation on ZnO Epitaxial Growth by Atmospheric-Pressure Metal Organic Chemical Vapor Deposition, *Jpn. J. Appl. Phys.* **46**, 342 (2007).
37) H. Heinke, V. Kirchner, S. Einfeldt, and D. Hommel, X-ray diffraction analysis of the defect structure in epitaxial GaN, *Appl. Phys. Lett.* **77**, 2145 (2000).
38) A. Krost, J. Christen, N. Oleynik, A. Dadgar, S. Deiter, J. Bläsing, A. Krtschil, D. Forster, F. Bertram, and A. Diez, Ostwald ripening and flattening of epitaxial ZnO layers during in situ annealing in metalorganic vapor phase epitaxy, *Appl. Phys. Lett.* **85**, 1496 (2004).
39) M. Fox, *Optical Properties of Solids* (Oxford Univ. Press, 2001) p. 58.
40) V. Srikant, and D. R. Clarke, On the optical band gap of zinc oxide, *J. Appl. Phys.* **83**, 5447 (1998).
41) K. Vanheusden, W. L. Warren, C. H. Seager, D. R. Tallant, J. A. Voigt, and B. E. Gnade, Mechanisms behind green photoluminescence in ZnO phosphor powders, *J. Appl. Phys.* **79**, 7983 (1996).
42) K. E. Knutsen, A. Galeckas, A. Zubiaga, F. Tuomisto, G. C. Farlow, B. G. Svensson, and A. Yu. Kuznetsov, Zinc vacancy and oxygen interstitial in ZnO revealed by sequential annealing and electron irradiation, *Phys. Rev. B* **86**, 121203(R) (2012).
43) M. A. Reshchikov, H. Morkoc, B. Nemeth, J. Nause, J. Xie, B. Hertog, and A. Osinsky, Luminescence properties of defects in ZnO, *Physica B* **401-402**, 358 (2007).
44) T. Yamada, H. Makino, N. Yamamoto, and T. Yamamoto, Ingrain and grain boundary scattering effects on electron mobility of transparent conducting polycrystalline Ga-doped ZnO films, *J. Appl. Phys.* **107**, 123534 (2010).
45) S. M. Sze, and Kwok K. Ng, *Physics of Semiconductor Devices Third Edition* (Wiley, New York, 2007) p. 22.
46) T. Oishi, Y. Koga, K. Harada, and M. Kasu, High-mobility β-$Ga_2O_3(\bar{2}01)$ single crystals grown by edge-defined film-fed growth method and their Schottky barrier diodes with Ni contact, *Appl. Phys. Express* **8**, 031101 (2015).

47) W. R. L. Lambrecht, A. V. Rodina, S. Limpijumnong, B. Segall, and B. K. Meyer, Valence-band ordering and magneto-optic exciton fine structure in ZnO, *Phys. Rev. B* **65**, 075207 (2002).

48) H. Nishiyama, H. Miura, K. Yasui, and Y. Inoue, Fabrication of high-electron mobility ZnO epilayers by chemical vapor deposition using catalytically produced excited water, *J. Cryst. Growth* **312**, 483 (2010).

49) K. Yasui, T. Takeuchi, E. Nagatomi, S. Satomoto, H. Miura, T. Kato, T. Konya, Properties of zinc oxide films grown on sapphire substrates using high-temperature H_2O generated by a catalytic reaction on platinum nanoparticles, *J. Vac. Sci. Tech. A* **32**, 021502 (2014).

50) H. Kato, M. Sano, K. Miyamoto, and T. Yao, High-quality ZnO epilayers grown on Zn-face ZnO substrates by plasma-assisted molecular beam epitaxy, *J. Cryst. Growth* **265**, 375 (2004).

51) K. Tamura, A. Ohtomo, K. Saikusa, Y. Osaka, T. Makino, Y. Segawa, M. Sumiya, S. Fuke, H. Koinuma, and M. Kawasaki, Epitaxial growth of ZnO films on lattice-matched $ScAlMgO_4$ (0001) substrates, *J. Cryst. Growth* **214/215**, 59 (2000).

52) A. Tsukazaki, A. Ohtomo, T. Onuma, M. Ohtani, T. Makino, M. Sumiya, K. Ohtani, S. F. Chichibu, S. Fuke, Y. Segawa, H. Ohno, H. Koinuma, and M. Kawasaki, Repeated temperature modulation epitaxy for p-type doping and light-emitting diode based on ZnO, *Nat. Mater.* **4**, 42 (2005).

53) S. T. Tan, X. W. Sun, Z. G. Yu, P. Wu, G. Q. Lo, and D. L. Kwong, p-type conduction in unintentional carbon-doped ZnO thin films, *Appl. Phys. Lett.* **91**, 072101 (2007).

54) D. C. Look, Recent advances in ZnO materials and devices, *Mater. Sci. Eng. B* **80**, 383 (2001).

55) S. Graubner, C. Neumann, N. Volbers, B. K. Meyer, J. Bläsing, and A. Krost, Preparation of ZnO substrates for epitaxy: Structural, surface, and electrical properties, *Appl. Phys. Lett.* **90**, 042103 (2007).

56) K. Matsumoto, K. Kuriyama, and K. Kushida, Electrical and photoluminescence properties of carbon implanted ZnO bulk single crystals, *Nucl. Instrum. Methods Phys. Res. B* **267**, 1568 (2009).

57) Y. Izawa, K. Matsumoto, T. Oga, K. Kuriyama, K. Kushida, and A. Kinomura, Evaluation of Carbon Interstitial in C-ion Implanted ZnO Bulk Single Crystals by a

Nuclear Reaction Analysis Study: An Origin of Low Resistivity, *AIP Conf. Proc.* **1399**, 69 (2011).

58) T. Minami, H. Sato, H. Nanto, and S. Takada, Highly Conductive and Transparent Silicon Doped Zinc Oxide Thin Films Prepared by RF Magnetron Sputtering, *Jpn. J. Appl. Phys.* **25**, L776 (1986).

59) A. K. Das, P. Misra, and L. M. Kukreja, Effect of Si doping on electrical and optical properties of ZnO thin films grown by sequential pulsed laser deposition, *J. Phys. D: Appl. Phys.* **42**, 165405 (2009).

60) C. G. Van de Walle, Defect analysis and engineering in ZnO, *Physica B* **308-310**, 899 (2001).

61) A. Kaschner, U. Haboeck, M. Strassburg, M. Strassburg, G. Kaczmarczyk, A. Hoffmann, C. Thomsen, A. Zeuner, H. R. Alves, D. M. Hofmann, and B. K. Meyer, Nitrogen-related local vibrational modes in ZnO:N, *Appl. Phys. Lett.* **80**, 1909 (2002).

62) S. Limpijumnong, X. Li, S.-H. Wei, and S. B. Zhang, Substitutional diatomic molecules NO, NC, CO, N_2, and O_2: Their vibrational frequencies and effects on *p* doping of ZnO, *Appl. Phys. Lett.* **86**, 211910 (2005).

63) I. Volintiru, M. Creatore, W. H. van Helvoot, J. L. Linden, and M. C. M. van de Sanden, Nitrogen incorporation during metal organic chemical vapor deposition of ZnO films using a remote Ar/N_2 plasma, *Appl. Phys. Lett.* **89**, 022110 (2006).

64) J. Gao, R. Qin, G. luo, J. Lu, Y. Leprince-Wang, H. Ye, Z. Liao, Q. Zhao, and D. Yu, First-principles study of the formation mechanisms of nitrogen molecule in annealed ZnO, *Phys. Lett. A* **374**, 3546 (2010).

65) P. Fons, H. Tampo, A. V. Kolobov, M. Ohkubo, S. Niki, J. Tominaga, R. Carboni, F. Boscherini, and S. Friedrich, Direct Observation of Nitrogen Location in Molecular Beam Epitaxy Grown Nitrogen-Doped ZnO, *Phys. Rev. Lett.* **96**, 045504 (2006).

66) Z. P. Wei, Y. M. Lu, D. Z. Shen, Z. Z. Zhang, B. Yao, B. H. Li, J. Y. Zhang, D. X. Zhao, X. W. Fan, and Z. K. Tang, Room temperature *p-n* ZnO blue-violet light-emitting diodes, *Appl. Phys. Lett.* **90**, 042113 (2007).

67) H. Kato, T. Yamamuro, A. Ogawa, C. Kyotani, and M. Sano, Impact of Mixture Gas Plasma of N_2 and O_2 as the N Source on ZnO-Based Ultraviolet Light-Emitting Diodes Fabricated by Molecular Beam Epitaxy, *Appl. Phys. Express* **4**, 091105 (2011).

68) A. Soudi, E. H. Khan, J. T. Dickinson, and Y. Gu, Observation of unintentionally incorporated nitrogen-related complexes in ZnO and GaN nanowires, *Nano Lett.* **9**, 1844 (2009).

69) C. L. Perkins, S.-H. Lee, X. Li, S. E. Asher, and T. J. Coutts, Identification of nitrogen chemical states in N-doped ZnO via x-ray photoelectron spectroscopy, *J. Appl. Phys.* **97**, 034907 (2005).

70) D. C. Look, J. R. Sizelove, Equivalence of Donor and Acceptor Fits of Temperature-Dependent Carrier-Concentration Data, *J. Appl. Phys.* **61**, 1650 (1987).

71) D. C. Look, Equivalence of donor and acceptor fits to temperature-dependent Hall data: General case, *J. Appl. Phys.* **62**, 3998 (1987).

72) D. C. Look, *Electrical characterization of GaAs materials and devices* (John Wiley & Sons, New York, 1989) p. 120.

73) S. Brochen, G. Feuillet, and J. Pernot, Equivalence of donor and acceptor fits of temperature dependent Hall carrier density and Hall mobility data: Case of ZnO, *J. Appl. Phys.* **115**, 163706 (2014).

Chapter 5: Novel chemical vapor deposition route of ZnO films: nonequilibrium N_2 plasma with small amount of O_2 below 1%

5-1 Introduction

Zinc oxide (ZnO) and its related alloys have been intensively studied for their excellent optical, electrical, and magnetic properties.[1–10] Although ZnO have many inherent advantages in terms of its material properties compared with III-V semiconductor such as gallium nitride (GaN),[11–13] the problem of oxygen deficiency (zinc excess) has still remained as an obstacle to the practical application of ZnO-based devices,[14] despite enormous efforts have been devoted to overcome the problem and various crystal growth techniques have been proposed and assessed.[15] Recent theoretical researches have predicted that nonequilibrium growth at an oxygen-rich environment is effective in suppressing representative donor-type defects such as zinc interstitials (Zn_i) and oxygen vacancies (V_O).[16,17] From an experimental point of view, the use of a reactive oxygen source such as O_3 and H_2O is also important for suppressing oxygen deficiency in oxide films.[18–21] Therefore, we focused on nonequilibrium plasma generated near atmospheric pressure (AP) which has an extremely high plasma density exceeding 10^{15} cm^{-3},[22] and a sufficiently high reactivity to achieve Si [23,24] and Ge [25] nitridation even at ambient temperatures. Using plasma generation and stabilization technology near AP,[26] we have developed a chemical vapor deposition (CVD) system and have reported the formation of ZnO films around 200 °C from β-diketonate complexes [Bis-2,4octanedionato zinc: $Zn(C_8H_{13}O_2)_2$] and N_2/O_2

plasma generated near AP, which would never be achieved without plasma (thermal CVD) around this temperature as discussed in chapter 2.[27,28]

Recently, our research group has reported the oxynitridation of Si by irradiating N_2 plasma with a small amount of additional O_2 near AP. This plasma remarkably enhanced Si oxidation rather than nitridation, leading to the formation of a dense silicon oxynitride layer with much lower leakage current compared with conventional radio-frequency plasma formed under low pressure.[29–31] Iwasaki *et al*. have adopted almost the same plasma system for surface modification process of ITO-coated glass substrates and glass substrates to find an extremely high hydrophilic efficiency.[32,33] Despite being oxidative, this plasma had never been used in the CVD of oxide films. In case of conventional vacuum processes such as MBE, PLD, sputtering, ZnO films show low resistivity due to a large number of shallow donor-type defects. In contrast, we have discovered in chapter 3 that N_2 plasma with a small amount of additional O_2 is able to form ZnO films with quite high specific resistivity of 4×10^6 Ωcm at room temperature while keeping high crystallinity,[34,35] suggesting that our CVD process is effective to reduce residual electron in ZnO films. However, it has not elucidated the formation processes of the ZnO films through N_2 plasma with a small amount of O_2.

In this chapter, therefore, we discuss the growth mechanism of ZnO films in this novel CVD route: N_2 plasma with a small O_2 concentration (O_2%) below 1%. Based on the analysis of excited species in the plasma, decomposition and oxidation processes of the Zn source material, and crystallization process are discussed in detail.[34] The electronic states of highly resistive ZnO films are investigated by thermally stimulated current (TSC) measurement to understand the reason of their high resistivity.[35]

5-2 Experimental

Referring to the schematic of our CVD system (**Fig. 5-1**), the flow rate of Bis-2,4octanedionato zinc: $Zn(C_8H_{13}O_2)_2$ (ADEKA CORPORATION) is fixed at 0.01 g/min by liquid mass flow controller (LMFC). Zn source material is splashed by irradiating N_2 (Top gas) of 1 slm, vaporized by thermal vaporizer kept at 190 °C, and transported using N_2 (Carrier gas) of 3 slm. The flow rate of the carrier gas introduced into the chamber is fixed at 60 ml/min. This carrier gas is mixed with N_2 and O_2 controlled by mass-flow controllers (MFC). The O_2 concentration in the N_2/O_2 mixture (denoted as O_2%) is varied from 0 to 1% and 20 to 90%, as an O_2% determines the type and concentration of excited species in the N_2/O_2 plasma, which strongly affects the crystallinity of ZnO films as described in chapter 3.[28)] The purity of N_2 and O_2 is 99.999% (5N). N_2/O_2 plasma by dielectric barrier discharging is generated between two parallel plate electrodes covered with aluminum nitride (AlN) separated by an uniform gap of 1.1 mm. Analysis of the plasma indicates that our plasma is nonequilibrium with the gas temperature and electron temperature of 410 - 430 K and 0.2 - 0.3 eV (~ 2900 K), respectively.[36)] Applied AC voltage and the frequency are 6.0 - 6.7 kV and 180 kHz, respectively. The discharging current is typically 200 - 230 mA. ZnO films are grown on glass substrates placed in the plasma. The deposition time, the total pressure of the chamber and the growth temperature are 40 min, 50 kPa and 200 °C, respectively. Detailed information of the CVD system is reported elsewhere.[27,28,34,35)] The excited species in the plasma are monitored by optical emission spectroscopy (OES) using a photonic multichannel spectral analyzer (PMA-C7473, Hamamatsu Photonics). The mass analysis of the exhaust gases after passing through the plasma is performed by a

quadruple mass spectrometer (Q-mass: Inficon, Transpector 2) combined with a differential exhaust system. The oxidizability of the exhausted gases is evaluated by the controlled potential electrolysis gas sensor (PS-4DP, New Cosmos Electric) for the exhausted gases after passing through the dry pump.

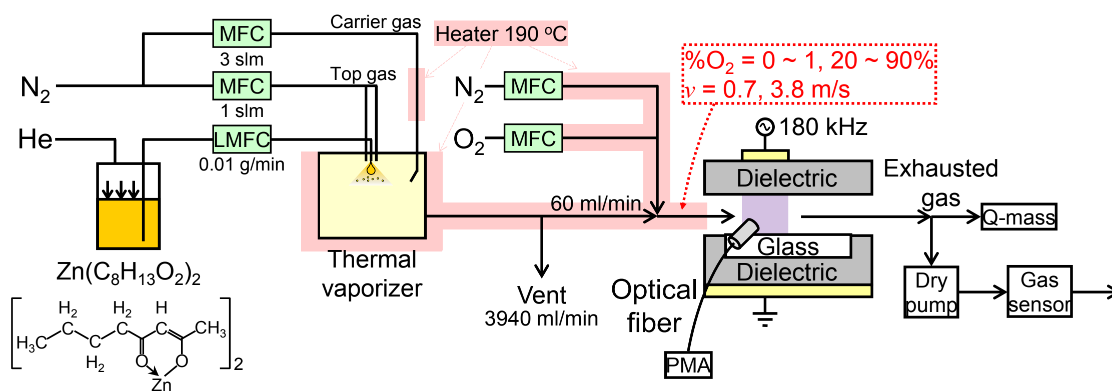

Fig. 5-1. A schematic illustration of CVD system using N_2/O_2 plasma generated near AP and diagnostic system. Chemical structural formula of Zn source material is also shown.

After deposition, the crystal structure of the films is evaluated through X-ray diffraction (XRD: X'pert MRD, Philips) using the optical geometry of 2θ-ω. Optical transmittance, optical bandgap and thickness of the films are simultaneously obtained using a UV-vis spectrophotometer (V-650, JASCO) assuming that the refractive index of ZnO in visible region is 1.95. For some uncrystallized samples, the thickness is measured using a field-emission-type scanning electron microscope (FE-SEM; S-4500, Hitachi Co Ltd) in cross-sectional view after cleaving the samples parallel to the gas flow direction. Prior to the SEM observation, ultrathin Pt-Pd alloy was coated on the sample to avoid the charge up problem during the SEM observation. The specific resistivity of ZnO layer is evaluated by van der Pauw's method using Hall-effect measurement system (TOYO-Corp., ResiTest 8310). Prior to the electrical measurements, Ohmic contacts consisted of indium dots are soldered onto the four corners of the films. In order to access effects of excited species in the plasma on the oxidation state of ZnO films, X-ray photoelectron spectroscopy (XPS: Kratos, AXIS-165) was performed using monochromatic Al-Kα radiation (1486.6 eV). Its energy resolution is 0.45 eV. Physical etching by Ar^+ ion was carried out in the XPS chamber to remove adsorbed contaminations on the surface.

Additionally, the trap levels of highly resistive ZnO films are evaluated by thermally stimulated current (TSC) measurement within the measurement temperature ranging from 78 to 300 K using pA Meter / DC voltage source (HP 4140B, Yokogawa-Hewlett-Packard Company), closed cycle cryostat (RDK-101D, Sumitomo Heavy Industries, Ltd.) and He compressor unit (CNA-11, Sumitomo Heavy Industries, Ltd.). The photo-excitation measurement and subsequent trap filling were performed at

78 K using UV-LED (OMRON, ZUV-C30H) with the central wavelength of 365 nm, which is slightly lower energy than the bandgap of ZnO at 78 K (3.43 eV) calculated from Varshni's parameters (α = 0.716 meV/K, β = 537 K). Details of the TSC measurement will be described later. (5-3-5)

5-3 Results and discussions

5-3-1 Effect of small amount of O_2 addition on the plasma and basic properties of ZnO films

OES of the plasma was performed to detect electronically excited atomic and molecular species in the plasma. Referring to **Fig. 5-1**, the edge of the optical fiber is fixed adjacent to the plasma to guide the optical emission (OE) into the PMA. **Fig. 5-2** shows the OE spectra of the plasma generated at the O_2 concentration (O_2%) of 0.2 and 90%. Strong emission lines corresponding to the N_2 second positive system (N_2 2ps: $C^3\Pi_u^+ \longrightarrow B^3\Pi_u^+$) are observed at wavelengths ranging from 300 to 450 nm in both

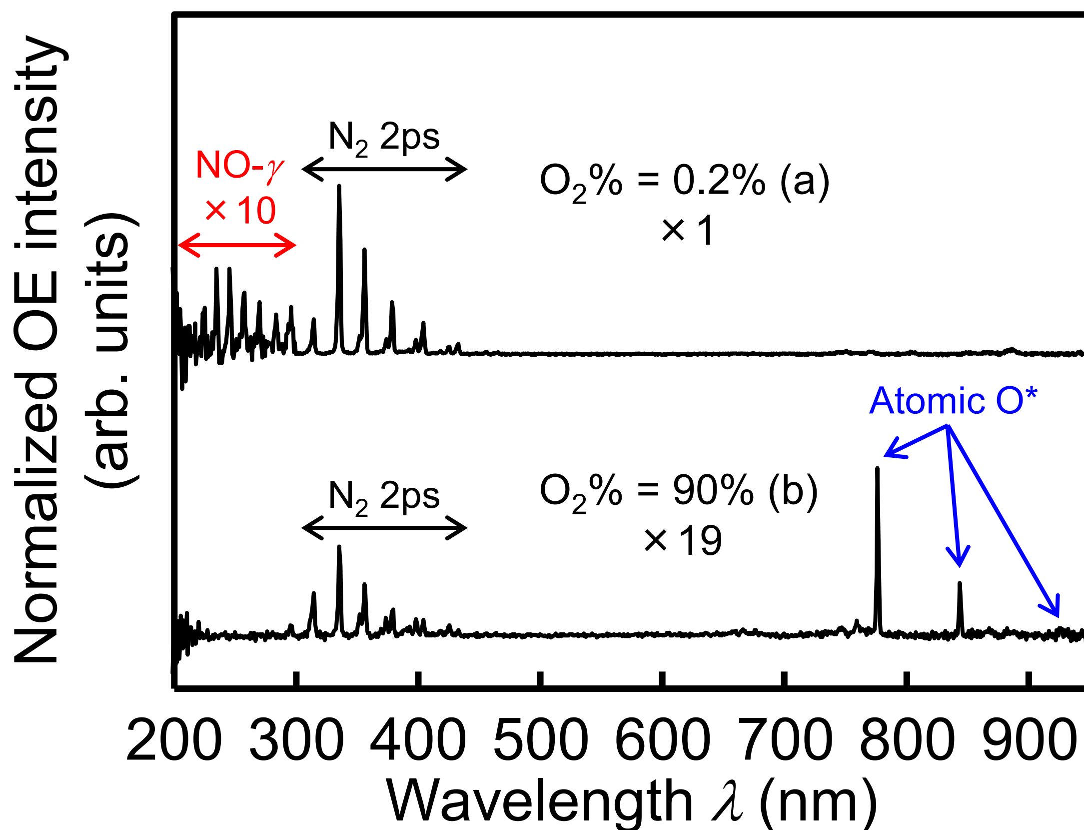

Fig. 5-2. Optical emission spectra of the plasma generated at the O_2% of 0.2% **(a)** and 90% **(b)**. The magnifications of the spectra are also shown.

spectra. We have also reported that the N_2 2ps are predominantly observed and the OE related to oxygen was barely observed in N_2/O_2 plasma at the O_2% less than 20%.[28] In **Fig. 5-2 (b)**, the OE lines attributed to atomic oxygen (Atomic O^*) are observed at wavelengths of 777 nm ($3p^5P \rightarrow 3s^5S$), 843 nm ($3p^3P \rightarrow 3s^3S$), and 927 nm ($3d^5D \rightarrow 3p^5P$), which are often observed in O_2 plasma generated at low pressure.[37,38] However, OE lines of nitric monoxide (NO) are observed at wavelengths of 213, 224, 234, 245, 257, 270, and 284 nm in the spectrum of 0.2% [**Fig. 5-2 (a)**] despite N_2 and O_2 being the only gases introduced. This electronic transition is generally called the NO-γ system (NO-γ: $A^2\Sigma^+ \longrightarrow X^2\Pi_\gamma^+$); its excitation processes up until the OE of NO-γ are given as follows.[39-41]

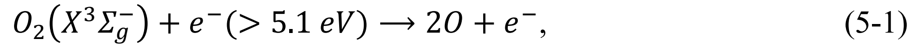

$$O_2(X^3\Sigma_g^-) + e^-(> 5.1\ eV) \longrightarrow 2O + e^-, \quad (5\text{-}1)$$

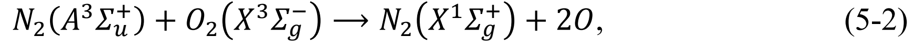

$$N_2(A^3\Sigma_u^+) + O_2(X^3\Sigma_g^-) \longrightarrow N_2(X^1\Sigma_g^+) + 2O, \quad (5\text{-}2)$$

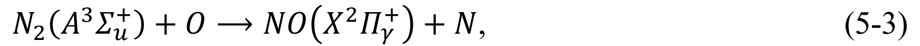

$$N_2(A^3\Sigma_u^+) + O \longrightarrow NO(X^2\Pi_\gamma^+) + N, \quad (5\text{-}3)$$

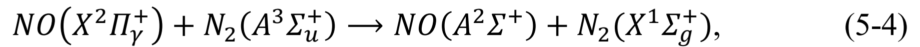

$$NO(X^2\Pi_\gamma^+) + N_2(A^3\Sigma_u^+) \longrightarrow NO(A^2\Sigma^+) + N_2(X^1\Sigma_g^+), \quad (5\text{-}4)$$

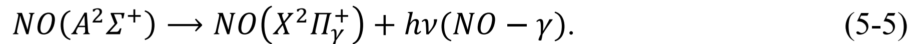

$$NO(A^2\Sigma^+) \longrightarrow NO(X^2\Pi_\gamma^+) + h\nu(NO-\gamma). \quad (5\text{-}5)$$

From our previous report, the OE of the NO-γ was observed in N_2 plasma with small O_2%. Using this plasma, the oxidation of Si wafer was drastically enhanced rather than the nitridation.[29–31] Based on these results, we considered that NO-γ should provide a new oxidation process for oxide films. Therefore, we have carried out OES for N_2 plasma generated at a small O_2% below 1%.

From plots of the OE intensities of N_2 2ps and NO-γ as a function of the O_2% (**Fig. 5-3**), the OE intensity for N_2 2ps rapidly decreases with the addition of O_2 and becomes almost constant at O_2% above 0.04%. The rapid quenching of N_2 2ps by the addition of O_2 is due to the decrease of electron density by the strong electronegativity of O_2 [33] or quenching reaction of $N_2(C^3\Pi_u^+)$ with O_2 [42] as described in chapter 3. Regarding NO-γ, that is observed even at an O_2% of 0% owing to oxygen-related residues in the N_2 gas cylinder such as O_2 or H_2O, which are observed even when we use N_2 gas of 99.9999% (6N) purity. The OE intensity of NO-γ increases and reaches a maximum value around an O_2% of 0.2% and then decreases with increasing O_2%. At an O_2% above 1%, OE from the NO-γ system disappears probably due to the decrease of $N_2(A^3\Sigma_u^+)$ concentration in the plasma according to eq. (5-4).[42]

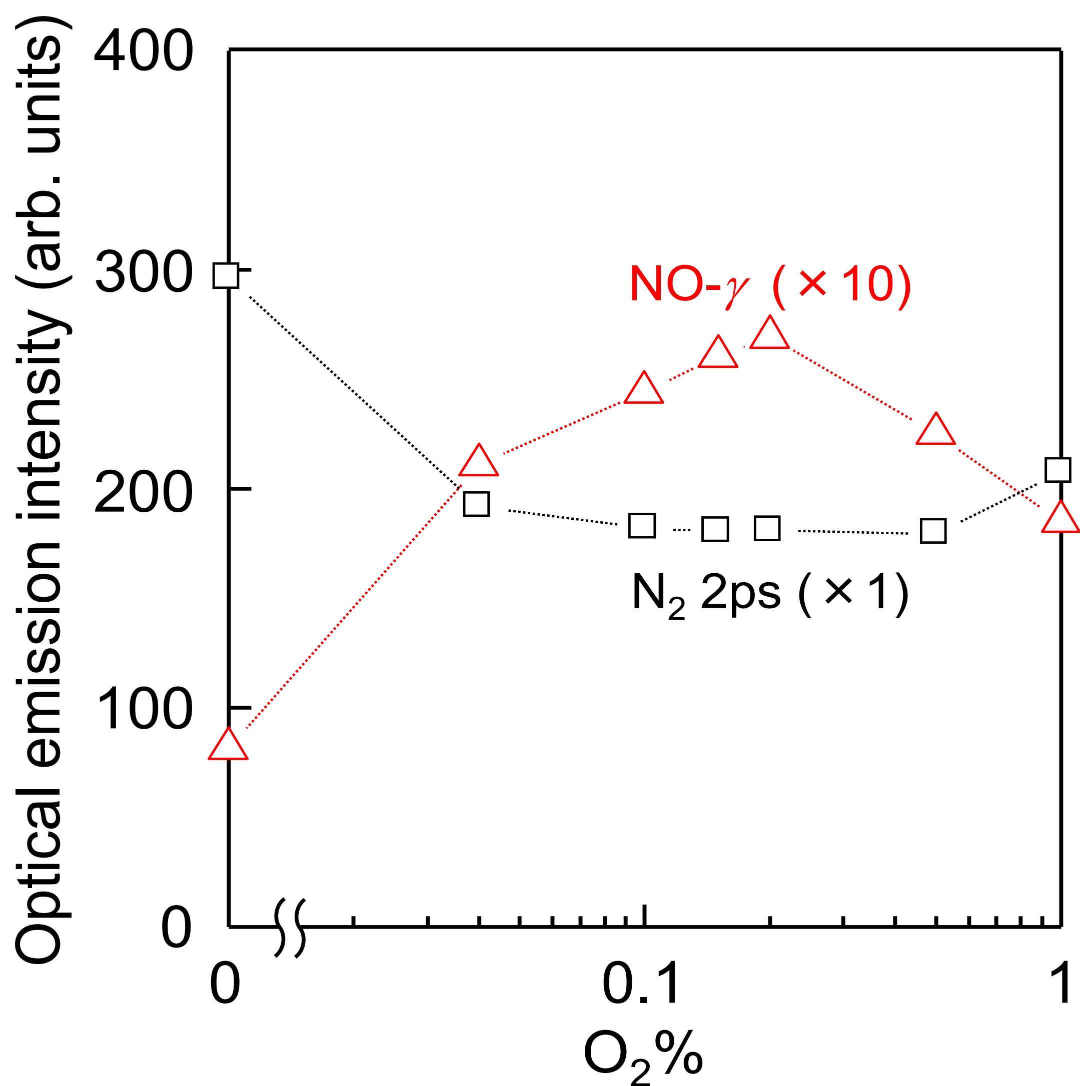

Fig. 5-3. Change of the OE intensity of N_2 2ps (337 nm: square, the magnification of ×1) and NO-γ (234 nm: triangle, the magnification of ×10) as a function of the O_2%.

To assess the contribution of NO-γ to the crystallinity of the ZnO films, XRD measurements were performed to obtain 2θ-ω scanned XRD profiles [**Fig. 5-4 (a)**] for the samples deposited at O_2%s of 0, 0.04, 0.1, 0.2, and 1.0%. No diffraction peaks are recognized for films fabricated at low O_2% of 0 and 0.04%. In contrast, a small diffraction peak from ZnO 0002 is observed at the O_2% of 0.1%, and that rapidly increases at the O_2% of 0.2%. At the O_2% of 1%, a diffraction peak from ZnO $10\bar{1}1$ appears, signaling deterioration in the (0001) preferred orientation for ZnO films. In general, $10\bar{1}1$ diffraction with the largest structural factor for ZnO (JCPDS 36-1451) is often observed and difficult to remove when the films are grown at low temperature.[43)]

The optical transmittance spectra of uncrystallized (0 and 0.04%) and crystallized samples (0.1, 0.2, and 1%) are shown in **Fig. 5-4 (b)**. The crystallized films show sharp basic absorption edge corresponding to the bandgap of ZnO (~ 3.3 eV),[44)] whereas uncrystallized films exhibit broad absorption edge which exceeds the band gap of the ZnO, suggesting that the Zn source material is not fully decomposed when the deposition is carried out at the O_2% below 0.04%.[45)]

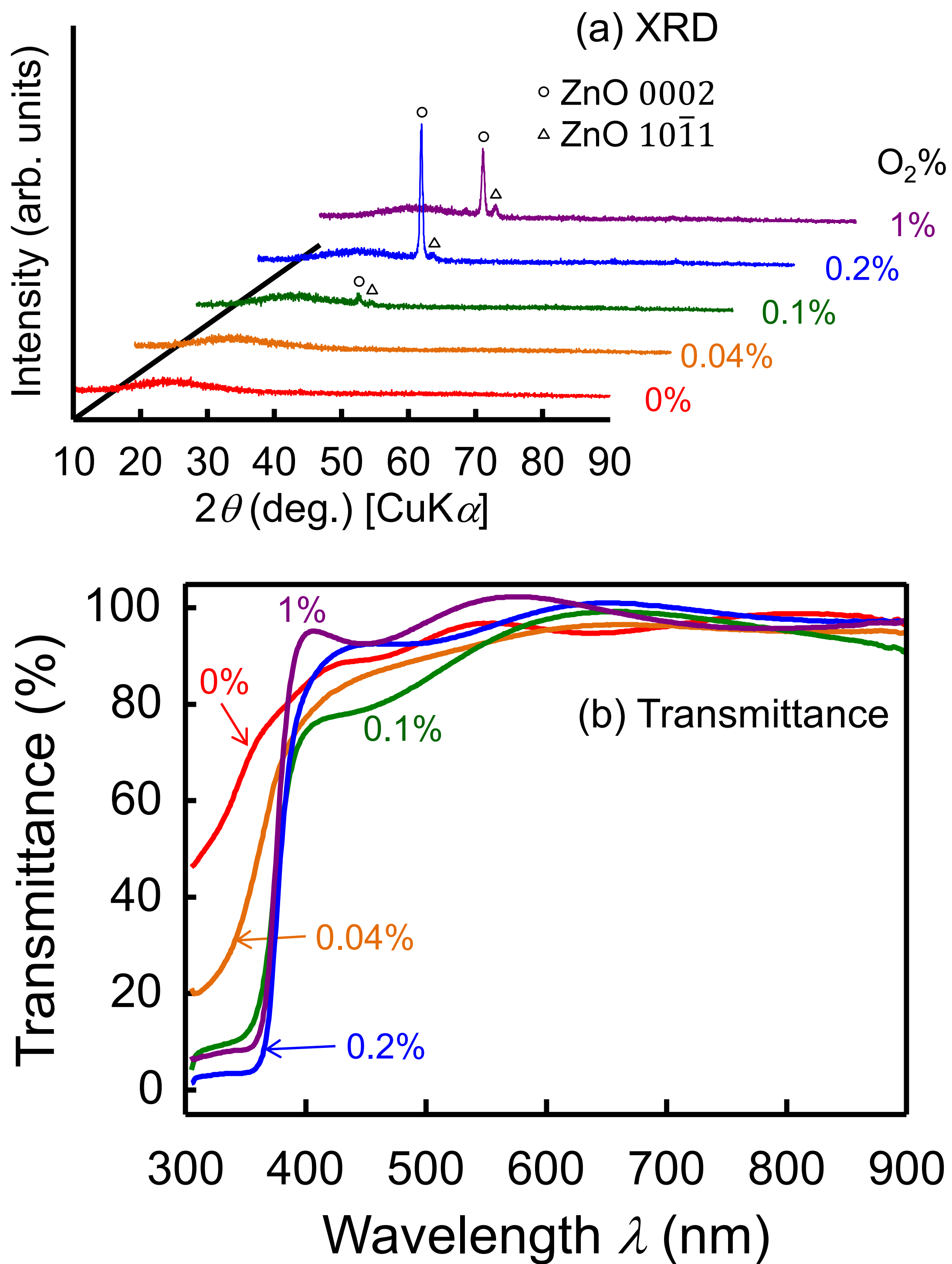

Fig. 5-4. 2θ-ω scanned XRD profiles **(a)** and optical transmittance spectra **(b)** for the films deposited at the various O_2% from 0 to 1%.

To understand the contribution of NO-γ for the chemical reaction during film growth, the growth rate and the state of crystallization against the logarithm of O_2% are summarized in **Fig. 5-5**. The crosses (×) and circles (○) indicate the crystallization state of the films. The deposition rate of the ZnO films decreases with increasing O_2% from 0 to 0.1% whereas it does not change regardless of the O_2% above 0.2%. The deposition rate of uncrystallized film (0%) is larger than that of crystallized one, because the Zn source material is not fully decomposed and included in the film as residual. At the O_2% above 0.2%, the deposition rate is almost independent on the O_2% and was regardless of the growth temperature ranging from 200 to 400 °C as well. Nevertheless, it depended on the flow rate of the Zn source material introduced into the chamber, suggesting that the growth governs the supply-limited process when the O_2% above 0.2%. Atomic O^* should contribute to the decomposition and the oxidization of the Zn source material at the O_2% above 20% as shown in **Fig. 5-2 (b)**, therefore, some oxidant with high oxidizability that is equivalent to Atomic O^* should be sufficiently produced at the small O_2% between 0.2 and 1%.

Based on these experimental results shown from **Fig. 5-3** to **Fig. 5-5**, the ZnO films with good crystallinity and optical property seem to originate from the contribution of NO-γ. However, OE of NO-γ is observed even at the uncrystallized regime (e.g. OE intensity of NO-γ at 0.04% is larger than that of 1%). Therefore, another non-radiative excited species which enhances the decomposition and oxidization of Zn source material toward the crystallization of ZnO should exist at the O_2% between 0.2 to 1%.

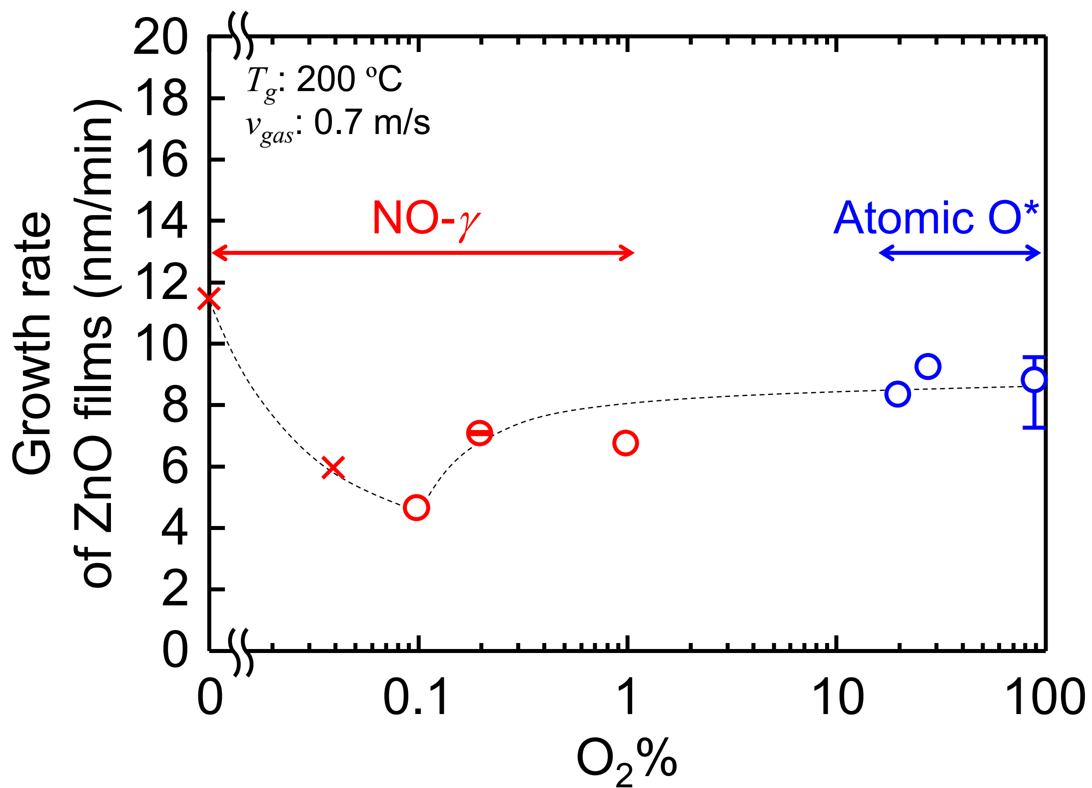

Fig. 5-5. O_2% dependence of the growth rate of ZnO films at the growth temperature of 200 ºC. The crosses (×) and circles (○) indicate uncrystallized and crystallized films, respectively. Error bars in the growth rate at 0.2 and 90% indicate maximum and minimum for some samples deposited at the same growth conditions. Dashed lines are guide to the eye.

5-3-2 Evaluation of non-radiative species using Q-mass and gas sensor

To clarify the contribution of this non-radiative species, mass spectrometry was performed using the exhausted gases after passing through the plasma. (see **Fig. 5-1** again) The mass spectrum [**Fig. 5-6 (a)**] of the exhausted gases with the O_2% of 0.2% can be classified in four different components corresponding to N, O, OH, and NO, after taking the isotope ratio and O_2% into account. From the O_2% dependence of the Q-mass signal of the representative ionized species [**Fig. 5-6 (b)**], the Q-mass signals for $^{14}N^+$ and $^{28}N_2^+$ are almost constant regardless of the O_2% because the N_2 flow rate is maintained constant throughout this experiment. Similarly, that for $^{17}OH^+$, possibly originating from the residual water in the gas cylinder, is constant. In contrast, the signal for O increases with increasing O_2%, which correlates with the increase in the O_2 flow rate. Note that the signal for $^{30}NO^+$ increase monotonically with increasing O_2% despite the OE of NO-γ disappearing at O_2% greater than 1%. This signal originates from NO in the ground state [NO($X^2\Pi_\gamma^+$)], because the effective radiative lifetime of NO($A^2\Sigma^+$) is estimated to be 210 ns,[46] which is too short for NO($A^2\Sigma^+$) to maintain and reach the Q-mass system. Therefore, the disappearance of NO-γ at O_2% greater than 1% must result from the decrease of metastable $N_2(A^3\Sigma_u^+)$ concentration in the plasma according to eq. (5-4).[42]

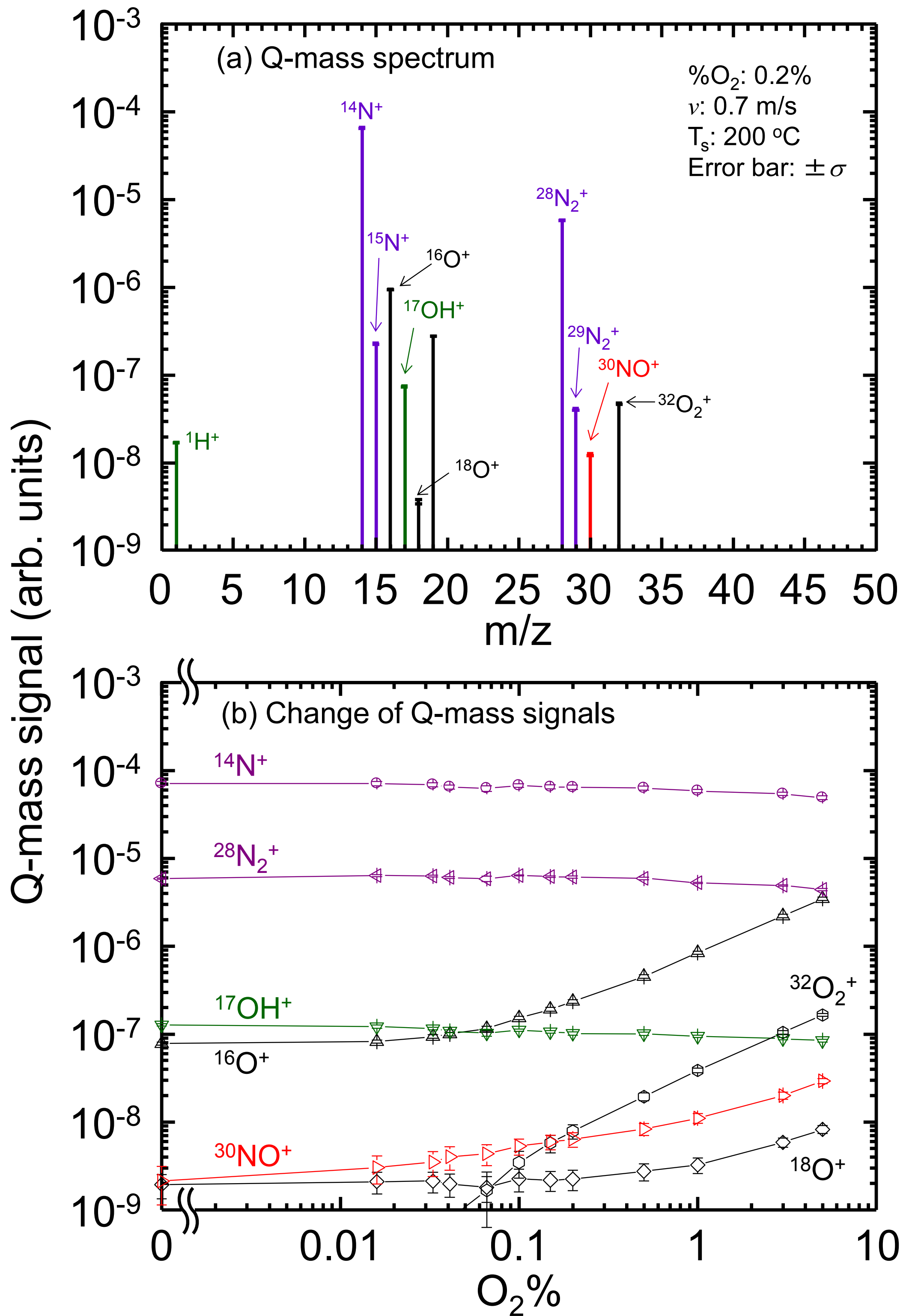

Fig. 5-6. Q-mass spectrum of the exhausted gas measured at the O_2% of 0.2%. **(a)** Change of the Q-mass signals from forcibly ionized species against the change of the O_2%. **(b)**

Our Q-mass system can detect only positively ionized species. To investigate the gas species with high electronegativity (high oxidizability), the oxidizability of the exhausted gases was evaluated using a controlled potential electrolysis gas sensor, which responds to the adsorption of oxidative gases such as F_2, Cl_2, and O_3. The time dependences of the sensor voltage at various O_2% were recorded (**Fig. 5-7**). Prior to each measurement (t < 0), the surface of the sensor was purged by dry nitrogen to remove the adsorbed unknown oxidative gases. Next, pure N_2 plasma was generated (t = 0) and subsequently supplied with O_2 (t > 0). The voltage of the gas sensor shows a slight but significant decrease at an O_2% of 0.2%, and then a rapid decrease at higher O_2% up until 5%, which indicates that the oxidizability of the exhausted gas is

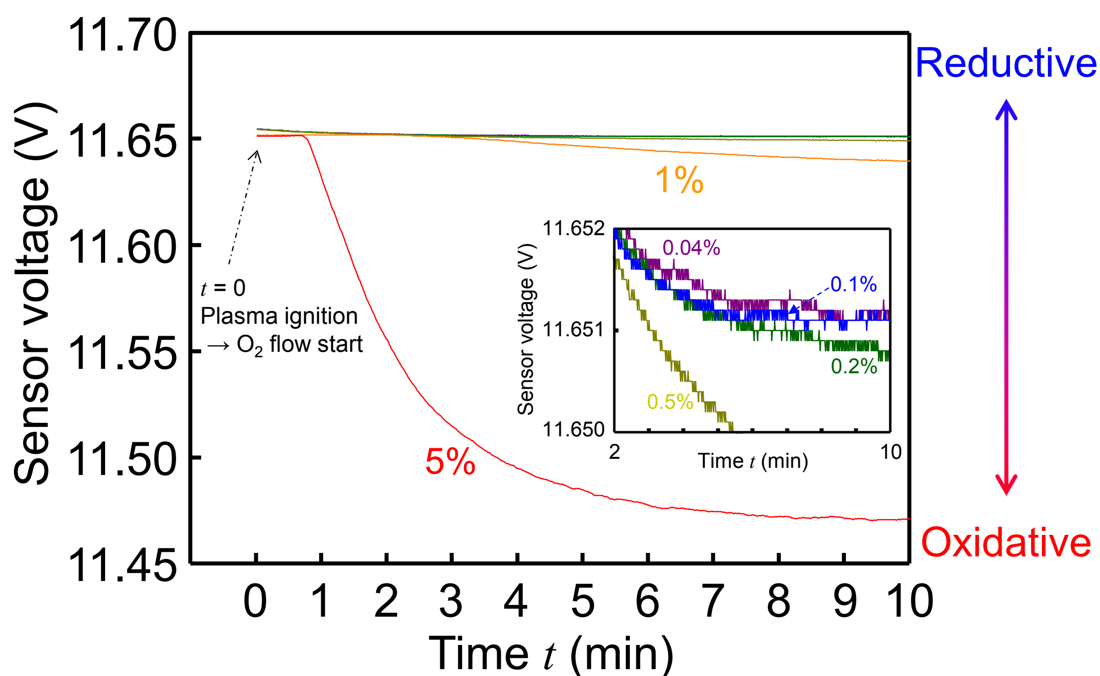

Fig. 5-7. Time variation of the sensor voltage recorded at various O_2% from 0.04 to 5%. Controlled potential electrolysis gas sensor is fixed at the downstream side of the dry pump. The inset is an enlarged view for the data of 0.04, 0.1 and 0.2%. Decrease of sensor voltage corresponds to the enhancement of the oxidizability of exhausted gases.

monotonically enhanced with increasing O_2%. This is probably owing to O_3 generated in the discharging region as the half-life of O_3 is sufficiently long for O_3 to reach the gas sensor. This contrasts with other excited oxidants with shorter lifetimes such as the atomic O radicals. In general, O_3 has a large absorption coefficient around 260 nm,[47,48] which corresponds to the central wavelength for the OE of NO-γ. The photo-induced dissociation of O_3 is described as follows:

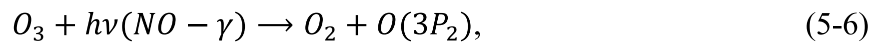

$$O_3 + hv(NO - \gamma) \longrightarrow O_2 + O(3P_2), \tag{5-6}$$

which indicates that a certain amount of O($^3P_2$) exists in the discharging region at an O_2% ranging from 0.2 to 1%, because strong OE of NO-γ and O_3 coexist in this O_2% regime. Moreover, the generation efficiency of O($^3P_2$) should rapidly decrease at O_2% greater than 1%, because the OE of NO-γ disappears in the regime.[49] This result strongly suggests that the highly crystalline ZnO film grown at a specific O_2% of 0.2% is produced by the contribution of both NO-γ and O_3.

5-3-3 Evaluation of the oxidation state by XPS

In order to access effects of excited species in the plasma on the oxidation state of ZnO films, X-ray photoelectron spectroscopy (XPS: Kratos, AXIS-165) was performed using monochromatic Al-Kα radiation. Its energy resolution is 0.45 eV. In general, chemical states (e.g. chemical bonding states, coordination states, valence states) are analyzed from XPS peak shift of core levels. In case of Zn, however, oxidation-induced peak shift of $Zn2p_{3/2}$ is as small as 0.3 eV, which makes it difficult to separate oxidized and non-oxidized components.[50)] On the other hand, oxidation-induced auger peak shift is as large as 5 eV. Therefore, we intended to separate oxidized component (ZnO) and not a fully oxidized component (ZnO_{1-x}) using auger spectra. **Fig. 5-8 (a)** shows Zn auger $L_3M_{45}M_{45}$ spectrum for ZnO film grown at the O_2% of 0.2%. In addition to the intense peak (ZnO) located at the kinetic energy of 988.4 eV, chemical shifted peak (ZnO_{1-x}) is observed at 991.8 eV as a right shoulder. To evaluate the effects of excited species in the plasma on the oxidation state of ZnO films, integrated intensity ratio (I_{ZnO} / I_{ZnO1-x}) is plotted as a function of the O_2%. [**Fig. 5-8 (b)**] The amount of peak shift (ΔE) including its standard deviation is approximately (3.37±0.05) eV, therefore the standard deviation is smaller than the energy resolution of our system. Prior to the measurement, physical etching by Ar^+ was performed for 0, 3 and 4 min in the XPS chamber to reduce the effects of contamination. Note that the value of I_{ZnO} / I_{ZnO1-x} increases and reaches a maximum value around an O_2% of 0.2%, where a highly crystalline ZnO film is obtained, and then decreases at 1%. At the O_2% above 1%, I_{ZnO} / I_{ZnO1-x} do not show much change. These results suggest the strong oxidizability of this novel CVD route compatible to Atomic O^*-based plasma.

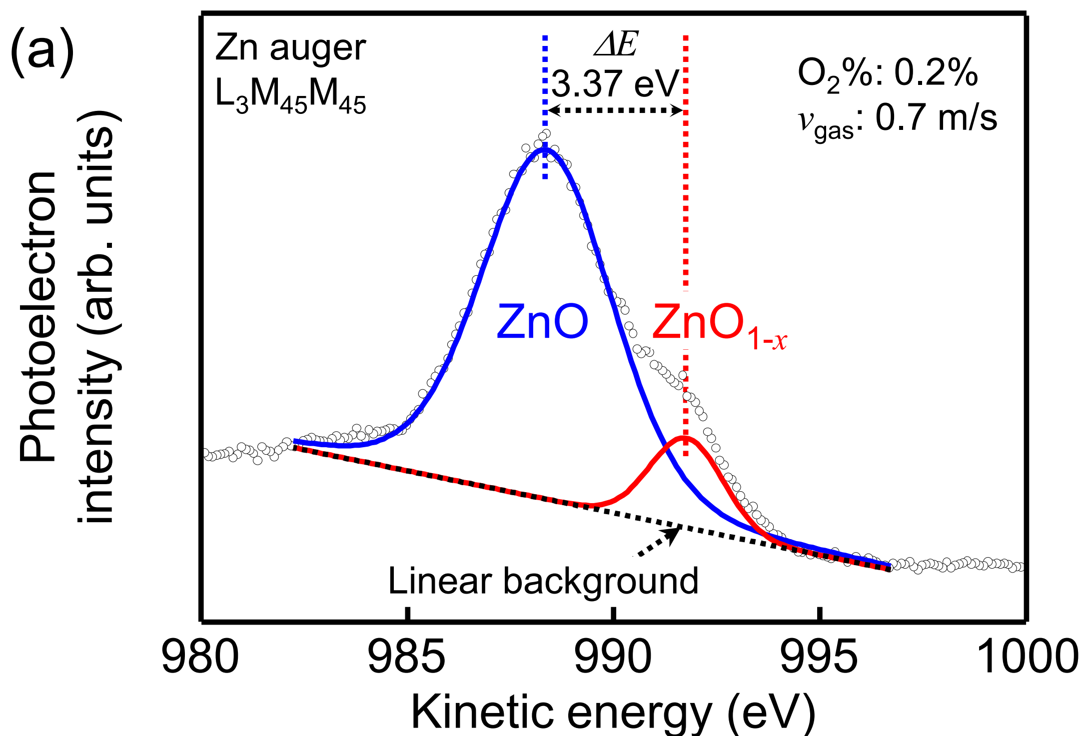

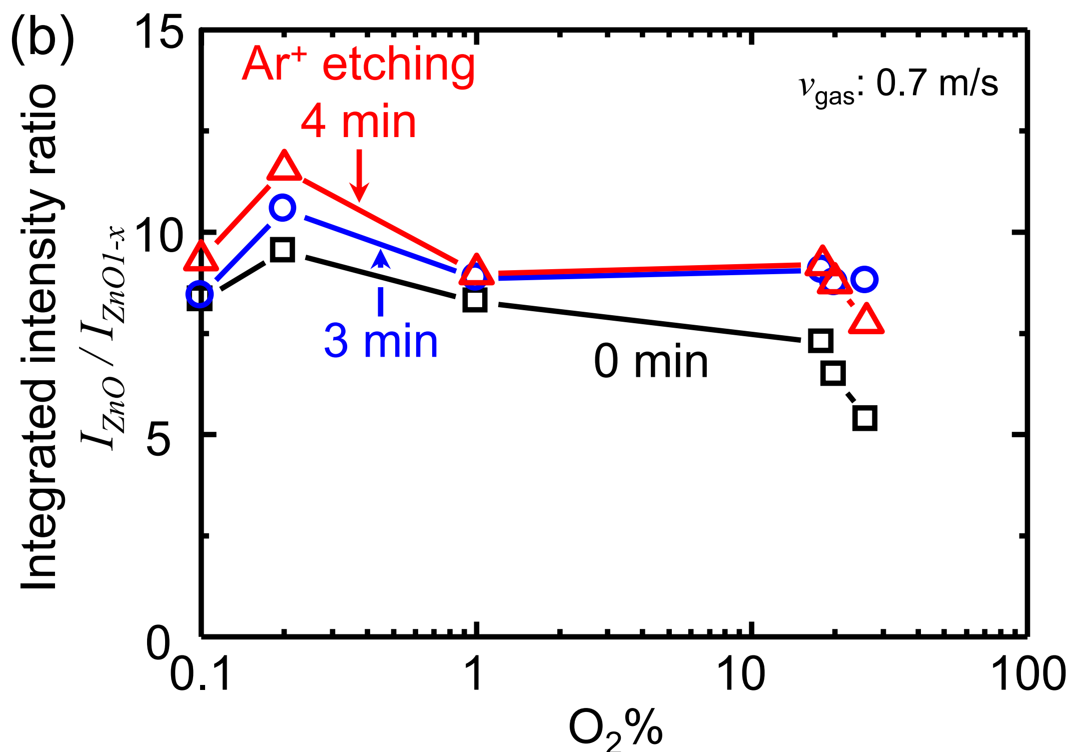

Fig. 5-8. Zn auger $L_3M_{45}M_{45}$ spectrum for ZnO film grown at the O_2% of 0.2%. **(a)** Plot of integrated intensity ratio (I_{ZnO} / I_{ZnO1-x}) as a function of the O_2%. **(b)** XPS measurement is performed after Ar^+ physical etching in the XPS chamber for 0, 3 and 4 min.

5-3-4 Reaction scheme

Based on the analysis of plasma (OES) and exhausted gas (Q-mass, Gas sensor), the detected excited species are summarized in **Fig. 5-9 (a)**. At a specific O_2% of 0.2%, where we could achieve the best crystallinity, NO-γ and O_3 coexist in the discharging region and might generate active oxidant such as $O(^3P_2)$. Iwasaki *et al*. have reported the hydrophilization of the ITO-coated glass substrate [32] and the glass substrate [33] by nonequilibrium AP N_2 plasma with small amounts of O_2 added. Their group systematically investigated the absolute density of non-radiative atomic oxygen [$O(^3P_2)$] generated by the photo-induced decomposition of O_3 at various O_2% by vacuum ultraviolet laser absorption spectroscopy, and pointed out that the extremely high hydrophilic efficiency was produced at a specific O_2% by the photo-induced decomposition of organic contaminants by NO-γ and the subsequent oxidation by $O(^3P_2)$.[49] Their result is similar to our case and strongly supports our claim that the highly crystalline ZnO film fabricated at a specific O_2% of 0.2% originates from the decomposition and oxidation of Zn source material by the coexistence of NO-γ and O_3 through the reaction scheme in **Fig. 5-9 (b)**.

(a) Excited species

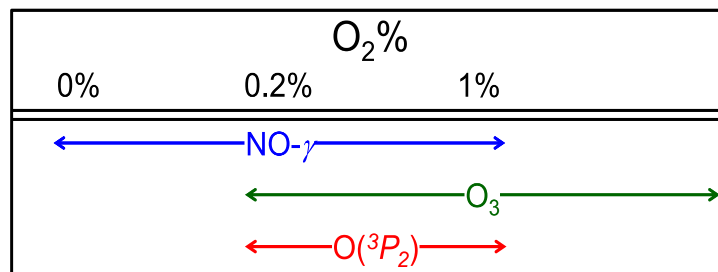

(b) Reaction scheme

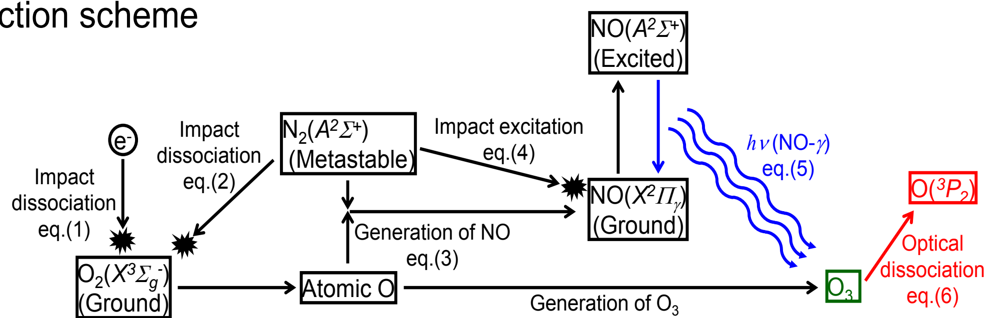

Fig. 5-9. Summary of excited species **(a)** and reaction scheme **(b)** in N_2 plasma with small amount of O_2 addition.

5-3-5 Evaluation of the deep levels by thermally stimulated current measurement

In the last section (5-3-4), we have found that the use of N_2 plasma with small amount of additional O_2 had remarkably enhanced the oxidation, which is compatible to that of atomic O^*-based plasma as used in chapter 2.[27] Using this plasma, extremely highly resistive ZnO films were successfully formed, which is difficult to obtain by the conventional vacuum processes such as MBE, PLD and sputtering methods.[34,35] Therefore, this section focuses on the electronic states of highly resistive ZnO films. Thermally stimulated current (TSC) measurement is used to understand the reason of their high resistivity.[35]

Based on the findings obtained through the last section, we demonstrate the further enhancement of crystallinity by increasing the gas flow velocity from 0.7 to 3.8 m/s. From a 2θ-ω scanned XRD profile [**Fig. 5-10 (a)**] of the film deposited at the optimized O_2% of 0.2% and at the faster gas flow velocity of 3.8 m/s, strong (0001) preferred orientation is seen without the diffraction from ZnO $10\bar{1}1$.

The transmittance spectrum of this film [**Fig. 5-10 (b)**] indicates high transmittance above 85% at wavelengths ranging from 405 to 900 nm simultaneously with a sharp basic absorption edge. The optical bandgap is calculated to be 3.30 eV [inset of **Fig. 5-10 (b)**], which is close to the bandgap of ZnO at room temperature.[44] A blue shift in the optical bandgap induced by the Burstein–Moss effect [51] or the amorphous phase [45] has not been confirmed despite the growth condition being O_2-poor.

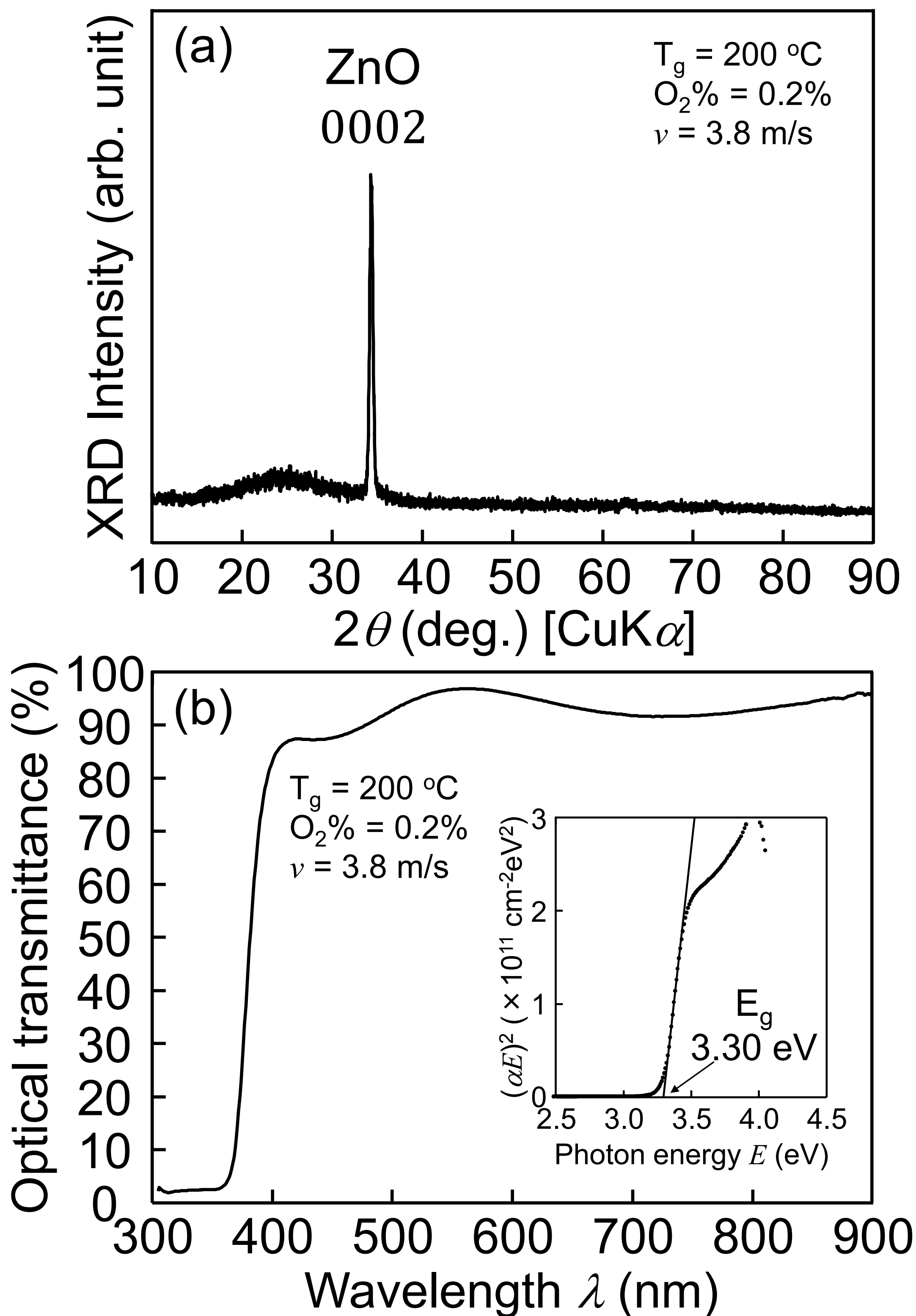

Fig. 5-10. 2θ-ω scanned XRD profile **(a)** and optical transmittance spectrum **(b)** of the film deposited at the O_2% and the gas flow velocity of 0.2% and 3.8 m/s, respectively. The inset in (b) is a plot of $(\alpha E)^2$ vs photon energy E calculated from this spectrum.

Resistivity measurement was performed by four probe method using van der Pauw's electrodes configuration. **Fig. 5-11** shows the change of the specific resistivity of ZnO films grown at 200 °C against the change of the O_2%. These films show a quite high specific resistivity of above 10^6 Ωcm, which is not easily obtained via conventional vacuum processes such as MBE, PLD, and sputtering unless the introduction of additional ion doping. Although Hall-effect measurement was also performed following the resistivity measurement, reliable Hall voltage was not detected due to the high resistivity of the samples.

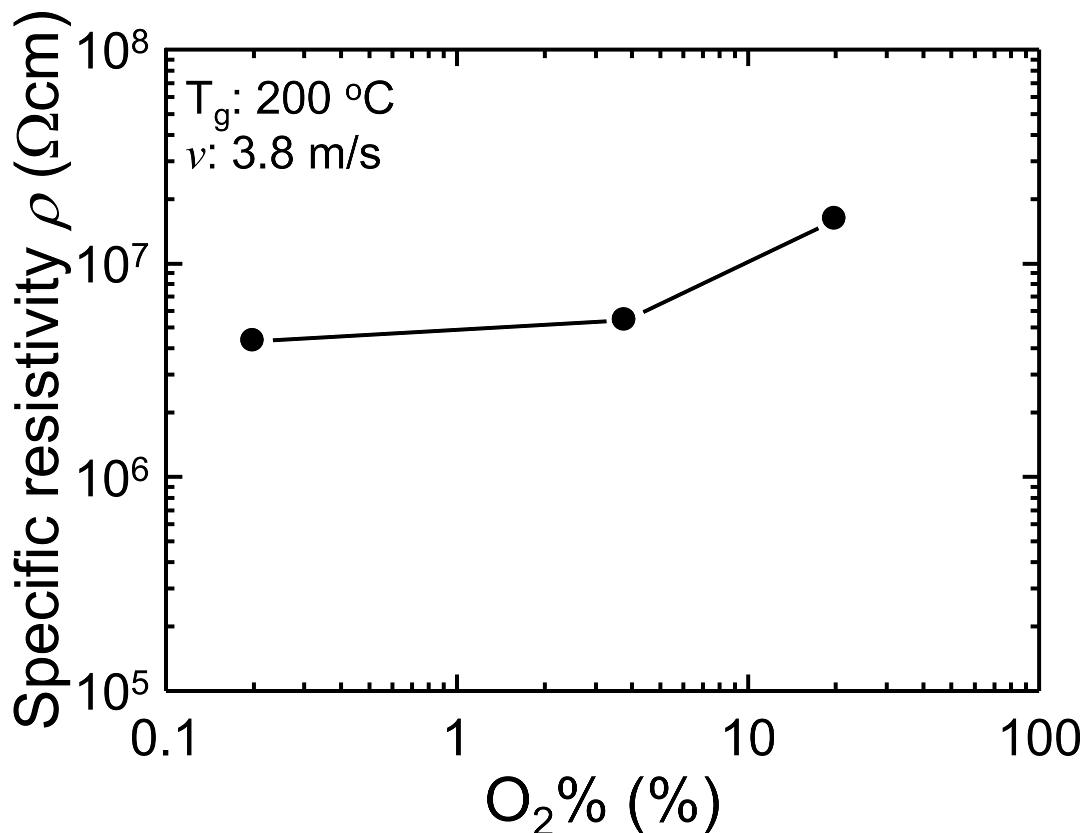

Fig. 5-11. Change of the specific resistivity ρ of ZnO films grown at 200 °C against the change of the O_2%.

In order to analyze the origin of the high resistivity, trap states were evaluated by TSC measurement which is a powerful tool for the electronical investigation of semi-insulating (SI) materials such as SI-GaAs,[52,53] SI-InP [54-57] and SI-GaN [58-60] etc. The experimental setup and measurement sequence are schematically illustrated in **Fig. 5-12**. TSC measurement consists of three different steps.[52] Samples are cooled down from 300 to 78 K in the dark environment as the first step. Following the cooling step, the carrier is injected from the electrodes and the trap states should be efficiently filled at 78 K by the illumination of UV-LED with the central wavelength of 365 nm for 5 min. Finally, the current due to the carrier emission from trap states (so called TSC signal) is

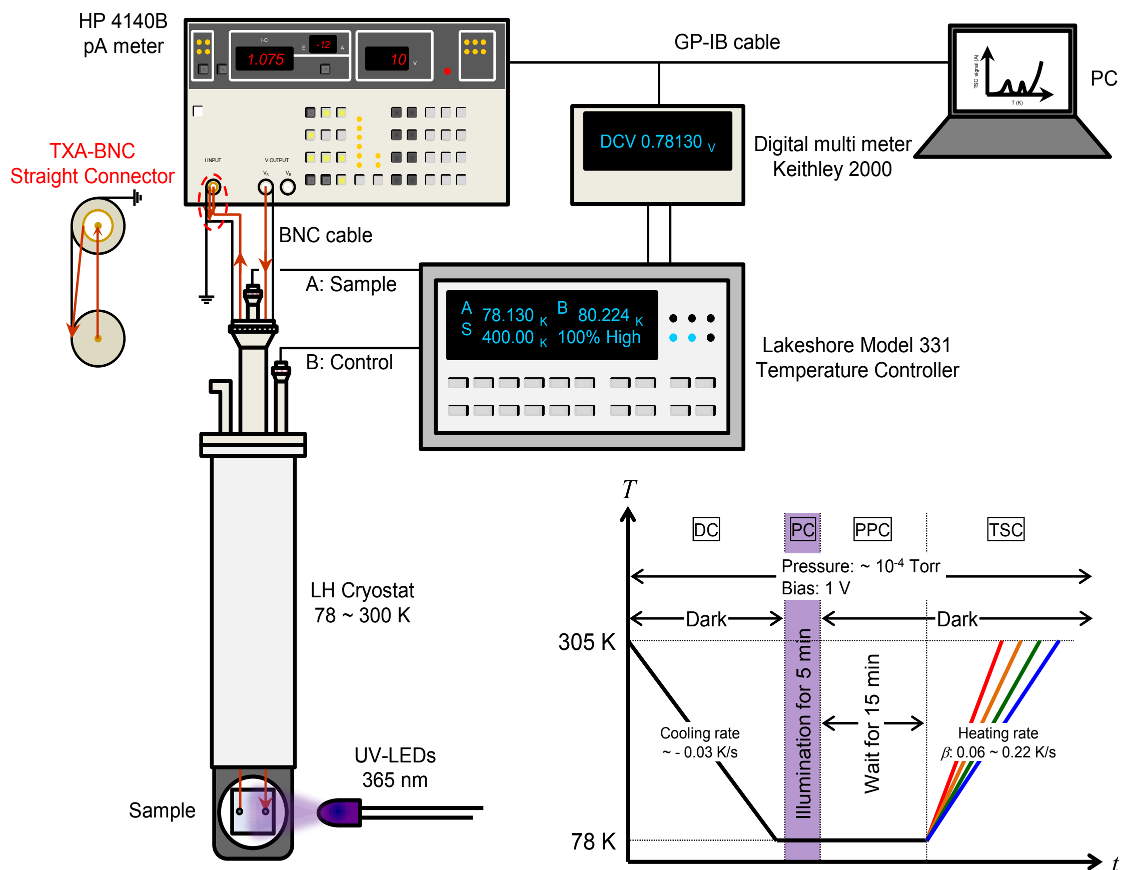

Fig. 5-12. A schematic illustration of the experimental setup for thermally stimulated current measurements. Time sequence of the TSC measurement is also shown.

recorded at the temperature ranging from 78 to 300 K in dark environment while keeping a constant heating rate. A bias voltage of 1 V was always applied to the sample throughout these three steps. **Fig. 5-13** shows the TSC curves for the highly resistive ZnO films shown in **Fig. 5-11**. Two prominent TSC peaks are observed at the temperature of 100 K (T_{m1}) and 290 K (T_{m2}) for the sample fabricated at the O_2% of 0.2%. In case of the samples deposited at 3.8 and 20%, although small and gradual cusps are confirmed near T_{m1} and T_{m2}, it is difficult to decide the reliable peak temperatures, which directly correspond to the trap level. In the following discussion, therefore, we focus on the TSC curve of the sample fabricated at 0.2%. From the peak temperature (T_m) of a given trap state, the activation energy of the trap (E_T) is approximately determined using the following equation: [52]

$$E_T = k_B T_m \ln(T_m^4/\beta), \qquad (5\text{-}7)$$

where k_B is Boltzmann constant, β is heating rate. From this equation, E_T corresponding to T_{m1} and T_{m2} are calculated to be 170 and 610 meV, respectively. Fang *et al.* have observed the TSC peaks with the E_T of 150 meV [61] and 160 meV [62] from hydrothermally grown highly resistive ZnO single crystals and have assigned as zinc vacancy (V_{Zn}) acceptor. Additionally, Kuriyama *et al.* have reported that 30 MeV-electron-irradiated ZnO single crystals showed broad TSC peak at around 550 to 660 meV that corresponds to our result. With considering the combination of the results of electron paramagnetic resonance (EPR) measurement, they concluded that those peaks could be assigned as V_{Zn} and O_i, respectively.[63]

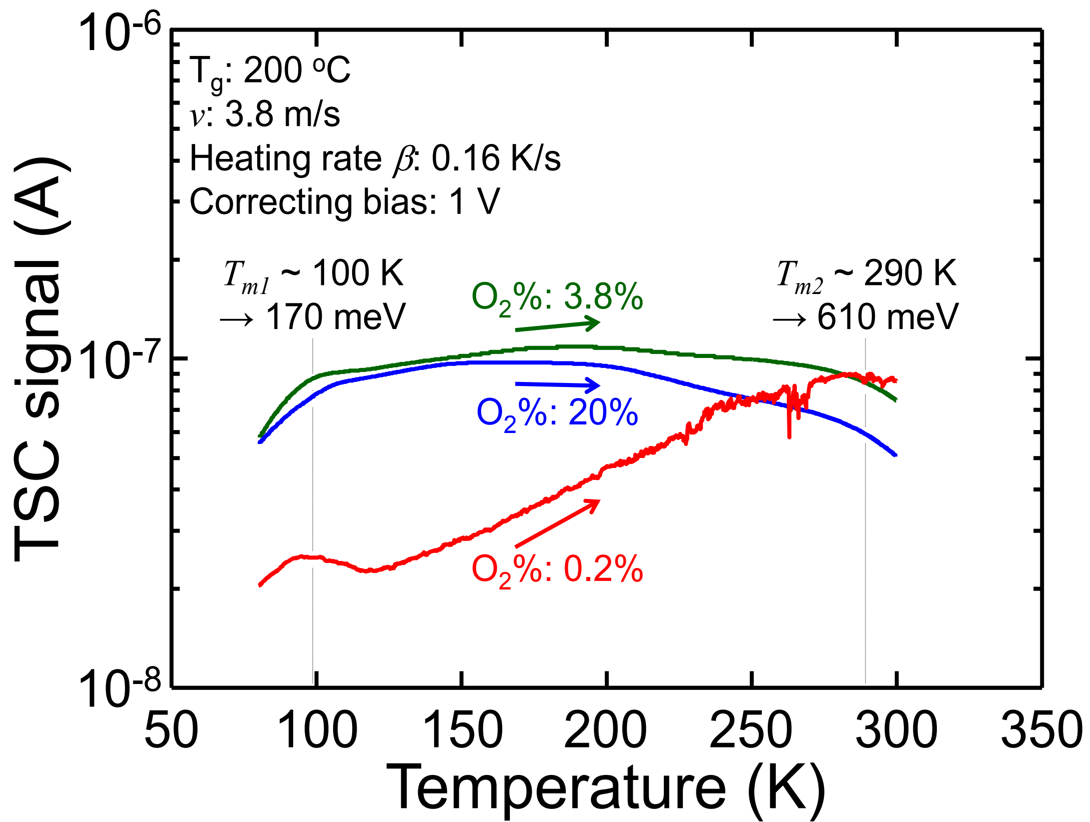

Fig. 5-13. TSC curves for highly resistive ZnO films grown at the O_2% of and 0.2, 3.8 and 20%. Prior to TSC measurement, trap states were efficiently filled at 78 K by the illumination of UV-LED with the wavelength of 365 nm for 5 min while applying the bias voltage of 1 V.

According to the literatures, nitrogen atom substituting oxygen site (N_O) also creates a deep acceptor level in ZnO with the activation energy of around 170 meV.[64)] From cryogenic PL measurement, that of N_O is estimated at 170 - 266 meV,[64-69)] which is close to the value of V_{Zn}. In our case, N_O acceptor should be taken into account as well, because dense and reactive nitrogen excited species exist in the plasma.[23-25)] In order to access the chemical bonding state of doped nitrogen, Raman spectroscopy was performed. (**Fig. 5-14**) In addition to the host vibration modes at 437 and 574 cm^{-1}, local vibration modes by N_O are observed at 275, 505, 582 and 636 cm^{-1} as discussed in chapter 4.[14,70,71)] Therefore, V_{Zn} and N_O are the candidates for T_{m1}. In order to clarify the origin of T_{m1}, further discussion is necessary.

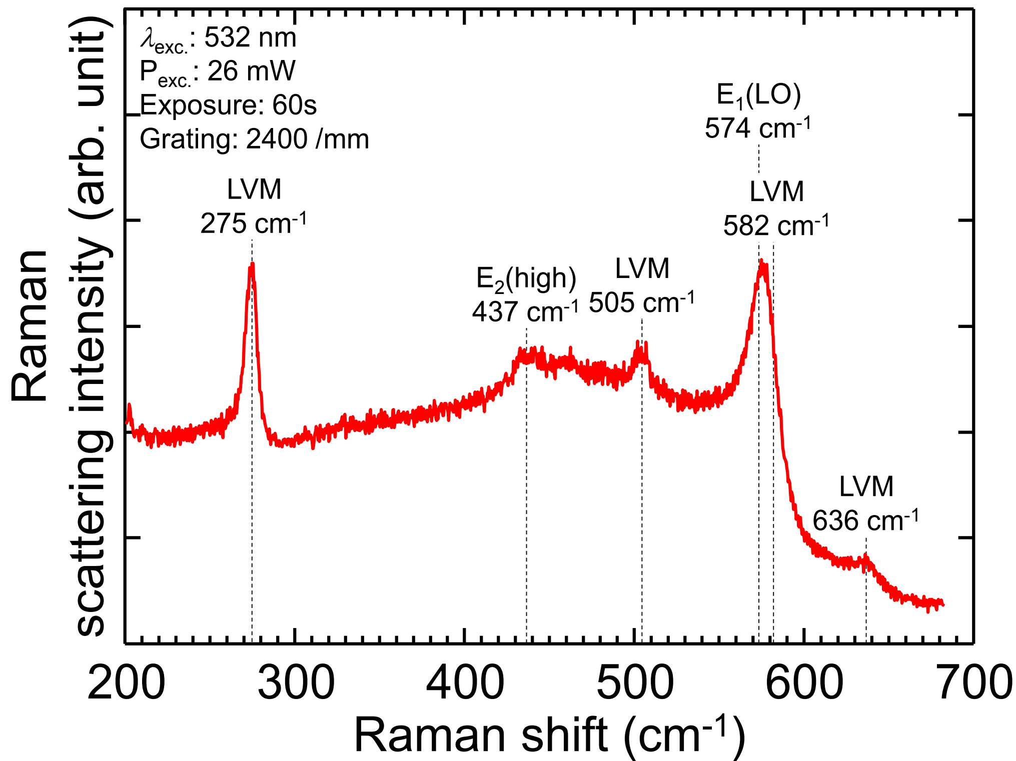

Fig. 5-14. Raman spectrum for the highly resistive ZnO film grown at the growth temperature and O_2% of 200 °C and 0.2%, respectively.

5-3-6 Assignment of the trap states

Fig. 5-15 (a) shows the TSC curve near T_{m1} recorded at various heating rate. T_{m1} shifts to higher temperature with increasing the heating rate from 0.06 to 0.2 K/s. Using this inherent nature of TSC processes, we can get further information from TSC curves. At a TSC peak temperature T_m, following formula can be described: [72)]

$$\frac{1}{\nu} exp\left(\frac{E_T}{kT_m}\right) = \frac{kT_m^2}{\beta E_T}, \quad (5\text{-}8)$$

$$\nu = N\sigma_T V, \quad (5\text{-}9)$$

where ν, N, σ_T and V are emission frequency, effective density of state of conduction or valence band, capture cross section and thermal velocity, respectively. Eqn. (5-8) and (5-9) lead to the following formula:

$$E_T = k_B T_m \left(\frac{N\sigma_T V k_B T_m^2}{\beta E_T}\right). \quad (5\text{-}10)$$

In case of crystal, effective density of state N and thermal velocity V at the peak temperature T_m can be written as follows:

$$N = 2\left(\frac{2\pi m^* m_0 k_B T_m}{h^2}\right)^{3/2}, \quad (5\text{-}11)$$

$$V = \sqrt{\frac{8k_B T_m}{\pi m^* m_0}}, \quad (5\text{-}12)$$

where $m^* m_0$, k_B and h are effective mass of carrier in the crystal, Boltzmann constant and Planck constant, respectively. From Eqs. (5-10), (5-11) and (5-12), following formula can be obtained.[56,72)]

$$\frac{E_T}{k_B T_m} = \ln\left(\frac{T_m^4}{\beta}\right) + \ln\left(\frac{16\pi m^* m_0 k_B^3 \sigma_T}{h^3 E_T}\right). \quad (5\text{-}13)$$

Therefore, the accurate activation energy and the capture cross section can be simultaneously obtained from the slope and intercept of $1/T_m$ - $\ln(T_m^4/\beta)$ plot,

respectively as shown in **Fig. 5-15 (b)**. Assuming that the effective mass of hole in ZnO is $0.54m_0$,[73,74] accurate trap level E_{T1} and capture cross section σ_1 can be calculated to be 160 meV and 2×10^{-16} cm^{-2}, respectively. Gu *et al.*[75] have detected the trap level from N^+-implanted ZnO with the E_T and σ_T of 170 meV and ~ 10^{16} cm^{-2}, respectively by deep level transient spectroscopy (DLTS) measurement, both of which are very close to our result. They performed DLTS measurement after the systematic recovery and activation annealing at various temperature ranging from 650 to 1200 °C. E_T of 170 meV was not detected as N^+-implanted sample. Interestingly, however, the trap suddenly appeared at the annealing temperature of 700 °C, and persistently remained even after 1200 °C-annealing, while the other DLTS peaks tend to disappear through the high temperature annealing and recovery process of crystal lattice of ZnO. These results strongly suggest that this trap level has thermally stable and/or thermally induced natures. From theoretically and experimentally, N_O in ZnO is considered to be unstable,[76-78] while V_{Zn} is artificially induced at a harsh environments such as high temperature annealing,[79] high energy beam irradiation,[61-63,80-83] and H_2O_2 etching.[84,85] In fact, we performed post deposition annealing (700 °C, 10 min) for 400 °C-grown epitaxial ZnO film (already shown in chapter 4) in O_2 atmosphere for 10 min similar to their experiment.[75] The LVMs of N_O acceptor were observed in the as-grown state, whereas those disappeared after the annealing treatment. [see **Fig. 4-9 (a)** again] Therefore, E_{T1} seems to be V_{Zn} rather than N_O.

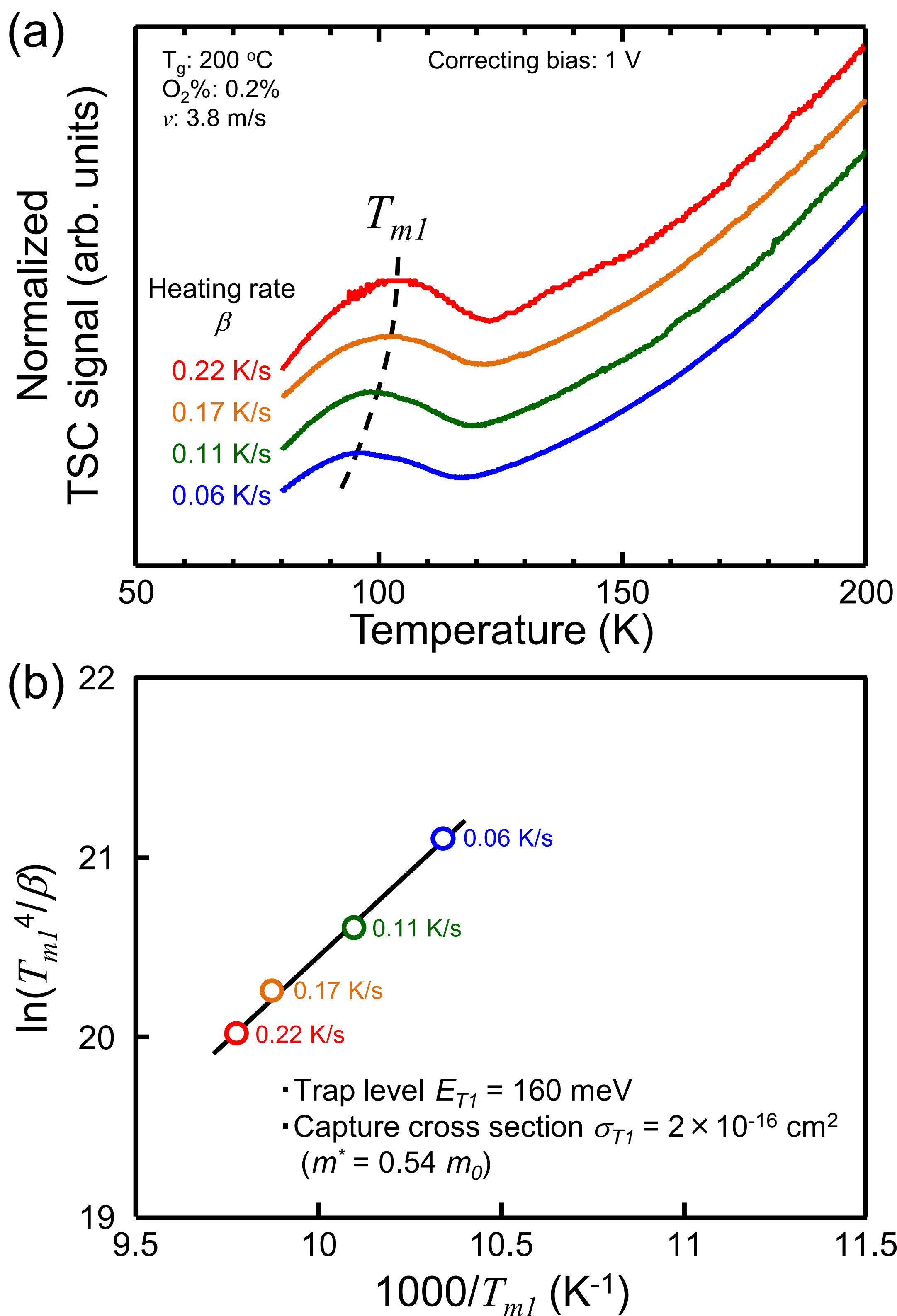

Fig. 5-15. TSC curves around T_{m1} recorded at various heating rates. **(a)** Dashed line is guide to the eye. Plot of $\ln(T_{m1}{}^4/\beta)$ as a function of reciprocal temperature $1000/T_{m1}$. **(b)**

By the way, E_T around 300 meV (generally called E3 electron trap) has often reported from deep level transient spectroscopy (DLTS),[84-88] thermal admittance spectroscopy (TAS),[89] TSC [82] and Hall-effect measurement [90,91] for ZnO single crystals regardless of the synthesis methods, and has been assigned as singly ionized V_O donor. Optical absorption measurements performed by Halliburton *et al.*,[92] Kappers *et al.*[93] and Srikant *et al.*[44] also detected the sub-gap absorption by E3 trap as a shoulder of basic absorption edge. Although we have also detected a single TSC peak possibly originate from E3 electron trap (T_m = 170 K, E_T = 320 meV) when we use HYD grown n-type resistive ZnO single crystal ($n_{300K} \sim 3\times10^{14}$ cm^{-3}) used in chapter 4 as a reference sample of photoluminescence (PL) measurements, the signal is not detected in the TSC curve for the sample fabricated at the O_2% of 0.2%, whereas the broad TSC peak seems to exist around 170 – 180 K for the samples fabricated at the O_2%s of 3.8 and 20%. Our TSC measurement was performed after illumination at low temperature, which should enhance the filling process for majority (electron) and minority (hole) carrier traps simultaneously.[94] Provided that the concentration of deep V_O donor is comparable to that of V_{Zn}, TSC signal from V_O donor should appear more clearly, because TSC current is also affected by the carrier mobility. ($\mu_e > \mu_h$ in ZnO) Therefore, ZnO film grown at the O_2% of 0.2% seems to include less V_O donors. Matsumoto *et al.* have reported that carbon-implanted ZnO also have the donor level of 310 meV from photoluminescence (PL) measurement and have assigned the level as carbon substituting zinc site (C_{Zn}),[95] but such peak is not observed in our highly resistive ZnO films at all.

Based on above discussions, the electronic states of highly resistive ZnO films are schematically illustrated in **Fig. 5-16** in addition to those of HYD-grown resistive ZnO single crystal. In case of ZnO single crystal, carrier emission from electron trap located at approximately E_c – 320 meV (so called E3 electron trap) is dominant, which is often observed by DLTS [84-88] or TSC measurement.[82] On the other hand, our highly resistive ZnO films are dominated by hole traps (acceptor-type defects) such as V_{Zn} (160 meV), and V_{Zn} or O_i (610 meV), which is hardly observed in as-grown ZnO films.

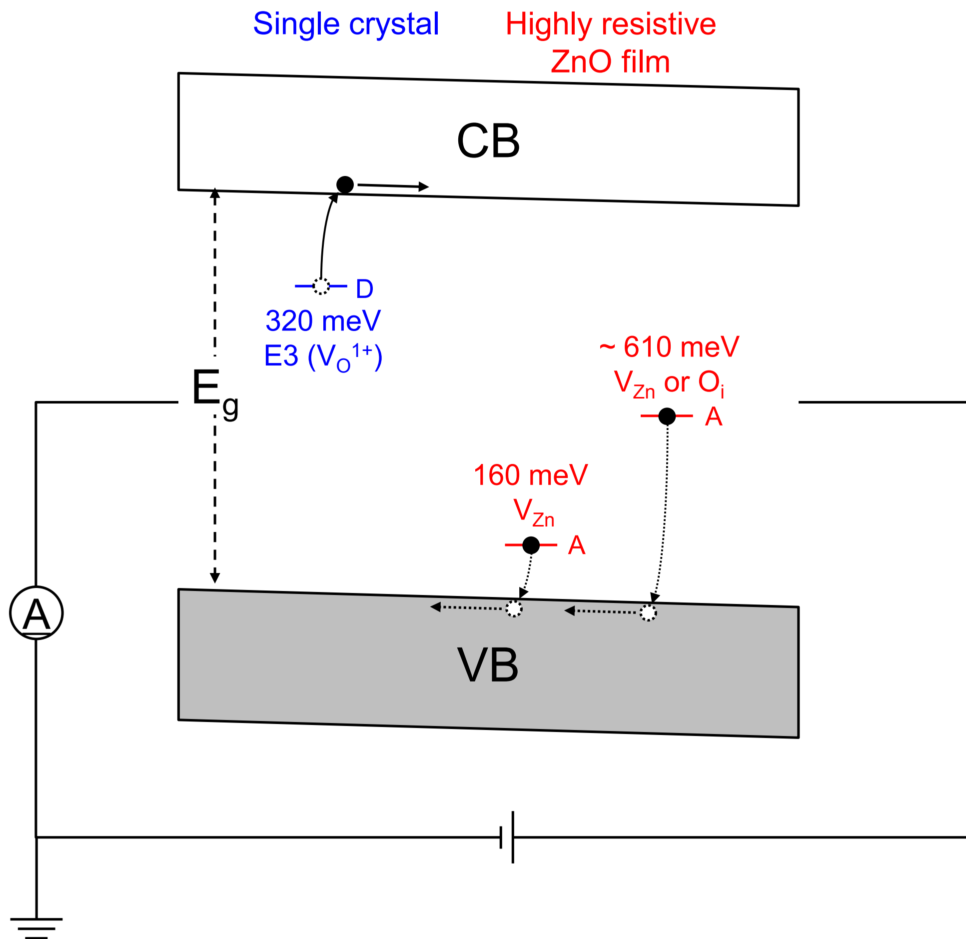

Fig. 5-16. A schematic illustration of carrier emission processes during the TSC measurement. D, A, V_O, V_{Zn} and O_i in this figure indicate donor level, acceptor level, oxygen vacancy, zinc vacancy and oxygen interstitial, respectively.

5-3-7 Application of this novel CVD process

Based on this work, we can conclude the several advantages of this novel CVD process utilizing N_2 plasma with small amount of O_2. It would be desirable to suppress unintentional parasitic reactions occurring in the gas line or upstream region of the reactors, because most of the CVD source materials have explosive reactivity with O_2 resulting in a deterioration in crystal quality.[15,96-98] N_2-based plasma improves the temporal and spatial homogeneity of the plasma through the work of the metastable $N_2(A^3\Sigma_u^+)$ with long radiative lifetime,[99,100] which also helps to enhance the extraction of excited species to the remote (downstream) region [101] resulting in damage-less remote plasma CVD processes near AP. NO under the effect of $N_2(A^3\Sigma_u^+)$ might be useful in forming nitrogen-doped p-type ZnO as theoretically predicted [102] and experimentally demonstrated.[103]

5-4 Conclusions

In conclusion, we have found a new CVD process for ZnO film using N_2 plasma with a small O_2 concentration (O_2%) generated near AP. In the OES of the plasma, OE lines corresponding to electron transitions of the N_2 2ps and the NO-γ were dominant at O_2% ranging from 0 to 1%. Despite a low O_2%, the growth rate is comparable to that of the films using the plasma including atomic O^* which plays an important role in forming oxide films at low pressure plasma processes. Our plasma analyses using OES, Q-mass, and gas sensor suggested that ZnO films with excellent crystallographic and optical properties were produced at the specific O_2% of 0.2% through the decomposition and oxidation of Zn source material by the coexistence state of NO-γ and O_3. By using this novel route, ZnO films with high crystallinity, excellent optical absorption property and high specific resistivity of 4×10^6 Ωcm were successfully obtained at the growth temperatures of as low as 200 °C at a wide process window, which is difficult to obtain through the conventional vacuum processes. TSC measurement detected two prominent trap states in our unique ZnO film grown at the O_2% of 0.2% with the activation energy of 170, and 610 meV, which were able to assign as acceptor-type defects: V_{Zn}, and V_{Zn} or O_i, respectively. This experimental result and theoretical prediction given by Janotti *et al.*[17)] suggests that AP plasma process is effective method for the realization of O-rich growth condition, which might leads to the formation of intrinsic and p-type ZnO films.

References

1) D. C. Reynolds, D. C. Look, and B. Jogai, Optically pumped ultraviolet lasing from ZnO, *Solid State Commun.* **99**, 873 (1996).
2) D. M. Bagnall, Y. F. Chen, Z. Zhu, T. Yao, M. Y. Shen, and T. Goto, High temperature excitonic stimulated emission from ZnO epitaxial layers, *Appl. Phys. Lett.* **73**, 1038 (1998).
3) T. Dietl, H. Ohno, F. Matsukura, J. Cibert, and D. Ferrand, Zener Model Description of Ferromagnetism in Zinc-Blende Magnetic Semiconductors, *Science* **287**, 1019 (2000).
4) T. Edahiro, N. Fujimura, and T. Ito, Formation of two-dimensional electron gas and the magnetotransport behavior of ZnMnO/ZnO heterostructure, *J. Appl. Phys.* **93**, 7673 (2003).
5) S. Ghosh, V. Sih, W. H. Lau, D. D. Awschalom, S.-Y. Bae, S. Wang, S. Vaidya, and G. Chapline, Room-temperature spin coherence in ZnO, *Appl. Phys. Lett.* **86**, 232507 (2005).
6) M. Nakano, T. Makino, A. Tsukazaki, K. Ueno, A. Ohtomo, T. Fukumura, H. Yuji, Y. Nishimoto, S. Akasaka, D. Takamizu, K. Nakahara, T. Tanabe, A. Kamisawa, and M. Kawasaki, $Mg_xZn_{1-x}O$-Based Schottky Photodiode for Highly Color-Selective Ultraviolet Light Detection, *Appl. Phys. Express* **1**, 121201 (2008).
7) K. Nakahara, S. Akasaka, H. Yuji, K. Tamura, T. Fujii, Y. Nishimoto, D. Takamizu, A. Sasaki, T. Tanabe, H. Takasu, H. Amaike, T. Onuma, S. F. Chichibu, A. Tsukazaki, A. Ohtomo, and M. Kawasaki, Nitrogen doped $Mg_xZn_{1-x}O$/ZnO single heterostructure ultraviolet light-emitting diodes on ZnO substrates, *Appl. Phys. Lett.* **97**, 013501 (2010).
8) K. Sato, L. Bergqvist, J. Kudrnovsky, P. H. Dederichs, O. Eriksson, I. Turek, B. Sanyal, G. Bouzerar, H. Katayama-Yoshida, V. A. Dinh, T. Fukushima, and H. Kizaki, First-principles theory of dilute magnetic semiconductors, *Rev. Mod. Phys.* **82**, 1633 (2010).
9) Aleksandra B. Djurišić, Xinyi Chen, Yu Hang Leung, and Alan Man Ching Ng, ZnO nanostructures: growth, properties and applications, *J. Mater. Chem.* **22**, 6526 (2012).
10) Y. Kozuka, A. Tsukazaki, and M. Kawasaki, Challenges and opportunities of ZnO-related single crystalline heterostructures, *Appl. Phys. Rev.* **1**, 011303 (2014).
11) J. D. Albrecht, P. P. Ruden, S. Limpijumnong, W. R. L. Lambrecht, and K. F.

Brennan, High field electron transport properties of bulk ZnO, *J. Appl. Phys.* **86**, 6864 (1999).

12) K. Maeda, M. Sato, I. Niikura, and T. Fukuda, Growth of 2 inch ZnO bulk single crystal by the hydrothermal method, *Semicond. Sci. Tech.* **20**, S49 (2005).

13) Bernard Gil, Didier Felbacq, and S. F. Chichibu, Exciton binding energies in chalcopyrite semiconductors, *Phys. Rev. B* **85**, 075205 (2012).

14) Ü. Özgür, Ya. I. Alivov, C. Liu, A. Teke, M. A. Reshchikov, S. Doğan, V. Avrutin, S.-J. Cho, and H. Morkoç, A comprehensive review of ZnO materials and devices, *J. Appl. Phys.* **98**, 041301 (2005).

15) R. Triboulet, J. Perrière, Epitaxial growth of ZnO films, *Prog. Cryst. Growth Charact.* **47**, 65 (2003).

16) M. D. McCluskey, and S. J. Jokela, Defects in ZnO, *J. Appl. Phys.* **106**, 071101 (2009).

17) A. Janotti, and C. G. Van de Walle, Native point defects in ZnO, *Phys. Rev. B* **76**, 165202 (2007).

18) T. Kawaharamura, H. Nishinaka, and S. Fujita, Growth of Crystalline Zinc Oxide Thin Films by Fine-Channel-Mist Chemical Vapor Deposition, *Jpn. J. Appl. Phys.* **47**, 4669 (2008).

19) S. Akasaka, K. Nakahara, A. Tsukazaki, A. Ohtomo, and M. Kawasaki, $Mg_xZn_{1-x}O$ Films with a Low Residual Donor Concentration ($<10^{15}$ cm^{-3}) Grown by Molecular Beam Epitaxy, *Appl. Phys. Express* **3**, 071101 (2010).

20) K. Sasaki, A. Kuramata, T. Masui, E. G. Víllora, K. Shimamura, and S. Yamakoshi, Device-Quality β-Ga_2O_3 Epitaxial Films Fabricated by Ozone Molecular Beam Epitaxy, *Appl. Phys. Express* **5**, 035502 (2012).

21) T. Kawaharamura, T. Uchida, D. Wang, M. Sanada, and M. Furuta, Enhancing carrier mobility of IGZO TFT fabricated by non-vacuum mist CVD with O_3 assistance, *Phys. Status Solidi C* **10**, 1565 (2013).

22) M. Iwasaki, H. Inui, Y. Matsudaira, H. Kano, N. Yoshida, M. Ito, and M. Hori, Nonequilibrium atmospheric pressure plasma with ultrahigh electron density and high performance for glass surface cleaning, *Appl. Phys. Lett.* **92**, 081503 (2008).

23) R. Hayakawa, T. Yoshimura, A. Ashida, T. Uehara, and N. Fujimura, Reaction of Si with excited nitrogen species in pure nitrogen plasma near atmospheric pressure, *Thin Solid Films* **506-507**, 423 (2006).

24) R. Hayakawa, M. Nakae, T. Yoshimura, A. Ashida, N. Fujimura, T. Uehara, M.

Tagawa, Y. Teraoka, Detailed structural analysis and dielectric properties of silicon nitride film fabricated using pure nitrogen plasma generated near atmospheric pressure, *J. Appl. Phys.* **100**, 073710 (2006).

25) R. Hayakawa, M. Yoshida, K. Ide, Y. Yamashita, H. Yoshikawa, K. Kobayashi, S. Kunugi, T. Uehara, and N. Fujimura, Structural analysis and electrical properties of pure Ge_3N_4 dielectric layers formed by an atmospheric-pressure nitrogen plasma, *J. Appl. Phys.* **110**, 064103 (2011).

26) M. Yuasa, and T. Yara, *Japan Patent* 3040358 (2000).

27) Y. Nose, T. Yoshimura, A. Ashida, T. Uehara, and N. Fujimura, Low Temperature Growth of ZnO Thin Films by Non-Equilibrium Atmospheric Pressure N_2/O_2 Plasma and the Growth Morphology of the Films, *Zairyo* **61**, 756 (2012) [in Japanese].

28) Y. Nose, T. Nakamura, T. Yoshimura, A. Ashida, T. Uehara, and N. Fujimura, Orientation Control of ZnO Films Deposited Using Nonequilibrium Atmospheric Pressure N_2/O_2 Plasma, *Jpn. J. Appl. Phys.* **52**, 01AC03 (2013).

29) R. Hayakawa, T. Yoshimura, A. Ashida, H. Kitahata, M. Yuasa, and N. Fujimura, Formation of Silicon Oxynitride Films with Low Leakage Current Using N_2/O_2 Plasma near Atmospheric Pressure, *Jpn. J. Appl. Phys.* **43**, 7853 (2004).

30) R. Hayakawa, M. Nakae, T. Yoshimura, A. Ashida, N. Fujimura, and T. Uehara, Effect of Additional Oxygen on Formation of Silicon Oxynitride Using Nitrogen Plasma Generated near Atmospheric Pressure, *Jpn. J. Appl. Phys.* **45**, 9025 (2006).

31) Y. Miyata, Y. Nose, T. Yoshimura, A. Ashida, and N. Fujimura, Evaluation of the electronic states in highly Ce doped Si films grown by low temperature molecular beam epitaxy system, *J. Cryst. Growth* **425**, 158 (2015).

32) M. Iwasaki, K. Takeda, M. Ito, T. Yara, T. Uehara, and M. Hori, Effect of Low Level O_2 Addition to N_2 on Surface Cleaning by Nonequilibrium Atmospheric-Pressure Pulsed Remote Plasma, *Jpn. J. Appl. Phys.* **46**, L540 (2007).

33) M. Iwasaki, Y. Matsudaira, K. Takeda, M. Ito, E. Miyamoto, T. Yara, T. Uehara, and M. Hori, Roles of oxidizing species in a nonequilibrium atmospheric-pressure pulsed remote O_2/N_2 plasma glass cleaning process, *J. Appl. Phys.* **103**, 023303 (2008).

34) Y. Nose, T. Yoshimura, A. Ashida, T. Uehara, and N. Fujimura, submitted to *J. Appl. Phys.*

35) Y. Nose, T. Yoshimura, A. Ashida, T. Uehara, and N. Fujimura, submitted to *Thin*

Solid Films.

36) R. Hayakawa, Dr. Thesis, Faculty of engineering, Osaka Prefecture University, Osaka, 2006.

37) Yefan Chen, D. M. Bagnall, Hang-jun Koh, Ki-tae Park, Kenji Hiraga, Ziqiang Zhu, and Takafumi Yao, Plasma assisted molecular beam epitaxy of ZnO on c-plane sapphire: Growth and characterization, *J. Appl. Phys.* **84**, 3912 (1998).

38) K. Nakahara, T. Tanabe, H. Takasu, P. Fons, K. Iwata, A. Yamada, K. Matsubara, R. Hunger, and S. Niki, Growth of undoped ZnO films with improved electrical properties by radical source molecular beam epitaxy, *Jpn. J. Appl. Phys.* **40**, 250 (2001).

39) M. Simek, V. Babicky, M. Clupek, S. DeBenedictis, G. Dilecce, and P. Sunka, Excitation of $N_2(C^3\Pi_u)$ and $NO(A^2\Sigma^+)$ states in a pulsed positive corona discharge in N_2, N_2-O_2 and N_2-NO mixtures, *J. Phys. D: Appl. Phys.* **31**, 2591 (1998).

40) Z. P. Wei, Y. M. Lu, D. Z. Shen, Z. Z. Zhang, B. Yao, B. H. Li, J. Y. Zhang, D. X. Zhao, X. W. Fan, and Z. K. Tang, Room temperature p-n ZnO blue-violet light-emitting diodes, *Appl. Phys. Lett.* **90**, 042113 (2007).

41) H. Kato, T. Yamamuro, A. Ogawa, C. Kyotani, and M. Sano, Impact of Mixture Gas Plasma of N_2 and O_2 as the N Source on ZnO-Based Ultraviolet Light-Emitting Diodes Fabricated by Molecular Beam Epitaxy, *Appl. Phys. Express* **4**, 091105 (2011).

42) E. Suetomi, T. Mizukoshi, K. Fukazawa, and A. Saito, Simulation of Atmospheric Pressure Glow Discharge Plasmas in Nitrogen-Oxygen Mixtures, *Konika Minolta Technology Report* **3**, 80 (2006) [in Japanese].

43) J. Nomoto, H. Makino, and T. Yamamoto, Carrier mobility of highly transparent conductive Al-doped ZnO polycrystalline films deposited by radio-frequency, direct-current, and radio-frequency-superimposed direct-current magnetron sputtering: Grain boundary effect and scattering in the grain bulk, *J. Appl. Phys.* **117**, 045304 (2015).

44) V. Srikant, and D. R. Clarke, On the optical band gap of zinc oxide, *J. Appl. Phys.* **83**, 5447 (1998).

45) S. T. Tan, B. J. Chen, X. W. Sun, W. J. Fan, and H. S. Kwok, Blueshift of optical band gap in ZnO thin films grown by metal-organic chemical-vapor deposition, *J. Appl. Phys.* **98**, 013505 (2005).

46) H. Bubert and F. W. Froben, Direct lifetime measurements of $NO(A^2\Sigma^+)$, *Chem.*

Phys. Lett. **8**, 242 (1971).

47) K. Watanabe, Edward C. Y. Inn, and M. Zelikoff, Absorption Coefficients of Oxygen in the Vacuum Ultraviolet, *J. Chem. Phys.* **21**, 1026 (1953).

48) M. Griggs, Absorption Coefficients of Ozone in the Ultraviolet and Visible Regions, *J. Chem. Phys.* **49**, 857 (1968).

49) Y. Iwata, H. Sakamoto, H. Inui, and M. Hori, Surface Modification of Solder Resist and Dry Film Resist by 60Hz Nonequilibrium Atmospheric Pressure Plasma Using O_2/N_2 Gas, *J. Surf. Finish. Soc. Jpn.* **62**, 311 (2011) [in Japanese].

50) The Surface Science of Japan (ed.), *X-ray Photoelectron Spectroscopy* (Maruzen, Tokyo 1998) p. 138 [in Japanese].

51) E. Burstein, Anomalous Optical Absorption Limit in InSb, *Phys. Rev.* **93**, 632 (1954).

52) D. C. Look, The Electrical and Photoelectronic Properties of Semi-Insulating GaAs, *Semiconductors and Semimetals* **19**, 75 (1983).

53) B. Šantić, and U. V. Desnica, Thermoelectric effect spectroscopy of deep levels-Application to semi-insulating GaAs, *Appl. Phys. Lett.* **56**, 2636 (1990).

54) Z.-Q. Fang, D. C. Look, and J. H. Zhao, Traps in semi-insulating InP studied by thermally stimulated current spectroscopy, *Appl. Phys. Lett.* **61**, 589 (1992).

55) K. Kuriyama, K. Sakai, K. Ushiyama, M. Okada, and K. Yokoyama, Thermally stimulated current study of electron-irradiated semi-insulating Fe-doped InP, *Solid State. Commun.* **100**, 389 (1996).

56) G. Hirt, T. Mono, and G. Müller, Spectroscopic investigation of deep levels related to the compensation mechanism of nominally undoped semi-insulating InP, *Mater. Sci. Eng. B* **28**, 101 (1994).

57) Z.-Q. Fang, D. C. Look, M. Uchida, K. Kainosho, and O. Oda, Deep Centers in Undoped Semi-Insulating InP, *J. Electron. Mater.* **27**, L68 (1998).

58) H. Witte, E. Schrenk, K. Flügge, A. Krost, J. Christen, B. Kuhn, and F. Scholz, Characterization of deep defects responsible for the quenching behavior in undoped GaN layers, *Phys. Rev. B* **71**, 125213 (2005).

59) D. C. Look, Z.-Q. Fang, W. Kim, Ö. Aktas, A. Botchkarev, A. Salvador, and H. Morkoç, Thermally stimulated current trap in GaN, *Appl. Phys. Lett.* **68**, 3775 (1996).

60) Z. C. Huang, J. C. Chen, and Dennis Wickenden, Characterization of GaN using thermally stimulated current and photocurrent spectroscopies and its application to

UV detectors, *J. Cryst. Growth* **170**, 362 (1997).

61) Z.-Q. Fang, B. Claflin, D. C. Look, G. C. Farlow, Electron irradiation induced deep centers in hydrothermally grown ZnO, *J. Appl. Phys.* **101**, 086106 (2007).

62) Z.-Q. Fang, B. Claflin, and D. C. Look, Effects of annealing in N_2 ambient on traps and persistent conduction in hydrothermally grown ZnO, *J. Appl. Phys.* **103**, 073714 (2008).

63) K. Kuriyama, K. Matsumoto, Y. Suzuki, K. Kushida, and Q. Xu, Persistent photoconductivity and thermally stimulated current related to electron-irradiation induced defects in single crystal ZnO bulk, *Solid State. Commun.* **149**, 1347 (2009).

64) A. Zeuner, H. Alves, D. M. Hofmann, B. K. Meyer, A. Hoffmann, U. Haboeck, M. Strassburg, and M. Dworzak, Optical Properties of the Nitrogen Acceptor in Epitaxial ZnO, *Phys. Stat. Sol. B* **234**, R7 (2002).

65) C. J. Pan, J. Y. Chen, G. C. Chi, B. W. Chou, B. J. Pong, F. Ren, C. Y. Chang, and S. J. Pearton, Optical investigation of nitrogen ion implanted bulk ZnO, *Vacuum* **83**, 1073 (2009).

66) K. Thonke, Th. Gruber, N. Teofilov, R. Schönfelder, A. Waag, and R. Sauer, Donor-acceptor pair transitions in ZnO substrate material, *Physica B* **308-310**, 945 (2001).

67) L. Wang, and N. C. Giles, Determination of the ionization energy of nitrogen acceptors in zinc oxide using photoluminescence spectroscopy, *Appl. Phys. Lett.* **84**, 3049 (2004).

68) K. Tamura, T. Makino, A. Tsukazaki, M. Sumiya, S. Fuke, T. Furumochi, M. Lippmaa, C. H. Chia, Y. Segawa, H. Koinuma, and M. Kawasaki, Donor-acceptor pair luminescence in nitrogen-doped ZnO films grown on lattice-matched $ScAlMgO_4$ (0001) substrates, *Solid State Commun.* **127**, 265 (2003).

69) D. C. Look, D. C. Reynolds, C. W. Litton, R. L. Jones, D. B. Eason, and G. Cantwell, Characterization of homoepitaxial p-type ZnO grown by molecular beam epitaxy, *Appl. Phys. Lett.* **81**, 1830 (2002).

70) L. Artús, R. Cuscó, E. Alarcón-Lladó, G. González-Díaz, I. Mártil, J. Jiménez, B. Wang, and M. Callahan, Isotopic study of the nitrogen-related modes in N^+-implanted ZnO, *Appl. Phys. Lett.* **90**, 181911 (2007).

71) A. Kaschner, U. Haboeck, M. Strassburg, M. Strassburg, G. Kaczmarczyk, A. Hoffmann, C. Thomsen, A. Zeuner, H. R. Alves, D. M. Hofmann, and B. K. Meyer,

Nitrogen-related local vibrational modes in ZnO:N, *Appl. Phys. Lett.* **80**, 1909 (2002).

72) M. Iwamoto, and D. Taguchi, *Thermally Stimulated Current in Electronic Materials -Analysis and Application-* (Corona, Tokyo, 2014), p. 102 [in Japanese].

73) Walter R.L. Lambrecht, Anna V. Rodina, Sukit Limpijumnong, B. Segall, and Bruno K. Meyer, Valence-band ordering and magneto-optic exciton fine structure in ZnO, *Phys. Rev. B* **65**, 075207 (2002).

74) T. Yamamoto (ed.), *State-of-the-Art Research and Prospective of Zinc Oxide*, (CMC shuppan, Tokyo, 2011) p. 9 [in Japanese].

75) Q. L. Gu, C. C. Ling, G. Brauer, W. Anwand, W. Skorupa, Y. F. Hsu, A. B. Djurisic, C. Y. Zhu, S. Fung, and L. W. Lu, Deep level defects in a nitrogen-implanted ZnO homogeneous p-n junction, *Appl. Phys. Lett.* **92**, 222109 (2008).

76) Eun-Cheol Lee, Y.-S. Kim, Y.-G. Jin, and K. J. Chang, Compensation mechanism for N acceptors in ZnO, *Phys. Rev. B* **64**, 085120 (2001).

77) J. Gao, R. Qin, G. luo, J. Lu, Y. Leprince-Wang, H. Ye, Z. Liao, Q. Zhao, and D. Yu, First-principles study of the formation mechanisms of nitrogen molecule in annealed ZnO, *Phys. Lett. A* **374**, 3546 (2010).

78) P. Fons, H. Tampo, A. V. Kolobov, M. Ohkubo, S. Niki, J. Tominaga, R. Carboni, F. Boscherini, and S. Friedrich, Direct Observation of Nitrogen Location in Molecular Beam Epitaxy Grown Nitrogen-Doped ZnO, *Phys. Rev. Lett.* **96**, 045504 (2006).

79) A. Kobayashi, H. Fujioka, J. Ohta, M. Oshima, Room Temperature Layer by Layer Growth of GaN on Atomically Flat ZnO, *Jpn. J. Appl. Phys.* **43**, L53 (2004).

80) F. Tuomisto, K. Saarinen, and D. C. Look, Irradiation-induced defects in ZnO studied by positron annihilation spectroscopy, *Phys. Stat. Sol. A* **201**, 2219 (2004).

81) A. Y. Polyakov, N. B. Smirnov, A. V. Govorkov, E. A. Kozhukhova, V. I. Vdovin, K. Ip, M. E. Overberg, Y. W. Heo, D. P. Norton, S. J. Pearton, J. M. Zavada, and V. A. Dravin, Proton implantation effects on electrical and recombination properties of undoped ZnO, *J. Appl. Phys.* **94**, 2895 (2003).

82) K. Kuriyama, M. Ooi, K. Matsumoto, and K. Kushida, Thermally stimulated current studies on deep levels in hydrothermally grown single crystal ZnO bulk, *Appl. Phys. Lett.* **89**, 242113 (2006).

83) N. T. Son, I. G. Ivanov, A. Kuznetsov, B. G. Svensson, Q. X. Zhao, M. Willander, N. Morishita, T. Ohshima, H. Itoh, J. Isoya, E. Janzén, and R. Yakimova, Recombination centers in as-grown and electron-irradiated ZnO substrates, *J. Appl.*

Phys. **102**, 093504 (2007).

84) Q. L. Gu, C. K. Cheung, C. C. Ling, A. M. C. Ng, A. B. Djurišić, L. W. Lu, X. D. Chen, S. Fung, C. D. Beling, and H. C. Ong, Au/n-ZnO rectifying contact fabricated with hydrogen peroxide pretreatment, *J. Appl. Phys.* **103**, 093706 (2008).

85) Q. L. Gu, C. C. Ling, X. D. Chen, C. K. Cheng, A. M. C. Ng, C. D. Beling, S. Fung, A. B. Djurišić, L. W. Lu, G. Brauer, and H. C. Ong, Hydrogen peroxide treatment induced rectifying behavior of Au/n-ZnO contact, *Appl. Phys. Lett.* **90**, 122101 (2007).

86) L. Scheffler, V. I. Kolkovsky, E. V. Lavrov, and J. Weber, Deep level transient spectroscopy studies of n-type ZnO single crystals grown by different techniques, *J. Phys.: Condens. Matter.* **23**, 334208 (2011).

87) J. C. Simpson, and J. F. Cordaro, Characterization of deep levels in zinc oxide, *J. Appl. Phys.* **63**, 1781 (1988).

88) G. Chicot, J. Pernot, J.-L. Santailler, C. Chevalier, C. Granier, P. Ferret, A. Ribeaud, G. Feuillet, and P. Muret, Electronic properties of E3 electron trap in n-type ZnO, *Phys. Stat. Sol. B* **251**, 206 (2014).

89) A. Y. Polyakov, N. B. Smirnov, A. I. Belogorokhov, A. V. Govorkov, E. A. Kozhukhova, A. V. Osinsky, J. Q. Xie, B. Hertog, and S. J. Pearton, Electrical properties and deep traps in ZnO films grown by molecular beam epitaxy, *J. Vac. Sci. Technol. B* **25**, 1794 (2007).

90) D. C. Look, Recent advances in ZnO materials and devices, *Mater. Sci. Eng. B* **80**, 383 (2001).

91) S. Graubner, C. Neumann, N. Volbers, B. K. Meyer, J. Bläsing, and A. Krost, Preparation of ZnO substrates for epitaxy: Structural, surface, and electrical properties, *Appl. Phys. Lett.* **90**, 042103 (2007).

92) L. E. Halliburton, N. C. Giles, N. Y. Garces, Ming Luo, Chunchuan Xu, Lihai Bai, and L. A. Boatner, Production of native donors in ZnO by annealing at high temperature in Zn vapor, *Appl. Phys. Lett.* **87**, 172108 (2005).

93) L. A. Kappers, O. R. Gilliam, S. M. Evans, L. E. Halliburton, and N. C. Giles, EPR and optical study of oxygen and zinc vacancies in electron-irradiated ZnO, *Nucl. Instrum. Methods Phys. Res. B* **266**, 2953 (2008).

94) D. K. Schroder, *Semiconductor Material and Device Characterization Third Edition* (Wiley, New York, 2007) p. 288.

95) K. Matsumoto, K. Kuriyama, and K. Kushida, Electrical and photoluminescence

properties of carbon implanted ZnO bulk single crystals, *Nucl. Instrum. Methods Phys. Res. B* **267**, 1568 (2009).

96) C. R. Gorla, N. W. Emanetoglu, S. Liang, W. E. Mayo, Y. Lu, M. Wraback, and H. Shen, Structural, optical, and surface acoustic wave properties of epitaxial ZnO films grown on $(01\bar{1}2)$ sapphire by metalorganic chemical vapor deposition, *J. Appl. Phys.* **85**, 2595 (1999).

97) J. Ye, S. Gu, S. Zhu, T. Chen, L. Hu, F. Qin, R. Zhang, Y. Shi, Y. Zheng, The growth and annealing of single crystalline ZnO films by low-pressure MOCVD, *J. Cryst. Growth* **243**, 151 (2002).

98) S. M. Smith, and H. B. Schlegal, Molecular Orbital Studies of Zinc Oxide Chemical Vapor Deposition: Gas-Phase Hydrolysis of Diethyl Zinc, Elimination Reactions, and Formation of Dimers and Tetramers, *Chem. Mater.* **15**, 162 (2003).

99) A. Lofthus and P. H. Krupenie, The spectrum of molecular nitrogen, *J. Phys. Chem. Ref. Data* **6**, 113 (1977).

100) R. Brandenburg, V. A. Maiorov, Y. B. Golubovskii, H.-E. Wagner, J. Behnke, and J. F. Behnke, Diffuse barrier discharges in nitrogen with small admixtures of oxygen: discharge mechanism and transition to the filamentary regime, *J. Phys. D: Appl. Phys.* **38**, 2187 (2005).

101) Y. Horikawa, K. Kurihara, and K. Sasaki, Effective Species in Inductively Coupled Nitrogen Plasma for Silicon Nitriding, *Appl. Phys. Express* **4**, 086201 (2011).

102) Y. Yan, S. B. Zhang, and S. T. Pantelides, Control of Doping by Impurity Chemical Potentials: Predictions for p-Type ZnO, *Phys. Rev. Lett.* **86**, 5723 (2001).

103) H. Matsui, H. Saeki, T. Kawai, H. Tabata, and B. Mizobuchi, N doping using N_2O and NO sources: From the viewpoint of ZnO, *J. Appl. Phys.* **95**, 5882 (2004).

Chapter 6: Chemical vapor deposition using nonequilibrium N_2/O_2 remote plasma generated near atmospheric pressure

6-1 Introduction

Nonequilibrium plasma generated near AP is classified into two different configurations: direct plasma and remote plasma,[1)] and the two types are employed for different purposes in accordance to the processing objects. As for the deposition process, direct plasma has been applied to the high speed deposition [2)] owing to the high plasma density.[3)] Nonequilibrium AP plasma besed on dielectric barrier discharge requires the covering of electrodes by dielectric materials and the narrow plasma gap of around 1 mm,[2)] which limits the conductivity and shape of the processing objects. On the other hand, remote plasma is able to apply for flexible substrate or metallic substrate, which allows a lot of process flexibility. The cleaning process of organic contaminant by remote plasma has partly put to the practical use in the manufacturing processes of liquid crystal display.[3,4)] Remote plasma is expected to reduce plasma damages to the substrates and films, which is often getting severe problem in the plasma deposition process of thin films. In case of He-based AP plasma, excited species expands and maintained far from the electrode owing to the benefit of quite long lifetime of metastable He.[5)] That of AP N_2/O_2-based plasma, however, the extraction of excited species to remote region should be the key issue due to the quite high collision frequency and short lifetime of excites species.[6,7)]

In chapter 5, we could obtain an important suggestion that the use of N_2 plasma with small amount of O_2 might be effective for the extraction of excited species to the remote region by the benefit of metastable N_2 species. In this chapter, therefore, we investigate the effect of experimental conditions on the extraction efficiency of excited species to the remote region at first. Based on the results of optical emission spectroscopy (OES) at the remote region, chemical vapor deposition (CVD) of ZnO films is demonstrated using N_2-based N_2/O_2 remote plasma generated near AP for the first time.

6-2 Difference in growth process: Direct and Remote regions

First of all, the difference of growth processes between direct and remote region is investigated return to the experiment performed in chapter 2 (see **Fig. 2-7** again). The distribution of film thickness and morphology along gas flow direction are summarized in **Fig. 6-1 (a)** and **(b)**, respectively. Based on these microscopic observations in **Fig. 6-1 (a)** and **(b)**, growth model along the gas flow direction is developed and schematically illustrated in **Fig. 6-1 (c)**. The regions are divided into five regions from upstream to downstream.

At region 1, where the gases are introduced in the plasma edge, hexagonal large grains with the diameter of 100 – 200 nm are observed. Although the shape is not film but pillar, this region seems to provide highly-crystallized ZnO compared with other downstream regions from 2 to 5. In this region, relatively small precursors (low molecular weight) such as Zn or ZnO should suspend in the vapor-phase and be incorporated into the crystal according to the isotropic surface free energy density of the pillar.[8)]

At region 2, where the gases are between the plasma edge and top electrode edge, the grain size is apparently smaller than that of region 1 and hexagonal structure is not confirmed. Similar phenomena have reported by Yasutake *et al.* during the AP-plasma enhanced CVD of Si films using horizontal reactor.[9)] According to their report, nucleation and condensation of precursors in the vapor phase, and subsequent formation of higher order particle result in the deterioration of crystal quality underneath the plasma edge. In our case, such higher order molecule [denoted as $(ZnO)_n$] might be generated at the transition region 2.

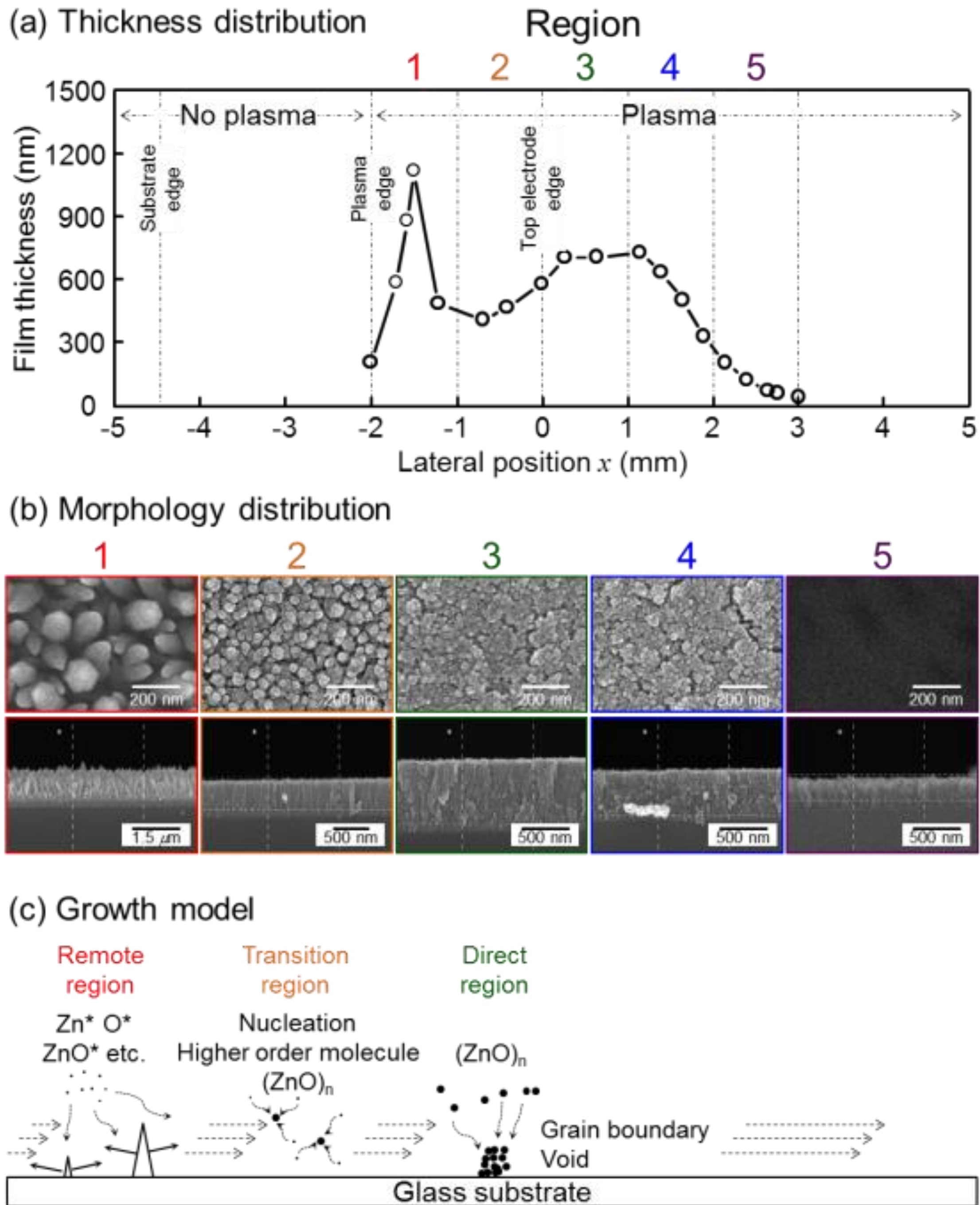

Fig. 6-1. Film thickness distribution along the gas flow direction **(a)**, surface and cross-sectional SEM images of ZnO films taken at various region **(b)** and growth model of ZnO films **(c)**.

At regions 3 - 5, where the gases are after entering the direct plasma, the grain size is even smaller than that of region 1 and 2. Cross-sectional high magnification SEM images confirm small spherical nano-grains with the diameter of 20 – 30 nm in these regions, suggesting that the higher order molecule formed in the vapor phase is incorporated in the crystal. Note that we could successfully achieve epitaxial growth of ZnO films even in direct plasma as shown in chapter 4. [see **Fig. 4-1 (b)** again] Therefore, we conclude that although the precursor of the direct plasma might be higher order molecules, the size are not as large as that disturb the epitaxial growth of ZnO films.

From this growth model, the author expects that the use of remote plasma might be effective for the enhancement of crystallinity, but the injection method of source materials should be carefully determined to avoid the formation of higher order molecules especially for the reactive source materials such as diethylzinc (DEZn).

6-3 Experimental setup for remote plasma CVD

According to the findings obtained in the last section, remote plasma CVD system was newly developed as shown in **Fig. 6-2**. N_2 plasma with small amount of O_2 addition is generated between two parallel prate electrodes covered with silicon nitride dielectric and separated by uniform spacing of 1 mm by applying an AC voltage and frequency of 2.3 - 2.5 kV and 160 kHz, respectively. N_2 flow rate (F_{N2}) and total pressure of the reactor (p) are fixed at 6 slm and 5.3 kPa, respectively. O_2 concentration in N_2/O_2 mixture is varied from 0 to 49% so as to access the expansion of plasma to the remote region. As for the deposition of ZnO films, diethyl zinc (DEZn) was selected as Zn source material. DEZn was supplied by bubbling of N_2 carrier gas and the saturated vapor was transported to underneath the substrates by stainless delivery tube at the constant flow rate of 0.23 μmol/min and subsequently mixed at the remote region, because DEZn have an explosive reactivity with oxidants.[10,11] Separate injection of source materials should be effective for the suppression of higher order molecules.[12] Additionally, the flow direction of the remote plasma is set perpendicular to the sample surface so as to deliver DEZn quickly after mixing with plasma. Such an idea has also been applied to the MOVPE growth of AlGaN films.[13,14] As a substrate, atomically flat sapphire (0001) was used as in the chapter 4 [see **Fig. 4-3 (a)** again], which is fixed 5 mm above the dielectric box and heated from 400 to 600 °C. After the deposition, the crystal structure was investigated by X-ray diffraction (XRD). The film thickness and the morphology were evaluated by field emission type scanning electron microscope (FE-SEM).

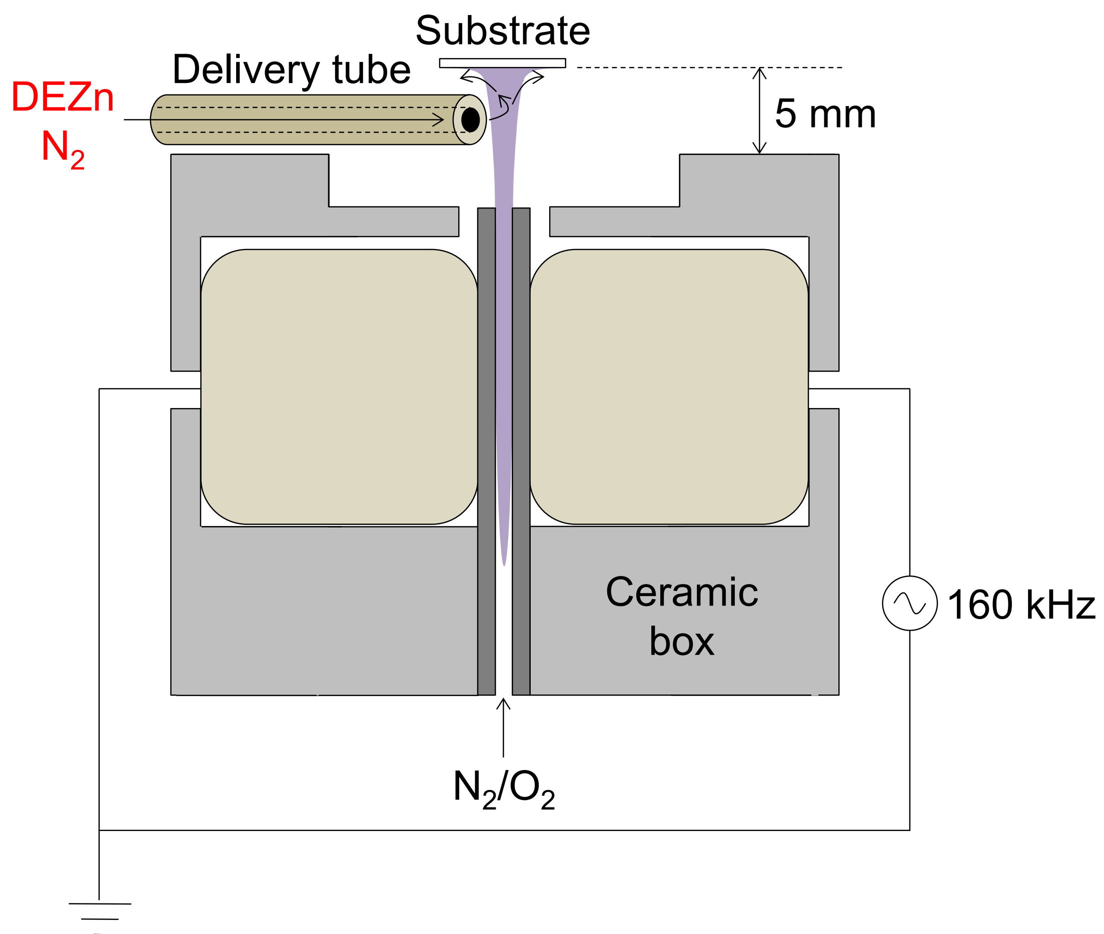

Fig. 6-2. A schematic illustration of CVD system using N_2/O_2 remote plasma generated near atmospheric pressure.

6-4 Results and discussions

6-4-1 Extraction of excited species to remote region

As discussed in chapter 5, the use of N_2 plasma with small amount of O_2 seems to be a key point for the effective extraction of excited species to the remote region. Based on this finding, OES was performed for N_2 plasma with small amount of O_2. OE of remote plasma was corrected through quartz view port. Optical fiber was fixed perpendicular to the view port so as to correct the OE at 5 mm above the ceramic box, which corresponds to the mounted position of substrates.

Fig. 6-3 (a) shows OE spectra of remote plasma generated at the O_2% of 0.017%. OE of NO-γ system [NO-γ: $A^2\Sigma^+ \longrightarrow X^2\Pi_\gamma^+$], N_2 second positive system [N_2 2ps: $C^3\Pi_u^+ \longrightarrow B^3\Pi_g^+$], N_2O [$O(1S)N_2 \longrightarrow O(1D)N_2$] and N_2 Herman's infrared system [N_2 HIR: $C^5\Pi_g \longrightarrow A^5\Sigma_g^+$] are simultaneously observed. N_2O and N_2 HIR were not observed in direct plasma, probably due to the long radiative lifetime of N_2O and the intense background OE of N_2 first positive system [N_2 1ps: $B^3\Pi_u^+ \longrightarrow A^3\Sigma_u^+$], respectively. In case of remote region, plasma should be maintained by the mutual collision of excited species, because most of the excited states have very short radiative lifetimes [e.g. Lifetime of $N_2(C^3\Pi_u^+)$ < 1μs]. As described in chapter 5 (see **Fig. 5-9** again), metastable $N_2(A^3\Sigma_u^+)$ play important role in the generation of NO from N_2/O_2 mixture. According to the plasma analysis reported by Hayakawa *et al*. employed the same experimental setup, mutual collision of metastable $N_2(A^3\Sigma_u^+)$s is the origin of N_2 HIR emission.[15] Therefore, the density of metastable $N_2(A^3\Sigma_u^+)$ should play a key role in maintaining N_2-based remote plasma.

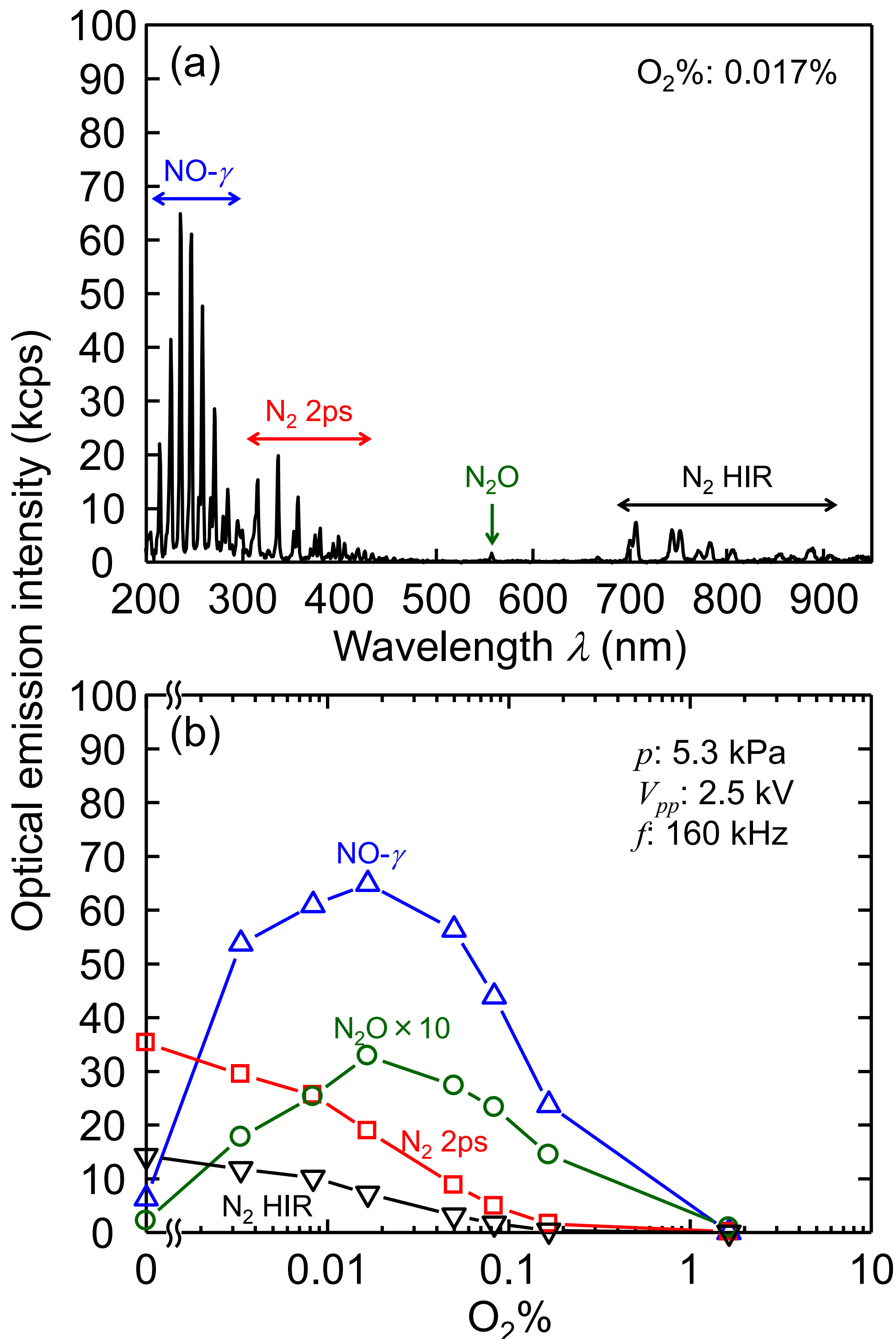

Fig. 6-3. OE spectrum of N_2/O_2 remote plasma generated at the O_2% of 0.17%. **(a)** Change of the OE intensity of NO-γ (234 nm), N_2 2ps (337 nm), N_2 HIR (707 nm) and N_2O (557 nm) against the change of the O_2%. **(b)** Throughout this experiment, discharge pressure p, applied voltage V_{pp} and frequency f are 5.3 kPa, 2.5 kV and 160 kHz, respectively.

Subsequently, the intensity of these four OE lines was plotted as a function of the O_2%. [**Fig. 6-3 (b)**] OE intensity of N_2 2ps and N_2 HIR show monotonic decrease against the increase of O_2% due to the decrease of metastable $N_2(A^3\Sigma_u^+)$ in the remote plasma as discussed in chapter 3 (3-3-2) and chapter 5 (5-3-1).[16] On the other hand, that of NO-γ and N_2O reaches to the maximum around the O_2% of 0.02% and then decrease at higher O_2% also affected by the concentration of metastable $N_2(A^3\Sigma_u^+)$.[16] At the O_2% > 1% the OE of plasma was hardly confirmed, suggesting that most of the radiative excited species are deactivated immediately after taking off from direct region. These results indicates that the metastable $N_2(A^3\Sigma_u^+)$ with long radiative lifetime plays the key role in the generation and maintenance of remote plasma.

6-4-2 Characterization of ZnO films

After the remote plasma CVD of ZnO films, the crystal structure and the crystallinity of the obtained films were investigated by XRD. **Fig. 6-4 (a)** shows 2θ-ω scanned XRD profile of ZnO films deposited on sapphire (0001) substrate at the T_g of 400 °C. ZnO film shows (0001) preferred orientation. In order to get information on the epitaxial relationship between ZnO and underneath sapphire substrate, ϕ-scan was performed following the 2θ-ω scan. As an inclined plane, ZnO $10\bar{1}1$ and Sapphire $10\bar{1}4$ was selected as shown in **Fig. 6-4 (b)**. Six folded peaks of ZnO indicate the epitaxial growth of ZnO films. The out-of-plane and in-plane epitaxial relationship are summarized as follows. (0001) ZnO // (0001) sapphire and $[10\bar{1}0]$ ZnO // $[10\bar{1}0]$ sapphire.

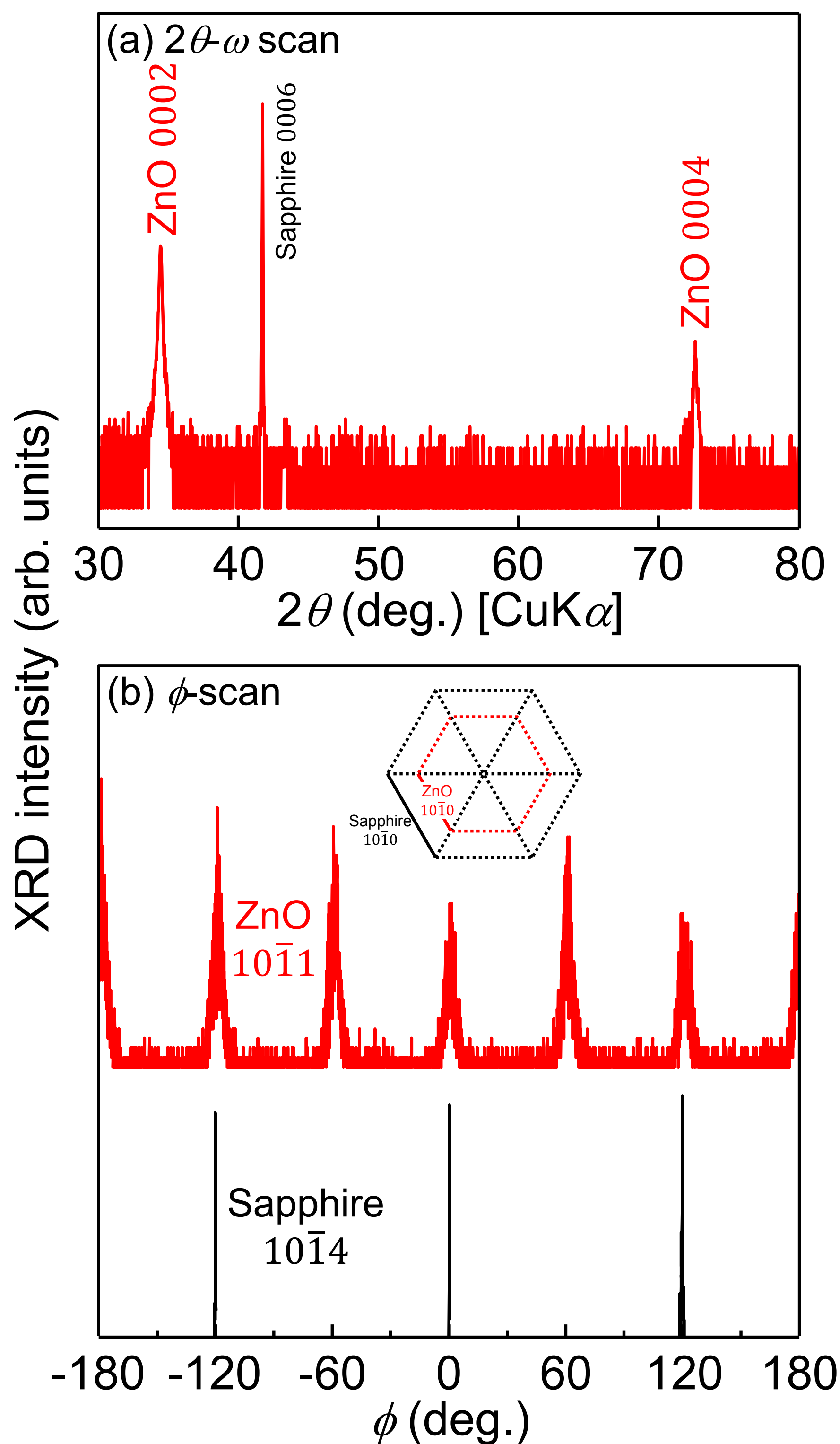

Fig. 6-4. 2θ-ω scanned **(a)** and ϕ scanned **(b)** XRD profiles for epitaxially grown ZnO films on sapphire (0001) substrate at 400 °C. Epitaxial relationships along out-of-plane and in-plane directions are (0001) ZnO // (0001) sapphire and $[10\bar{1}0]$ ZnO // $[10\bar{1}0]$ sapphire, respectively.

Fig. 6-5 shows cross-sectional SEM image of this sample. The picture of cross-section is taken after cleaving the sample. ZnO films are composed of dense columnar grain with the diameter of approximately 100 nm. Small spherical nano grains possibly originate from the formation of higher order molecule as observed region 3 and 4 in **Fig. 6-1** is not confirmed, suggesting that the growth mode is similar to that of region 1 in **Fig. 6-1** even for the use of DEZn with explosive reactivity with oxidant. Although the film is as thick as 2.3 μm, the surface flatness seems to be maintained.

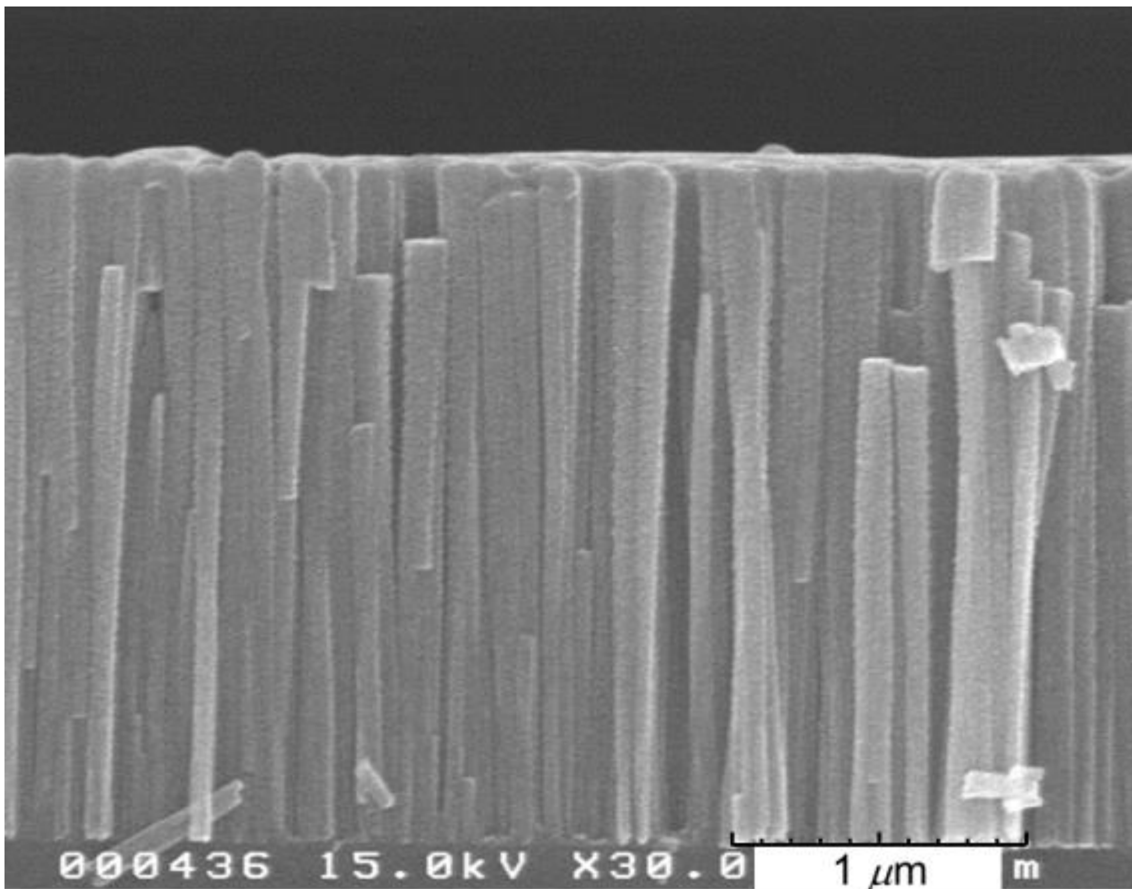

Fig. 6-5. Cross sectional SEM image of ZnO films. This picture was taken after cleaving the sample.

In order to access the macroscopic growth mechanism, growth rate was evaluated at various growth conditions (O_2%, T_g). The results are summarized in **Fig. 6-6**. At first, note that the difference of the growth rates by plasma CVD and thermal CVD (without plasma ignition) for ZnO films grown at the O_2% and T_g of 1.6% and 400 ^{o}C, respectively. The growth rate of ZnO films grown by plasma CVD becomes nearly 5 times higher than that by thermal CVD, indicating that the growth is undoubtedly accelerated by the excited species in the remote plasma. Next, O_2% is changed from 0.16 to 49% to investigate the contribution of radiative species to the formation of ZnO films refer to the result of OES shown in **Fig. 6-3 (b)**. The growth rate of ZnO gradually increases against the increase of O_2%. According to the OES shown in **Fig. 6-3 (b)**, All the OEs monotonically decrease with increasing the O_2% from 0.16%. Therefore, non-radiative excited species should be a source of oxygen in ZnO films. The most possible candidate of non-radiative excited species are O_3 and O($^3P_2$) from the discussion in chapter 5 (see **Fig. 5-9** again). Finally, T_g is increased from 400 to 600 ^{o}C for both of plasma and thermal CVD. The growth rate is rapidly increase to as high as 400 nm/min and apparently affected by the T_g for both cases, indicating that the growth is limited by the surface reaction of DEZn. Note that the yield is as high as 35%. This result also suggests that the remote plasma CVD with the flow direction of the remote plasma perpendicular to the sample surface as in our system has pussing effects of Zn source materials, which result in the high yield while avoiding the source material loss. Provided the growth mode can be changed to supply limited mode, the yield should be enhanced more.

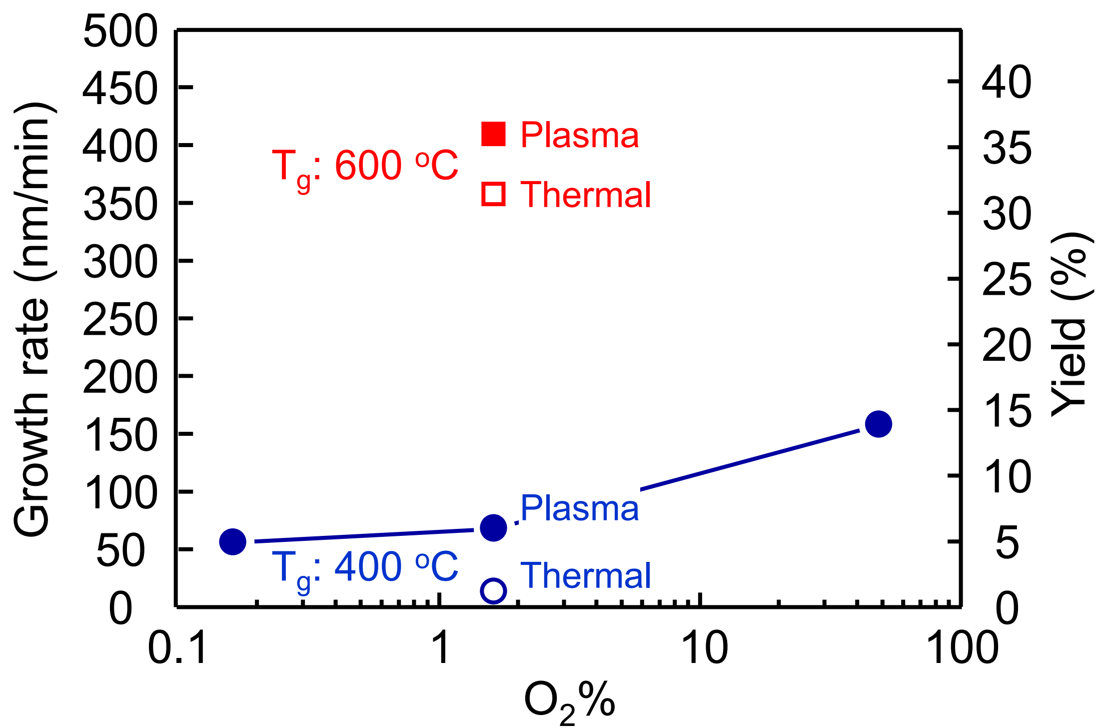

Fig. 6-6. Change of the growth rate of ZnO films against the change of the O_2%. Deposition was performed at the T_g of 400 and 600 °C by plasma and thermal CVD. Yield in the right axis is approximately calculated from the volume of films on sapphire substrate.

6-5 Conclusions

According to the position dependence of the growth morphology, remote plasma region is useful for the deposition of highly crystalline ZnO films. Thus, N_2 plasma with small amount of O_2 was proposed for the realization of remote plasma CVD near AP. OES at the remote region indicates that the radiative excited species is effectively generated at the O_2% below 1%. Nonequilibrium N_2/O_2 remote plasma near AP was employed to the CVD of ZnO films for the first time using diethyl zinc (DEZn) as Zn source material. ZnO films were epitaxially grown on sapphire (0001) substrate with the epitaxial relationship of (0001) $[10\bar{1}0]$ ZnO // (0001) $[10\bar{1}0]$ sapphire. Although the growth of ZnO was limited by the surface reaction of DEZn, the growth rate and material yield of DEZn was as high as 400 nm/min and 35%, respectively. These values are rather high compared with the other reports regarding the CVD of ZnO films.[17)] This result also suggests that the remote plasma CVD with the gas flow is perpendicular to the sample surface as in our system has pussing effects of Zn source gases result in the high material yield while avoiding the source material loss and unintentional vapor phase reaction even when we use metal organic (MO) compound with explosive reactivity with oxidant near AP.

References

1) G. Lucovsky, and D. V. Tsu, Plasma enhanced chemical vapor deposition: Differences between direct and remote plasma excitation, *J. Vac. Sci. Tech. A* **5**, 2231 (1987).
2) D. Merche, N. Vandencasteele, and F. Reniers, Atmospheric plasmas for thin film deposition: A critical review, *Thin Solid Films* **520**, 4219 (2012).
3) M. Iwasaki, H. Inui, Y. Matsudaira, H. Kano, N. Yoshida, M. Ito, and M. Hori, Nonequilibrium atmospheric pressure plasma with ultrahigh electron density and high performance for glass surface cleaning, *Appl. Phys. Lett.* **92**, 081503 (2008).
4) M. Iwasaki, Y. Matsudaira, K. Takeda, M. Ito, E. Miyamoto, T. Yara, T. Uehara, and M. Hori, Roles of oxidizing species in a nonequilibrium atmospheric-pressure pulsed remote O_2/N_2 plasma glass cleaning process, *J. Appl. Phys.* **103**, 023303 (2008).
5) G. R. Nowling, S. E. Babayan, V. Jankovic, and R. F. Hicks, Remote plasma-enhanced chemical vapour deposition of silicon nitride at atmospheric pressure, *Plasma Source Sci. Technol.* **11**, 97 (2002).
6) J. Loureiro, P. A. Sá, and V. Guerra, Role of long-lived $N_2(X^1\Sigma_g^+,v)$ molecules and $N_2(A^3\Sigma_u^+)$ and $N_2(a'^1\Sigma_u^-)$ states in the light emissions of an N_2 afterglow, *J. Phys. D: Appl. Phys.* **34**, 1769 (2001).
7) H. H. Brömer, and F. Spieweck, Lifetime and diffusion coefficient of the $N_2(A^3\Sigma_u^+)$ state of N_2, *Planet. Space Sci.* **15**, 689 (1967).
8) N. Fujimura, T. Nishihara, S. Goto, J. Xu, and T. Ito, Control of preferred orientation for ZnO_x films: control of self-texture, *J. Cryst. Growth* **130**, 269 (1993).
9) K. Yasutake, H. Ohmi, H. Kakiuchi, T. Wakamiya, and H. Watanabe, Characterization of Epitaxial Si Films Grown by Atmospheric Pressure Plasma Chemical Vapor Deposition Using Cylindrical Rotary Electrode, *Jpn. J. Appl. Phys.* **45**, 3592 (2006).
10) C. R. Gorla, N. W. Emanetoglu, S. Liang, W. E. Mayo, Y. Lu, M. Wraback, and H. Shen, Structural, optical, and surface acoustic wave properties of epitaxial ZnO films grown on $(01\bar{1}2)$ sapphire by metalorganic chemical vapor deposition, *J. Appl. Phys.* **85**, 2595 (1999).

11) J. Ye, S. Gu, S. Zhu, T. Chen, L. Hu, F. Qin, R. Zhang, Y. Shi, Y. Zheng, The growth and annealing of single crystalline ZnO films by low-pressure MOCVD, *J. Cryst. Growth* **243**, 151 (2002).
12) K. Matsumoto, and A. Tachibana, Growth mechanism of atmospheric pressure MOVPE of GaN and its alloys: gas phase chemistry and its impact on reactor design, *J. Cryst. Growth* **272**, 360 (2004).
13) H. Amano, N. Sawaki, I. Akasaki, and Y. Toyoda, Metalorganic vapor phase epitaxial growth of a high quality GaN film using an AIN buffer layer, *Appl. Phys. Lett.* **48**, 353 (1986).
14) J. R. Creighton, W. G. Breiland, M. E. Coltrin, and R. P. Pawlowski, Gas-phase nanoparticle formation during AlGaN metalorganic vapor phase epitaxy, *Appl. Phys. Lett.* **81**, 2626 (2002).
15) R. Hayakawa, T. Yoshimura, A. Ashida, N. Fujimura, H. Kitahata, and M. Yuasa, Analysis of nitrogen plasma generated by a pulsed plasma system near atmospheric pressure, *J. Appl. Phys.* **96**, 6094 (2004).
16) E. Suetomi, T. Mizukoshi, K. Fukazawa, and A. Saito, Simulation of Atmospheric Pressure Glow Discharge Plasmas in Nitrogen-Oxygen Mixtures, *Konika Minolta Technology Report* **3**, 80 (2006) [in Japanese].
17) R. Triboulet, J. Perriere, Epitaxial growth of ZnO films, *Prog. Cryst. Growth Charact.* **47**, 65 (2003).

Chapter 7: General conclusions

This thesis has been devoted to the experimental verification of the advantages of N_2-based nonequilibrium N_2/O_2 plasma generated near atmospheric pressure (AP) to the reduction of residual electron and nitrogen doping to ZnO films for the application to next generation CVD process of ZnO based semiconductors. On the basis of various plasma analysis and film characterization techniques, reaction processes in the plasma and resulting electronic state of ZnO films are elucidated in detail. The result of this thesis is comprehensively summarized as follows.

In chapter 2, the author developed a chemical vapor deposition (CVD) system using O_2-based N_2/O_2 direct plasma generated near atmospheric pressure (AP), which is expected to be the most effective use of the reactivity of excited species in the plasma. As a Zn source material, β-diketonate complexes: Bis-2,4octanedionato zinc [$Zn(C_8H_{13}O_2)_2$ denoted as $Zn(OD)_2$] was selected, which is free from spontaneous combustibility and liquid at ambient conditions. In the plasma, optical emission (OE) lines corresponding to the atomic oxygen (Atomic O^*) were predominantly observed, which often plays important roles in low pressure plasma processes such as sputtering of oxide films. The growth of thin films was carried out using this plasma. X-ray diffraction for deposited films indicated the successful formation of ZnO films with (0001) preferred orientation at the growth temperature of as low as 200 ºC. ZnO film showed high optical transmittance in the visible light region with no noticeable in-gap light absorption and sharp basic absorption edge corresponding to the bandgap of ZnO. The film thickness distribution was measured along the gas flow direction in the

horizontal reactor. Growth of ZnO films was not confirmed at the most upstream region where no plasma was generated (thermal CVD), whereas the growth started as soon as the mixed gases were introduced into the remote plasma, indicating that the excited species in the plasma are responsible for the decomposition and oxidation reaction of $Zn(OD)_2$. Furthermore, change of the growth rate of ZnO films in direct plasma was investigated against the change of $Zn(OD)_2$ flow rate [$F_{Zn(OD)2}$], O_2 flow rate [F_{O2}] and growth temperature [T_g] to evaluate the growth process from macroscopic viewpoint based on the chemical reaction formula. As a result, the growth rate of ZnO films was susceptible to the $F_{Zn(OD)2}$, and independent on the F_{O2} and T_g. From these results, the growth process of ZnO films was in a supply limited state even at the T_g of as low as 200 ºC, indicating the advantage of nonequilibrium plasma generated near AP toward the low temperature growth of ZnO films.

In chapter 3, the author accessed the effects of radiative activated species in the plasma on crystallinity and electrical property of ZnO films. The O_2 concentration in the N_2/O_2 mixture gases was systematically varied from 0 to 100%. Optical emission (OE) of the N_2 second positive system (N_2 2ps) was observed over a wide range of O_2% other than 100%. In addition, OE lines of nitric monoxide molecule (NO) corresponding to NO-γ system (NO-γ) were recognized only at the O_2% of below or 1%. Meanwhile, OE lines of atomic oxygen (Atomic O^*) which should take part in the formation of ZnO film in chapter 2 were observed at the O_2% ranging from 20 to 100%. These results enabled the selection and control of the type and density of each active species by adjusting the O_2%. Based on the finding, CVD was performed at various O_2% to investigate the relationship between active species and properties ZnO films. ZnO films

showed (0001) preferred orientation as shown in chapter 2 at wide range of O_2% from 0.1 to 90%, however, the magnitude of (0001) preferred orientation on the basis of texture coefficient increased at specific O_2%s of 0.2 and 20%, indicating the possibility of texture control by active species without increasing T_g. Subsequently, the specific resistivity of ZnO films was evaluated. Although that is affected by O_2%, ZnO films showed high resistivity of 10^3 - 10^6 Ωcm, which had been difficult to obtain by conventional vacuum processes. Moreover, the gas flow velocity was increased from 0.7 to 3.8 m/s to reduce unintentional parasitic reactions. As a result, the texture coefficient was increased while keeping quite high resistivity of 10^6 -10^7 Ωcm. This result indicates that ZnO films with low residual electron concentration are able to form even at a small O_2 concentration, which is very important for the nitrogen doping to ZnO films.

In chapter 4, the author intended to clarify the origin of high resistivity. ZnO films were grown by epitaxial growth technique using N_2-based nonequilibrium N_2/O_2 plasma generated near AP in order to approach a more intrinsic origin of high resistivity. As a result, ZnO epitaxial films without noticeable incorporation of 30° rotational domain were obtained. Photoluminescence measurement was carried out to evaluate the in-gap states of highly resistive epitaxial films. Control samples (PLD-grown ZnO epitaxial film and ZnO single crystal) showed broad green luminescence around 2.3 eV possibly originate from oxygen vacancy (V_O) donor, whereas our highly resistive ZnO films showed dominant red emission around 1.8 eV, suggesting the existence of zinc vacancy (V_{Zn}) acceptor. In order to approach the origin of high resistivity directly, temperature-dependent Hall-effect (TDH) measurement was carried out using Hall-bar

structure and found that the residual electron concentration was on the order of 10^{13} - 10^{15} cm^{-3} even at 400 K, indicating that the high resistivity is due to the extremely low electron concentration. Secondary ion mass spectrometry (SIMS) measurement and Raman spectroscopy in conjunction with the analysis of TDH measurement suggested that the density of shallow donor is rather lower than that of deep donor, and electron from the deep donor is partially compensated by acceptors such as V_{Zn}. This result suggests the advantage of nonequilibrium plasma generated near AP for the reduction of not only residual electron but also shallow donor, which had been the biggest issue for the practical application of ZnO.

In chapter 5, the author discovered a new CVD process for ZnO films using N_2 plasma with a small O_2 concentration (O_2%) generated near AP. In the OES of the plasma, OE lines corresponding to electron transitions of the N_2 2ps and the NO-γ were dominant at O_2% ranging from 0 to 1%. Despite a low O_2%, the growth rate of ZnO films was comparable to that of ZnO films grown by atomic O^* which plays an important role in forming oxide films at low pressure plasma processes. Our plasma analysis using OES, Q-mass, and gas sensor suggested that ZnO films with excellent crystallinity, optical transparency and low residual electron concentration were produced at the specific O_2% of 0.2% by the coexistence state of NO-γ and O_3. Moreover, the trap level and capture cross section, both of which are inherent physical quantity of a specific defect, were evaluated by thermally stimulated current (TSC) measurements. As a result, V_{Zn} acceptor was identified again as in epitaxial films shown at chapter 4, but V_O donor was not observed in the TSC curve. From the above, the

author proposed the advantage N_2 plasma with a small O_2% as a novel oxidative growth method of ZnO films.

In chapter 6, the author focused on the use of remote plasma for the deposition of ZnO films. In addition to the film thickness distribution along gas flow direction discussed in chapter 2, the distribution of growth morphology was evaluated. As a result, highly crystallized hexagonal pillars were grown at the remote region where the source gases were soon after entering the discharging region. Therefore, the plasma generation condition was investigated by OES from the viewpoint of extraction efficiency of excited species to remote region. In OE spectra, the extraction of radiative species was confirmed only at the O_2% of 1.6% or less. CVD of ZnO films was performed on sapphire substrate located at 5 mm above the plasma outlet by mixing diethylzinc (DEZn) separately in the vicinity of the substrate. As a result, epitaxial growth of ZnO thin films was confirmed at the growth temperature of 400 ºC. Cross-sectional observation by scanning electron microscope (SEM) found highly crystallized and dense columnar grains with the diameter of approximately 100 nm, suggesting that the unintentional vapor phase reaction was suppressed by the use of remote plasma. Although the growth was limited by the surface reaction, very high growth rate of 400 nm/min and material utilization efficiency of 35% were achieved. From above, remote plasma is effective for the suppression of vapor phase reactions, which enabled the use of highly reactive source materials such as metal organic compounds.

These results show the advantages of N_2-based nonequilibrium N_2/O_2 plasma generated near AP for overcoming the problems of residual electron, shallow donor and oxygen deficiency in ZnO films, which will open up a new window not only for the

reduction of oxygen deficiency in oxides but for the nitrogen doping to oxides and for the formation of oxinitrides.

Acknowledgement

The works summarized in this doctoral thesis were performed throughout the doctoral course in Physics of Novel Devices Laboratory at Osaka Prefecture University.

First of all, the author would like to express his sincerest appreciation to Prof. Norifumi Fujimura, Department of Physics and Electronics, Osaka Prefecture University, for the guidance, advice and encouragement to this work regardless of day and night. The author is grateful to Prof. Yoshihiko Hirai and Prof. Hiroaki Kawata for their useful advices and reviewing this thesis based on their deep insights on the semiconductor processes and plasma processes. The author appreciates to Prof. Takekazu Ishida, Prof. Hajime Ishihara, Prof. Hiroyoshi Naito, Prof. Seiji Akita, Prof. Hiromichi Horinaka, Prof. Satoru Noguchi and Prof. Atsushi Ashida for their constructive advices to this thesis.

The author is indebted to Associate Prof. Takeshi Yoshimura for their dedicated guidance and advices since the beginning of this research.

The author enormously appreciates to Mr. Motokazu Yuasa, Mr. Tsuyoshi Uehara, Mr. Junichiro Anzai, Dr. Shunsuke Kunugi, Ms. Sachiko Asao, Mr. Satoshi Yoguchi in Sekisui Chemical Co. Ltd. for their kind suggestion and collaborate research.

The author appreciates to Associate Prof. Yoshihiko Togawa and Mr. Yu Matsumoto for their advices and discussions on magnetotransport measurements.

The author would like to acknowledge to Dr. Hiroya Kitahata and Dr. Masato Miyake for their precise advices to this research based on their deep insights on the

chemical vapor deposition processes.

The author is deeply indebted to Dr. Takahiro Nagata of National Institute for Materials Science for his useful advices especially in XPS measurement.

This thesis is based on the research given by Dr. Ryoma Hayakawa of National Institute for Materials Science. The author would like to express great respect to his pioneering works and appreciate to his valuable advices.

The author also thanks heartily Ms. Sakiko Haji, Ms. Mami Yoneta and Ms. Tomomi Omura for their sincere helps to this research.

Acknowledgement are also due to Dr. Tatsuru Nakamura, Mr. Kota Ide, Mr. Takuma Terakawa, Mr. Takuya Kiguchi, Mr. Hironori Iwasaki, Mr. Xiangqian Zhao, Mr. Guangzhi Yu, Mr. Kenshi Takada and their cooperation to this research. Special thanks are similarly due to graduated, graduate and undergraduate students in Professor Fujimura's laboratory.

A part of this research was financially supported by a Grant-in-Aid for Japan Society for the Promotion of Science Fellows (Grant No. 14J11730).

Finally, I wish to express appreciation to my parents: Yoshitaka Nose and Masayo Nose and to my brother: Tomotsugu Nose for their support and encouragement for a long time. I am particularly grateful for the assistance given by my wife: Hitomi Nose. This thesis would not have been possible without her dedicated support.

Yukinori Nose

February 2016

Original Articles Regarding this thesis

No.	Title	Authors	Journal	Related chapter
1	大気圧非平衡酸窒素プラズマを用いた ZnO 薄膜の低温形成とその成長形態	野瀬 幸則 吉村 武 芦田 淳 上原 剛 藤村 紀文	材料, Vol. 61, No. 9, pp. 756 – 759 (2012).	Chapter 2
2	Orientation control of ZnO films deposited using nonequilibrium atmospheric pressure N_2/O_2 plasma	Y. Nose T. Nakamura T. Yoshimura A. Ashida T. Uehara N. Fujimura	Japanese Journal of Applied Physics, Vol. 52, No. 1S, Paper No. 01AC03, Total 3 pages (2013).	Chapter 3 Chapter 4 Chapter 5
3	Chemical vapor deposition of ZnO films with low residual electron concentrations using N_2-based nonequilibrium N_2/O_2 plasma generated near atmospheric pressure	Y. Nose Y. Miyata T. Kiguchi T. Yoshimura A. Ashida T. Uehara N. Fujimura	Applied Physics Express, submitted.	Chapter 4 Chapter 5
4	Novel chemical vapor deposition process of ZnO films using nonequilibrium N_2 plasma generated near atmospheric pressure with small amount of O_2 below 1%	Y. Nose T. Yoshimura A. Ashida T. Uehara N. Fujimura	Journal of Applied Physics, submitted.	Chapter 5
5	Low temperature formation of highly resistive ZnO films using nonequilibrium N_2/O_2 plasma generated near atmospheric pressure	Y. Nose T. Yoshimura A. Ashida T. Uehara N. Fujimura	Thin Solid Films, submitted.	Chapter 5

Other Article Regarding this thesis

No.	Title	Authors	Journal
1	Evaluation of the electronic states in highly Ce doped Si films grown by low temperature molecular beam epitaxy system	Y. Miyata Y. Nose T. Yoshimura A. Ashida N. Fujimura	Journal of Crystal Growth, Vol. 425, pp. 158 – 161 (2015).